DESIGN OF HETEROGENEOUS BIFUNCTIONAL CATALYST FOR UPGRADING BIOETHANOL THROUGH THE GUERBET REACTION

BY

MALEK Y. S. IBRAHIM

THESIS

Submitted in partial fulfillment of the requirements
for the degree of Master of Science in Chemical Engineering
in the Graduate College of the
University of Illinois at Urbana-Champaign, 2015

Urbana, Illinois

Advisors:

Professor Paul J. A. Kenis
Professor Hong Yang

ABSTRACT

Catalytic conversion of ethanol through the Guerbet reaction to higher carbon number molecules allows efficient transformation of biomass to liquid fuels and commodity chemicals. A selective and stable heterogeneous catalyst is required to render this conversion possible in an economic way. The reaction was found to proceed through two parallel mechanisms on basic magnesia where acetaldehyde, formed from ethanol dehydrogenation, can either couple with itself or with adsorbed ethoxide to form new carbon-carbon bonds and the ethanol to acetaldehyde pressure ratio was found to determine which of these two mechanisms predominates. Amphoteric titania, and acidic alumina were found to have very low ethanol dehydrogenation activity and can only catalyze the Guerbet reaction through the acetaldehyde self-coupling mechanism. Strong acidic sites were found to catalyze alcohol dehydration while strong basic sites were found to catalyze esterification and show poor stability under humid conditions. Mild acid-base sites on titania were found to selectively catalyze acetaldehyde aldol condensation and exhibit high stability under humid conditions.

To overcome the low dehydrogenation activity of titania, addition of a metallic function was proposed. Among several metals tested, copper was found to be the most selective catalyst for dehydrogenation either as unsupported powder or supported nanoparticles. A synergetic effect was obtained from deposition of the copper nanoparticles on the titania surface since it was found to facilitate product desorption, a step that was found to be the rate limiting for acetaldehyde aldolization. Supported copper nanoparticles were found to catalyze the undesired alcohol esterification reaction. To suppress this side reaction, alloying copper with gold and promotion with chromium and potassium were found to be beneficial. A hybrid sequential-simultaneous reaction configuration was proposed to allow preliminary alcohol selective dehydrogenation on a monofunctional catalyst followed by simultaneous dehydrogenation, aldolization, and product hydrogenation on a bifunctional catalyst.

ACKNOWLEDGEMENTS

The author wishes to express his sincere appreciation to the committee of professors for their assistance in the preparation of this thesis and to the research assistants who made this work possible; Lan Wei, Han Xiao, Rogan Kipp, Kenan Al-bardan, and Mark Triezenberg. In addition, special thanks to the Energy Bioscience Institute (EBI) and BP for their generous financial support to this project, Dow Chemcials and 3M for their student fellowships, and to the Material Research Laboratory (MRL, UIUC) for providing easy access to equipment and instrumentation needed for research. Part of the experimental work was done in the laboratory of Dr. D.W. Flaherty. At the end, I would like to thank my friends, and family, and everybody else who helped me through earning my Master's Degree.

TABLE OF CONTENTS

LIST OF ABBREVIATIONS

ATW	Atmospheric Thin Window
bal.	balance
BET	Brunauer–Emmett–Teller
C-C	carbon to carbon
COP3	Conference of Parties III
DFT	Density Function Theory
EDS	Energy Dispersive Spectroscopy
EtOH	Ethanol
FID	Flame Ionization Detector
FTIR	Fourier Transform Infra-Red
GC	Gas Chromatography
ICP	Inductively Coupled Plasma
ID	Inner diameter
IE	Ion Exchange
IW	Incipient Wetness
MFC	Mass Flow Controller
MS	Mass Spec
NP	nanoparticles
NRTL	Non Random Two Liquids
OD	outer diameter
OES	Optical Emission Spectroscopy
PID	Proportional Integral Derivative
STEM	Scanning Transmission Electron Microscope
TCD	Thermal Conductivity Detector
TEM	Transmission Electron Microscope
TPD	Temperature Programmed Desorption
TPR	Temperature Programmed Reduction
UV	Ultra Violet
wt	weight
XRD	x-Ray diffraction

Chapter 1: Introduction

1.1. Bioethanol Production

World energy consumption is expected to continue to expand due to the rapid economic growth in Asia and Latin America along with the increasing world population. The majority of world energy comes from limited nonrenewable fossil fuels which creates a pressing need to find other sustainable alternatives to serve as energy sources in the future.[1-3] It is also necessary to mitigate the climatic consequences resulting from the increasing carbon dioxide emissions expected from the increase in energy consumption.

Bioethanol, a carbon neutral feedstock as per the Kyoto Protocol COP3 (1997)[4] can be efficiently produced from the biological depolymerization of non-edible biomass containing lignocellulose either as a single product or accompanied by acetone and butanol in the mass ratio of 1:3:6 ethanol: acetone: butanol.[5-8] The fermentation products distribution can be controlled by engineering the microorganism used, which has been the focus of extensive research for the last few decades to achieve highly efficient conversion.[9] Through extensive research efforts in metabolism, reaction engineering, and separation, fermentation process conversion efficiency has been continuously improved while production cost and energy consumption have been reduced.[5,10,11] This improvement in production economics has led to an increased interest in upgrading the C_2-C_4 oxygenates produced from biomass fermentation to more valuable chemicals and fuels.[4,12,13]

1.2. Conversion of Bioethanol to Longer Chain Oxygenates

The main use for bioethanol nowadays is the direct blend in the gasoline pool.[14,15] While this can minimize the dependence on fossil fuels for automotive gasoline, it can only be applied to a limited degree due to ethanol high water solubility and low Reid vapor pressure; both are undesirable properties in automotive gasoline.[16] Unlike ethanol, butanol and higher alcohols have lower water solubility, vapor pressure, and higher energy content[17] as shown in Table 1 which allows their blend with refinery gasoline at higher ratios compared to ethanol without the need for modifications in the vehicles engines or the existing gasoline distribution infrastructure.[18]

In addition to gasoline blend, hydro-deoxygenation of the longer chain alcohols yields a mixture of paraffins that can be used as sulfur free diesel, jet fuel, or detergents raw materials depending on the product carbon number and degree of branching. Dehydration and cyclization of the produced long chain alcohols, on the other hand, yield olefins and aromatics used as building blocks for polymers and rubber production as shown in Figure 1. Thanks to these advantages, it is more sustainable and environmental benign to convert the bioethanol to longer chain alcohols.

1.3. Formation of New C-C Bonds via the Guerbet Reaction

Ethanol conversion to longer chain alcohols is possible through alcohol polymerization condensation, also known as the Guerbet reaction, a reaction first introduced and named after Marcel Guerbet[19] in 1899 and since then was extensively studied as a pathway for making new carbon to carbon C-C bonds required for synthesizing certain specialty chemicals possessing certain branching characteristics.[20,21] Several catalysts have been patented for coupling of ethanol at high temperature and pressure to produce butanol and longer alcohols since 1933.[22] Butanol conversion to longer alcohols is also widely applied by Exxon and Henkel to produce 2-ethyl-1-hexanol,[20] an important intermediate in plasticizers, perfumes, alkyd resins, hydraulic oils, and lubricants production.[23] Higher alcohols produced by Guerbet reaction also have high oxidation resistance, and low pore point and hence widely used in personal-care products, plastic mold release, and paper processing.[21]

Alcohols produced from the Guerbet reaction are typically hydrophobic and β branched since the new C-C bonds are formed between one molecule carbonyl carbon and another molecule α carbon.[21] Ethanol, unlike longer alcohols, has only two carbon atoms, and hence the coupling of ethanol with any other linear alcohol from the linear alcohol carbonyl carbon position always yields a linear alcohol which suggests that by controlling reaction conditions and especially reactants partial pressure, the product degree of branching can be controlled.

The Guerbet reaction can proceed without a catalyst at very slow rate but with the aid of a metallic function and alkali metal alkoxides, high reaction rates can be achieved at high temperature and autogenous pressure.[24] Such catalytic systems and reaction conditions have been applied until the

1970's when homogeneous complexes of transition metals such as Rh, Ru, Ir and Pt were found to catalyze the reaction at lower temperature and pressure[25] with lower side products yield such carboxylic acids.[20]

The main drawback in all the catalytic systems mentioned above is that they are homogeneous, corrosive, and require continuous expensive catalyst separation and recycle in addition to their waste disposal issues.[26-30] It was also reported that during the course of reaction, the basic metal alkoxide gets hydrolyzed to the less active metal hydroxide[31-34] and the basic reaction medium causes excessive metals leaching when supported metallic functions are used as co-catalysts[35-37] which limits the long term usability of such systems.

Replacing the aforementioned catalysts with solid heterogeneous catalyst enhances the system stability and eliminates the need for separations and recycles[26,27,29,38] which allows the application of the Guerbet reaction on large scale and makes it economically feasible to convert ethanol to longer chain alcohols in a continuous affordable way. Several metal oxides, and phosphates, are highly insoluble, and resemble the soluble transition metal complexes in terms of harboring high valence metal sites surrounded by electronegative atoms with no metal-metal bonds.[39] which make these materials possible replacement for Guerbet catalysts.

This thesis shows how the effect of changing the acid-base properties of heterogeneous metal oxides affects the ethanol conversion activity and selectivity towards the Guerbet products. The mechanism of the Guerbet reaction is also studied on metal oxides to understand the reaction pathway, rate determining step(s), and the required catalyst properties. It can be concluded from this work that an amphoteric metal oxide harboring mildly acidic and basic sites promoted with copper as a dehydrogenation function can catalyze the Guerbet reaction at relatively lower temperature without excessive side reactions or catalyst deactivation.

1.4. Figures and Tables

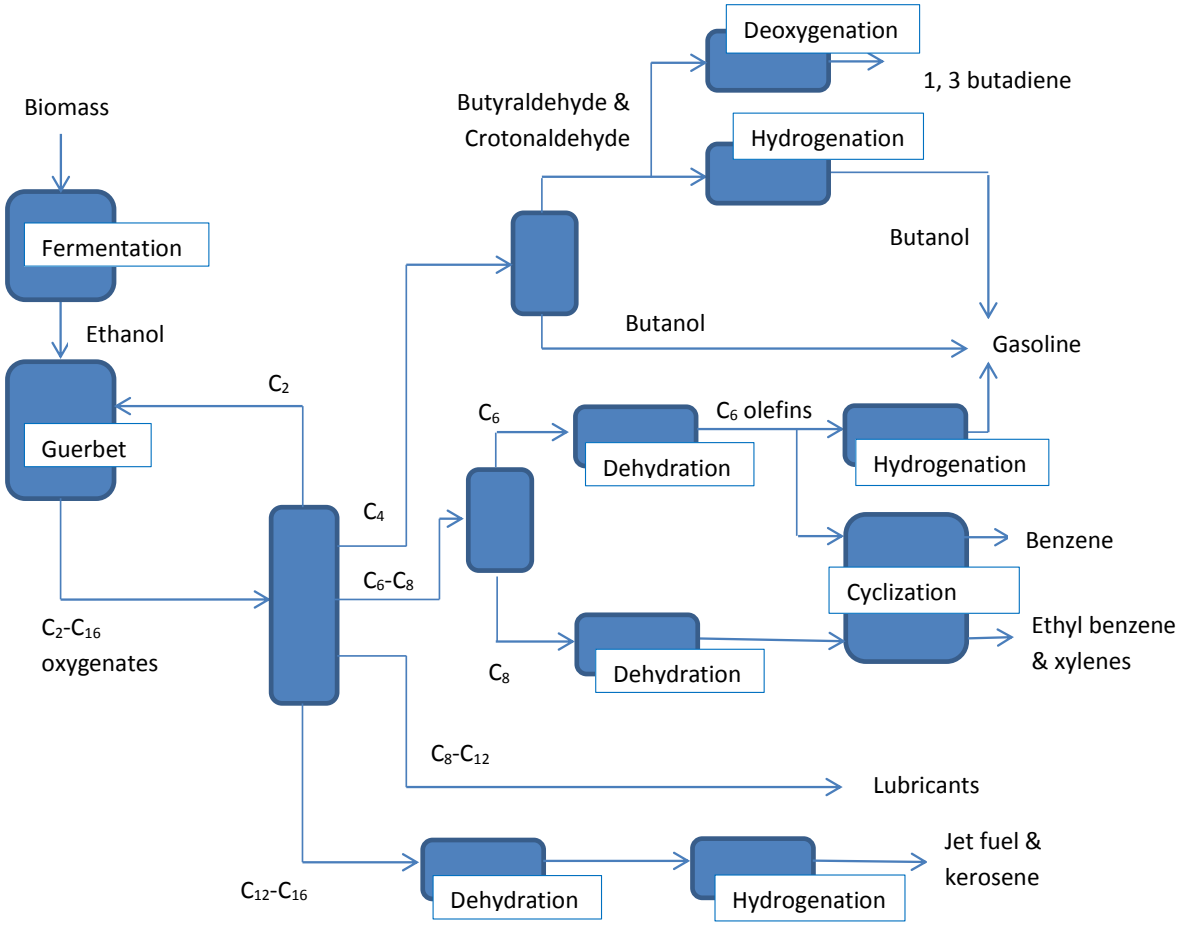

Figure 1. Conversion of biomass through fermentation-Guerbet process to liquid fuels and commodity chemicals

Table 1. Effect of increasing carbon number on linear alcohol fuel properties

Alcohol	Water solubility (mole/100 g water) at 20 ^{o}C	Reid vapor pressure (kPa)	Energy content (kJ/g)
Ethanol	∞	16	29.7
n-butanol	0.11	2.2	36.1

Chapter 2: Reaction of Ethanol on Metal Oxides with Different Acid-Base Properties

2.1. Introduction

Due to its high water solubility and low Reid vapor pressure, the maximum amount of ethanol that can be directly blended with automotive gasoline is about 15% by volume[40,41] which limits the application of the biomass fermentation process to a small fraction of the gasoline market. To overcome this limitation, bioethanol can be converted to longer chain alcohols in the range of C_4 to C_{16} through the controlled formation of new C-C bonds.

The intra-molecular coupling of alcohols to form new C-C bonds is a useful reaction in synthesizing a group of branched, long chain alcohols known as Guerbet alcohols that are often used as lubricants and plasticizers.[20,21] Moreover, the aforementioned reaction can be applied to upgrade the ethanol produced biologically from biomass fermentation through conversion to more valuable fuels and chemicals. This approach can minimize the dependence on fossil fuels by producing liquid fuels from biomass such as aviation gasoline and diesel fuel in addition to certain monomers building blocks and intermediates.

Homogeneous catalysts such as basic metal alkoxides, hydroxides, or bicarbonates, and transition metals or their complexes have been traditionally used as catalysts different alcohol Guerbet processes.[24,25,42] However, catalyst recovery and recycle make the process expensive and catalyst waste disposal creates environmental issues.[26-29] To eliminate the need for catalyst recovery and make the process economically feasible while mitigating its impact on the environment, it is of significant interest to replace the homogeneous catalysts with a heterogeneous catalytic system that is able to conduct this reaction at reasonable rate and high selectivity.

The reaction of alcohols on heterogeneous catalysts has been extensively studied. Products resulting from the formation of new C-C bonds were observed through the reaction of alcohols over on a panel of oxides including alkaline earth oxides,[43-47] rare earth oxides,[48] transition metal oxides[43,49,50], mixed oxides,[28,51-56] hydroxyapatites,[57-60] aluminophosphates,[61] hydrotalcites,[62] Zeolites,[63,64] and other heterogeneous catalysts with different degrees of success depending on the

catalyst surface acid-base properties and the reaction conditions applied. To optimize the catalyst surface properties for this reaction, it is required to understand how acid-base interaction affect the new C-C bonds formation. In addition to the new C-C bond formation, other reactions such as esterification, etherification, decarbonylation, and dehydration were also found to be affected by surface acid-base properties.

In this chapter, effect of the surface acid-base properties on C-C formation activity and selectivity is elucidated by observing formed products distribution on highly acidic (Al_2O_3), highly basic (MgO), and amphoteric, or acid-base balanced, (TiO_2). All oxides were able to form new C-C bonds providing that ethanol dehydrogenation to acetaldehyde occurs on a separate catalyst. In absence of a dehydrogenation catalyst, only the highly basic MgO is able to form new C-C bonds directly from ethanol. The highly acidic oxides catalyze dehydration of ethanol to ethylene and diethyl ether while the highly basic oxides catalyze ethanol conversion to ethyl ester and ketones and become deactivate rapidly under reaction conditions. The amphoteric metal oxides are found to catalyze the C-C formation reaction at high selectivity while maintaining its activity during operation under acetaldehyde-ethanol reaction conditions.

2.2. Materials and Methods

2.2.1. Catalysts Preparation

Magnesium oxide (MgO, Aldrich, 99.995%), titanium oxide (TiO_2, Aldrich, 99.8%), aluminum oxide (Al_2O_3, Aldrich, >99.9%) were washed with deionized water (17.9 MΩ resistivity), overnight dried in static air at 343 K, then treated in flowing dry air (S.J. Smith, Ultra Zero) by heating to 773 K at 3 K min^{-1} and holding for 8 h. Samples were cooled down to room temperature, pelletized, and sieved to size range of 35-60 mesh.

2.2.2. Catalysts Characterization

BET surface area was measured by Micromeritics® using multipoint N_2 physisorption at 77 K. Prior to experiment, samples were outgassed at 673 K for 2 h in helium. Measured surface areas

are reported in Table 2. The crystal phase of catalysts was determined using X-ray diffraction XRD (Bruker D-5000, Cu K- α radiation) and data is reported in Table 2.

2.2.3. Conversion and Selectivity Measurements

Reactions rates were measured using a quartz tubular reactor (0.5" OD) with plug flow hydrodynamics, which is contained within a three-zone electrically heated furnace (Applied Test Systems) controlled using an electronic PID controller (Watlow, EZ-Zone®) as described in Figure 2. The bed temperature was measured with a type K thermocouple touching the outer surface of the tube at the catalyst bed position. Catalysts were mixed with additional quartz (SiO_2, Supelco, analytical grade) to optimize vapor mixing with catalyst. Inertness of the quartz powder was tested at 633 K and no measurable reactions were observed.

Prior to the experiment, catalyst was in situ treated in 30 kPa H_2 (S.J. Smith, 99.99%), 71 kPa He (S.J. Smith, 99.99%) flowing at 200 $cm^3\ min^{-1}$ for 1 h at 773 K then cooled down to the experiment temperature. All pretreatments and experiments were done at ambient pressure. The volumetric flow rates of gaseous feed components were controlled using calibrated mass flow controllers (Parker, MFC 600) while liquid components; ethanol (Decon, 200 Proof), acetaldehyde (Sigma Aldrich, 99.5%), and deionized water were injected using two programmable syringe pumps (KD Scientific, Legato 110). Liquid feeds were injected to feed transfer lines heated by means of heat tape set at 393 K while reactor effluent lines were kept heated at 473 K to prevent high boiling point components condensation.

Reactor effluent was cooled and bubbled in ethanol to capture condensable products, the products containing solution was injected to an offline Gas Chromatography coupled with a Mass Spectrometer (Shimadzu, 2010 GC-MS) to identify the formed products. The quantitative analysis was determined using an online Gas Chromatography (Agilent, HP 6890) equipped with a capillary column (Agilent, J&W HP-PLOT Q, L = 30 m, ID = 0.32 mm, film thickness = 20μm) connected to a Flame Ionization Detector (FID) to detect hydrocarbons and oxygenates and a packed column (Restek, HayeSep Q, L = 2m, ID = 2 mm) connected to a Thermal Conductivity Detector (TCD) to detect H_2, CO, CO_2, and H_2O.

The retention time for each component was determined by injecting prepared standard solutions of the following chemicals in ethanol; 2-butanone (Supelco, analytical standard), 2-ethyl-1-hexanol (Fluka, analytical standard), 2-ethyl-1-butanol (Aldrich, 98%), 2-ethyl-2-hexenal (Aldrich^{CPR}), butyraldehyde (Fluka, 99%), butanol (Fisher, ACS grade), octanol (Alfa Aesar, 99%), hexanol (Sigma Aldrich, 98%), crotyl alcohol (Aldrich, 96%), hexanal (Aldrich, 98%), crotonaldehyde (Aldrich, 99%), acetone (Macron, ACS grade), Acetic acid (J.T.Baker, ACS grade). Retention time calibration for gaseous products was done by injecting gas mixture standards (Supelco, analytical standard) containing carbon monoxide, carbon dioxide, methane, ethane, ethylene, acetylene (1w/w% in N_2), propane, propylene, and butane (15 ppm in N_2)

Reaction parameters were measured under differential conditions (<10% reactant conversion) to minimize the effect of reactant depletion on measured parameters. Conversion and selectivity are defined as following:

$$EtOH\ Conversion(\%) = \frac{mole\ ethanol\ in - mole\ ethanol\ out}{mole\ ethanol\ in} X\ 100$$

$$Pool\ Conversion(\%) = \frac{mole\ ethanol + acetaldehyde\ in - mole\ ethanol + acetaldehyde\ out}{mole\ ethanol + acetaldehyde\ in} X\ 100$$

$$Product\ Selectivity(\%) = \frac{mole\ ethanol\ converted\ to\ product}{moles\ ethanol\ converted} X\ 100$$

2.2.4. Thermodynamic equilibria calculations

The thermodynamic equilibrium distribution of reactant and products was calculated using Virial equation of state to count for the intramolecular interactions in the vapor phase while components properties were estimated using Non Random Two Liquids NRTL equations.

2.3. Results and Discussions

2.3.1. Reaction of Ethanol on Metal Oxides

Figure 3a shows the ethanol conversion at 633 K on equal masses of Al_2O_3, MgO, and TiO_2. The three oxides were chosen as examples for acidic, basic, and amphoteric metal oxides respectively. Despite not having the largest surface area per unit mass, Al_2O_3 was found to be the most active material at the testing reaction conditions. MgO and TiO_2 showed similar steady state activity, however, MgO showed excessive deactivation at the first few hours of operation (not shown). To understand the difference in activity of these materials, it is important to study the main reactions pathways that ethanol undergoes on each of these materials.

Figure 3b shows the main products selectivity resulting from the reaction of ethanol on the three materials. The products represented in two main groups; the first group contains acetaldehyde produced from ethanol dehydrogenation, and Guerbet products resulting from C-C formation including C_{4+} alcohols, aldehydes, and hydrocarbons. The other group contains ethylene and diethyl ether resulting from ethanol dehydration plus ethane produced from ethylene hydrogenation. Besides these two groups of chemicals, small amounts of acetone and ethyl ester were also formed as discussed in the following sections. Figure 4 summarizes the main ethanol reaction pathways on the three metal oxides.

Al_2O_3 was found to selectively dehydrate ethanol to ethylene at 633 K. In addition to ethylene, traces amount of ethane were produced as well. The only group of products containing new C-C bonds formed on this material were saturated and unsaturated C_4 hydrocarbons with no oxygenates containing new C-C bonds or acetaldehyde being formed. Comparable selectivities towards both the unimolecular dehydration to ethylene and the bimolecular dehydration to diethyl ether were observed on TiO_2 and traces amounts of acetaldehyde and higher oxygenates including ketones and aldehydes were also detected suggesting that dehydrogenation and formation of new C-C bonds is possible on this amphoteric material but at very low selectivity. Unlike Al_2O_3 and TiO_2, dehydration products were not the main products formed on MgO, instead, high selectivity towards

acetaldehyde and butanol, a component containing newly formed C-C bonds, was observed. In addition to these two products, ethyl ester was formed in measurable quantities on MgO.

To understand the difference in products selectivity on these materials, it is required to understand how acid and base sites catalyze different chemistries. Theoretically, all metal oxide surfaces are harboring Lewis acid and Brønsted base sites represented by the surface metal cations and oxygen anions respectively.[27,39,65,66] Moreover, the surface hydroxyl groups resulting from protonation of the surface oxygen atoms can act as additional Brønsted acid sites.[67-69] The difference in the products identity and distribution at similar reaction conditions on the three catalysts is potentially resulting from the difference in the acid-base balance on their surfaces. It has been proven through temperature programmed desorption TPD,[70-72] acid-base titration,[73-75] calorimetric measurements,[76] FTIR,[30,77-79] UV absorption and luminescence,[27] theoretical methods,[80,81] DFT[82] and other methods[83] that the basicity strength of the oxide generally increases with its cation size going from right to left and down to up on the periodic table while acidity follows the opposite direction. This behavior can be explained by the ability of the larger cation to transfer electrons to the oxygen atom making it stronger base while the cation ability to share electrons with adsorbing species becomes attenuated making it a weaker Lewis acid.

Dehydration is found to be the main reaction pathway on highly acidic oxide, as in the case of Al_2O_3. Ethanol can undergo two types of dehydration either monomolecular to yield ethylene or bimolecular to yield diethyl ether. Both reactions are known to be acid catalyzed.[73,84-87] On the other hand, acidic surfaces exhibit poor activity towards ethanol dehydrogenation to acetaldehyde. Moreover, acidic surfaces are less active towards Guerbet oxygenate containing newly formed C-C bonds. It is worth mentioning here that the observed C_4 hydrocarbons on Al_2O_3 are probably resulting from dimerization of ethylene not through the dehydration of Guerbet products since no oxygenates containing new C-C bonds were detected in this case. The following section explains how acid and base sites contribute to the formation of different products from ethanol.

2.3.1.1. Dehydration to olefins

Alcohol dehydration to olefins can proceed through one of two mechanisms on metal oxides as proposed by Di Cosimo et al.[88] The E_2 elimination mechanism occurs through coordination of the

surface basic oxygen with a hydrogen atom attached to the alcohol β carbon while the surface metal site forms a bond with the hydroxyl oxygen as shown in Figure 5a. A new O-H bond is formed between the positively charged proton and the negatively charged hydroxyl oxygen to form water molecule that desorbs to the gas phase and double C=C bond gets formed between the **α** and the β carbons in the newly formed olefin. This reaction is a single step mechanism[89] that does not involve formation of ionic species.

On the other hand, the E_{1CB} elimination mechanism proceeds through the dissociative adsorption of the alcohol to form adsorbed alkoxide[90] and a proton as shown in Figure 5b. A strong basic site is required in this mechanism to abstract a proton from the alkoxide β carbon and form a surface carbanion followed by breaking the C-O bond. This mechanism has shown to be two to three order of magnitudes slower than the E_2 elimination on Al_2O_3[88] so it reasonable to propose the E_2 elimination mechanism as the major ethanol dehydration pathway to ethylene on the acidic metal oxides. This is also in agreement with the results of DFT calculations for alcohol dehydration on γ-Al_2O_3 where E_2 elimination was found to be the most favorable mechanism.[87]

Ethanol dehydration to ethylene was found to occur to a lesser extent on basic MgO which probably proceed through the E_{1CB} mechanism. Despite the low ethanol dehydration activity of the basic MgO, dehydration of longer or branched alcohols can proceed with higher rates since it has lower activation barrier[86,91] and hence the E_{1CB} elimination effect becomes more significant at higher conversions at which longer and branched alcohols concentrations become higher. This can lead to an excessive formation of undesired olefins lacking the carbonyl functionality required to form new C-C bonds through Guerbet reaction. Olefins, on the other hand, can still oligomarize to form higher olefins and aromatics through a different acid catalyzed mechanism that is described in the following section.

Ethylene oligomerization to C_4 hydrocarbons was observed on the acidic oxide. Such reaction can be catalyzed by either Lewis or Brønsted acids.[92] Lewis acid-catalyzed oligomerization involves the formation of carbocation intermediate with a hydrogen atom transfer followed by coupling with another olefin while Brønsted acid-catalyzed oligomerization proceeds through the formation of the carbocation as described earlier or through the formation of a surface alkoxide structure. The former mechanism is known to yield branched oligomers while the latter is known to yield

linear ones. Both mechanisms can occur on Al_2O_3 surface since the Al^{3+} sites act as strong Lewis acid while surface hydroxyl, formed from the dissociative adsorption of ethanol,[93] act as Brønsted acid sites.

2.3.1.2. Dehydration to ethers

Bimolecular alcohol dehydration to ether requires acid sites similar to the unimolecular dehydration to olefins. The main factor that sets which pathway is the prevailing on the metal oxide surface is the acidity strength of the surface sites.[94,95] It is generally agreed that the stronger the acid site, the higher the olefins to ethers ratio in the product.[88,96] This relation can be explained by the need for strong surface Lewis acid sites to weaken the alcohols C-O bond and break it in the monomolecular dehydration case unlike in the bimolecular dehydration where one of the two alcohols C-O bond is conserved and another C-O bond is formed as described in Figure 6. This can explain why the mildly acidic TiO_2 is more selective towards diethyl ether compared to the highly acidic Al_2O_3 as shown in Figure 7. In addition to Lewis acid strength, higher temperature also increases the ratio of olefins to ethers in the product due to the difference in activation barrier between the rate determining steps in these two mechanisms.[87]

Under the mentioned reaction conditions, diethyl ether was the only ether formed in measurable quantities on TiO_2. However, at higher conversions, it is expected that other ethers will be formed through the intra-molecular reaction of the higher alcohols formed from Guerbet reaction with ethanol. While ethers are high molecular weight oxygenates, they are considered undesirable products in the product pool due to their higher water solubility and Reid vapor pressure. Ethers are also considered as terminal products in terms of C-C bond formation as they do not harbor carbonyl carbons required to undergo such reaction. In addition to these disadvantages, dehydration of ethers yields undesirable shorter chain molecules due to the existence of the C-O links in the center of the molecule carbon chain. All these factors make it necessary to minimize alcohol dehydration to ethers by optimizing catalyst properties and process conditions.

2.3.1.3. Dehydrogenation to aldehydes

Strong basic sites on MgO and high reaction temperature are able to dehydrogenate ethanol to acetaldehyde at 633 K. Since the dissociative adsorption of ethanol to alkoxide and surface proton occurs at low temperatures on metal oxides.[90,93,97] It is possible that the high reaction temperature is required to overcome the activation barrier associated with elimination of the β hydrogen of the adsorbed alkoxide as shown in Figure 8 or associated with the desorption of the formed aldehyde to the gas phase. In addition to overcoming the kinetics activation barrier, dehydrogenation is an endothermic reaction that requires high temperature to shift the thermodynamic equilibrium towards the aldehydes formation direction as shown in Figure 9.

2.3.1.4. Dehydrogenation to esters

Esters, or acetates, formation is a C-O bond formation reaction that proceeds through a different mechansims from that leading to the C-O bond formed in dehdyration to ethers. Several mechansims were proposed for the formation of ethyl ester from ethanol. The direct acid catalyzed dehydration of an alcohol with a carboxylic acid was proposed as a mechansim for ester formation.[98] Carboxylic acids formation from alcohols requires dehydrogenation of the alcohol to the aldehyde followed by oxidation of the aldehyde to the carboxylic acid through Cannizaro reaction.[30,99,100] This mechansim is unlikely in the presented case since high selectivity to esters was observed on the highly basic material as shown in Figure 10 which suggests that it is not a specifically acid catalyzed reaction and no carboxylic acids were detected along with the esters.

An alternative, base-catalyzed, mechanism is proposed in which the alcohol becomes dehydrogenated to the aldehyde which reacts directly with another alcohol in Tishchenko type reaction[27,47,88] to form the hemiacetal intermediate which decomposes to ester[53,93,101,102] This mechanism requires both acid and base functionality to proceed where surface oxygen is required to coordinate with the carbonyl carbon of the deprotonated aldehyde while a C-O bond is formed with an adsorbed alkoxide. According to Idriss et al.[93], adsorbed alkoxide is formed by the absrtraction of α hydrogen from one aldehyde molecule by another adosrbed aldehdye to form the enolate and the alkoxide species respectivly, however, since the alcohol is presented in the reaction

medium, alkoxides can be formed directly by the dissociative adsorption of the alcohol as discribed in Figure 11 in the present case. According to this mechanism, alcohol esterification activity depends on the basic sites strength of the oxide. This is in agreement with the findings reported by Tanabe et al.[103] where esterification rates on alkaline earth oxide were found to follow the order of basicity as following MgO < CaO < SrO < BaO. This sort of esterification reaction was also reported on basic SnO, U_2O_3[104], and Cu-Zn-Al mixed oxide.[105]

Since the reaction involves the formation of the aldehydes as the reactive intermediates, it is important to notice that If the formed aldehydes is lacking α hydrogen, it reacts mainly through Tishchenko reaction to produce esters while aldehydes with α hydrogen can undergo both Tishchenko C-O formation and aldol C-C formation condensation.[63] Earlier studies by Hattori[27,106] showed that butyraldehyde, an example of an aldehyde with α hydrogen, is selectively converted to esters through Tishchenko reaction on stronger alkaline earth oxides such as SrO and BaO. Controversy, less basic MgO was more selective to aldol products suggesting that stronger basic sites are more selective towards esterification.

Similar to ethers, esters are undesirable in Guerbet products since they act as terminal products lacking the carbonyl functionality required for C-C bond formation and their dehydration yields shorter chains hydrocarbons. Separation of ethyl ester from ethanol is costly as the two components form an azeotrope.[107,108] In addition to these drawbacks, esters bind strongly to surface acid sites and inhibit the Guerbet C-C formation reaction as demonstrated in the next chapter.

2.3.1.5. Ketonization

Ketones, including acetone and methyl ethyl ketone, were also formed on basic metal oxide. More than one reaction mechanism was proposed for ethanol conversion to acetone. An oxidative mechanism involves the ethanol dehydrogenation to acetaldehyde followed by acetaldehyde oxidation to acetic acid was proposed similar to that described for esters formation. Two of the formed acetic acid molecules undergo a C-C formation reaction leading to the formation of acetone, carbon dioxide and water.[30,109] This mechanism is unlikely since no acetic acid or carbon dioxide were detected with ketones.

Another ethanol to acetone conversion mechanism was proposed by Murthy et al.[109] where acetaldehyde undergoes aldol condensation reaction to form acetaldol (3-hydroxy butyraldehyde) which undergoes an intermolecular hydrogen transfer reaction leading to the isomerization of the acetaldol to 4-hydroxy-2-butanone as shown in Figure 4. The 4-hydroxy-2-butanone can either be dehydrated to form methyl ethyl ketone or be decomposed to form acetone and formaldehyde. This reaction mechanism is more likely to occur under the testing conditions as both ketones were detected in addition to other aldol condensation products. Formaldehyde was not detected in the reaction product possibly due to its rapid decomposition to hydrogen and carbon monoxide which were detected in reaction products as well.

2.3.1.6. Guerbet C-C coupling to longer oxygenates

Since basic MgO is active for both dehydrogenation of alcohol to aldehyde and formation of the new C-C bonds in Guerbet reaction, it is not clear whether this ability of basic surfaces to form new C-C bonds through Guerbet reaction is due to its ability to dehydrogenate the alcohol to the corresponding aldehyde which is, in turn, the reactive intermediate in the C-C bond formation reaction or that the basic sites participate in a different C-C formation mechanism that involves the direct interaction with the alcohol itself without the need for dehydrogenation.

Figure 12a shows the breakdown of the dehydrogenation and C-C formation products group selectivity from the reaction of ethanol on MgO at varying conversion. It can be seen that at higher conversion, the acetaldehyde selectivity decreases while the butanol selectivity increases. Also while the selectivity versus conversion curve for acetaldehyde does not pass by the origin, butanol selectivity curve does which suggests that acetaldehyde is a primary product while butanol is not. These findings show that the direct ethanol-ethanol interaction with the basic sites leading to C-C coupling to form butanol is less likely in this case and acetaldehyde is the reactive intermediate in butanol formation. The C_4 products distribution at variable conversion shown in Figure 12b shows that butanol is formed primarily to other C_4 aldehydes and hydrocarbons on MgO suggesting that these later species are formed from butanol dehydrogenation and dehydration respectively.

2.3.2. Effect of Acid-Base Properties on Products Selectivity

It can be hypothesized from the products analysis that the selectivity towards dehydration versus dehydrogenation depends on the acid-base balance of the catalyst surface. The more acidic the surface is, the more selective towards dehydration it becomes while the more basic the oxide is, the more selective towards dehydrogenation and C-C formation it becomes. The stronger the acid sites, the more selective to dehydration to olefins they are, while mildly acidic sites are more selective towards ethers. Both olefins and ethers are undesired products that need to be minimized through minimization of surface acidity. Esterification and ketonization, on the other side, are undesired products that were found to require strong basic sites to be formed. From these findings, it can be concluded that a certain balance of the acid-base properties is required to optimize the metal oxide performance for the ethanol Guerbet reaction. The following section is a general literature review that summarizes the reaction of ethanol and other oxygenates on metal oxides of different groups in the periodic table as part of the efforts for searching of the optimum oxide for the Guerbet reaction.

2.3.2.1. Alkaline earth metal oxides

Due to their strong Brønsted basicity, alkaline earth oxides are widely studied for aldol C-C formation reactions. Zhang et al.[110] reported that C-C bond formation activity in acetone aldol addition, normalized by surface area, follows the same order of basicity as measured by CO_2 TPD going down along the periodic table with BaO being the most active oxide followed by SrO, CaO, and then MgO. A similar trend was observed in butyraldehyde aldol condensation,[111]however, besides aldol condensation, aldehydes undergo Cannizaro disproportionation leading to the formation of carboxylates on this family of oxides.[99]

A correlation between CO_2 uptake and ethanol conversion to ethyl ester and acetone was demonstrated by Idriss et al.[93] for different metal oxides. This confirms that the activity towards these side reactions depends on surface basicity. Efforts to enhance the performance of MgO, the least basic oxide of this group, by supporting its nanoparticles on silica lead to lower selectivity to higher oxygenates from ethanol compared to the unsupported MgO while supporting the

nanoparticles of Ca and Ba oxides on MgO was found to decrease both surface basicity and C-C formation activity of the catalyst.[44] A contradicting conclusion was reported by Shen et al.[47] where supported alkaline earth oxides showed higher C-C formation activity but rapid deactivation at temperatures less than 623 K. Despite their high C-C formation activity, these oxides suffer from loss of selectivity and stability issues.

2.3.2.2. Alkali metal oxides

Unlike bulk alkaline earth metal oxide catalysts, alkali metals and their oxides and hydroxides are normally supported when used as catalysts and are also highly soluble in liquid reaction media. Supports of these oxides can be acidic, basic, or amphoteric. Addition of alkali metals to acidic alumina decreases alumina acidity and enhances its basicity. The effectiveness of different metals in enhancing the basicity was found to follow this order of K>Na>Cs>Rb.[44] It was also found out that alkali treatment of alumina increases selectivity towards aldol versus Tishchenko esterification of butyraldehyde with selectivity order of Rb>K>Na. However, when Iwasa et al.[112] treated Cu/Al_2O_3 with KOH, the aldol products yield was significantly reduced compared to the untreated catalyst. The difference in selectivity behavior in case of Cu promoted Al_2O_3 can be explained by the reduced catalyst dehydrogenation ability due to blocking of Cu active sites by KOH.

When alkali metals cations are supported on acidic zeolite, they create strong basic sites able to convert ethanol to butanol as in the case of Rb-LiX[113]. Interestingly, Li, Na and K exchanged zeolite still showed high selectivity towards alcohol dehydration products suggesting that the metals were not very efficient in suppressing the zeolite acidity or creating strong basic sites.

Opposite to what is expected, doping Na and Cs on basic MgO drastically reduced MgO alcohol Guerbet activity when tested under a mixture of methanol and ethanol[43] or ethanol only[44] possibly due to creating very strong basic sites that are rapidly deactivated as suggested by Ueda et al.[43] however, this could not be verified by the CO_2 TPD done up to 1173 K by Coville et al.[44]

Addition of Cs and Rb hydroxides to the acid-base balanced Cu-Zn mixed oxide increased propanol yield from ethanol and methanol reaction while addition of Na and K hydroxides almost

had no effect.[114] Addition of K to Cu/Ce-Mg mixed oxides reduced surface acidity as well and decreased the formation of ethers and hydrocarbons.[115] Addition of K[56] or K_2O[116] to the Zn-Cr mixed oxide reduced dehydration activity but increased ketonization selectivity in expense of aldolization. This was attributed to the ability of K doping to inhibit the acetaldol intermediates dehydration step leading to the formation of the aldol products but this phenomenon can also be explained by the transformation of the aldol intermediate to ketone through the mechanism described in Figure 4. Promotion of relatively inert supports such as silica with Na showed activity towards butyraldehyde conversion to 2-ethyl-2-hexenal but a rapid deactivation was also observed possibly due to poisoning of active sites by reaction byproducts.[117]

Despite being difficult to use as separate heterogeneous catalysts, alkali metals and their oxides can be used to attenuate the acidity or promote the basicity of other, more stable oxides. The selection of the alkali metal and its optimum surface ratio is a matter of trial and error depending on the oxide support and the reaction conditions.

2.3.2.3. Rare earth metal oxides

Rare earth oxide basicity and activity change based on the cation oxidation state, when in the M_2O_3 susquioxides form, rare earth oxides exhibit stronger basic sites that are able to catalyze aldol reaction and even the more difficult reactions such as hydrogenation and isomerization.[70] When the cation oxidation state is higher than 3 such as in oxides CeO_2, Tb_4O_7, Pr_6O_{11}, mild basic sites are exhibited that are able to selectively catalyze aldol reaction but none of the other side reactions.[27]

The reaction of propanol at 773 K on rare earth oxides yielded 3-pentanone as the main product.[48] Deactivation was observed when starting with oxides with cations oxidation state higher than 3 as catalysts which was attributed to the catalyst reduction under reaction conditions and loss of strong basic sites. Based on complete conversion of propanol, Ce oxide was the least selective to 3-pentanone compared to other rare earth oxides followed by Y and Ho oxides.

When tested for acetone aldol condensation, oxides of Y, Pr and, Nd where the most active catalysts in this family followed by Tb, Dy and, La, then Ho, Er, Tm, Sn, Eu, Gd while Ce was again the least active oxide[70] which generally follows the basicity order as measured by Choudhary et al.[118] in a separate study. The low selectivity of CeO_2 towards aldol can be explained by the different structure and higher acidity of this oxide as measured by NH_3 TPD[118] and demonstrated by the high dehydration products selectivity from ethanol at 673 K in a separate study done by Nakajima et al.[49] Acetaldehyde TPD on thin film fully oxidized CeO_2 showed no reaction of acetaldehyde while TPD on reduced CeOx showed conversion to dehydration products but no aldolization.[119]

When compared to other groups of oxides, the rare earth oxide La_2O_3 was found to be less active for acetone aldol condensation than the more basic, alkaline earth oxide MgO but more active than the early transition, less basic oxide ZrO_2[120]. It was also observed that La_2O_3 was deactivated more rapidly than other rare earth oxides at 773 K when tested by Claridge et al.[48] possibly due to CO_2 poisoning leading to the formation of Lanthanum oxycarbonate, a material that showed to be strongly acidic and highly selective towards ethylene production from ethanol.[49] While certain rare earth oxides exhibit enough basicity to catalyze C-C bond formation through aldehyde aldol condensation, their weaker basicity compared to alkaline earth oxides can be used to avoid catalyzing esterification and ketonization reactions. The main drawback in this case is that the catalyst dehydrogenation activity is low and hence the formation of the aldehyde from the alcohol requires high reaction temperature.

2.3.2.4. Transition metal oxides

This group of metal oxides can be divided into three subgroups; early, middle, and late transition metal oxides. Late transition metal oxides such as oxides of Cu, Ni and Co are reduced to the metallic form under ethanol vapor at 673 K while partial reduction of middle transition metals oxides occurs such as the reduction of Mn_2O_3 to MnO, Fe_2O_3 to Fe_3O_4, and V_2O_5 to V_2O_3. Other metals oxides including Zn, Cd, and Cr remain in their initial oxide form under the mentioned reaction conditions.[49]

The products distribution from this type of oxide is highly dependent on the metal oxidation state and the catalyst phase. Fe_3O_4 is highly selective towards acetaldehyde production[49,93] but under oxidative environment where Fe_2O_3 is formed, the catalyst shows comparable selectivities towards both acetaldehyde and ethyl acetate.[65] On the other hand, the more acidic middle transition metal oxides such as Cr_2O_3 and V_2O_5 showed comparable selectivities towards ethylene and acetaldehyde at 673 K. The basic, non-reducible, oxides such as ZnO and CdO are able to catalyze dehydrogenation of ethanol to acetaldehyde with reasonable selectivity[43,49] while the reaction of ethanol on nano-sized ZnO lead to acetone formation in addition of acetaldehyde.[51]

Unlike late and middle transition metals, early transition metals such as TiO_2 and ZrO_2 can catalyze the formation of other products than ethylene, acetaldehyde, and ethyl ester from ethanol including acetone, ethyl ether and Guerbet products.[43,49,93] One example of this group of oxides that has several applications in industry is ZrO_2. a key property of this material is the mild strength of its acid and base sites which protects them from poisoning by water and CO_2 but at the same time allows them to work cooperatively to catalyze acid-base reactions.[27,121]

However, Sun et al.[51] reported high ethylene yield from ethanol at 723 K while Ueda et al.[43] reported high ether yield at 633 K on ZrO_2 which suggests that the acid-base balance on this material is more skewed towards the acidity side than that required for the Guerbet reaction of ethanol. Interestingly, despite having similar structure and coordination number, the acidic strength of HfO_2 seems to be significantly less than that of ZrO_2 as demonstrated by the lower selectivity on HfO_2 to 2-octanol dehdyration[122] which makes it a possible selective catalyst for Guerbet reaction.

2.3.2.5. Post-transition metal oxides

Al_2O_3 is selective towards alcohol dehydration and etherification[88]. Addition of KF to this oxide yields strong basic sites, stronger than MgO as shown by Climent et al.,[123] which are highly active for aldol reaction of benzaldehyde with heptanal. Addition of Ni or Cu to alumina was also used for butanol production from ethanol with selectivity up to 70% at 30% conversion.[16]

SiO_2 shows negligible basicity as demonstrated by CO_2 uptake and ethanol dehydrogenation activity when heat treated at relatively low temperatures, however, when treated at temperature as high as 870 K, he oxide shows some activity due to removal of surface silanol groups and exposure of relatively strong basic sites. The more basic SnO_2 and Pb_2O_3 showed complete selectivity towards acetaldehyde from ethanol at 673 K[49] with no other products reported while SnO was found to catalyze ethanol esterification.[105]

2.3.3. Reaction of Ethanol-Acetaldehyde Mixture on Metal Oxides

Since acetaldehyde is found to be the reactive intermediate in the new C-C formation reaction, it is required to decouple the effect of surface basicity effect on dehydrogenation from its effect on new C-C bonds formation. To fulfill this target, acetaldehyde was co-fed with ethanol to eliminate the need for active dehydrogenation function and allow us to study the effect of the surface acid-base balance on the C-C formation independently. At the specified reaction temperature for each material, conversion was varied by changing the feed mixture flow rate while keeping both acetaldehyde and ethanol pressures constant. This is achieved by keeping the feed pool conversion less than 10% where both the production of acetaldehyde from ethanol dehydrogenation and the acetaldehyde consumption to from C_4 products had minor effect on the reactants pressure.

2.3.3.1. Acidic Al_2O_3

Due to the high reactivity of acetaldehyde compared to ethanol, significantly higher conversion was achieved when feeding acetaldehyde-ethanol mixture compared to feeding the pure ethanol. To keep conversion low and be able to perform kinetics measurements, reaction temperature was lowered from 633 K to 483 K. It is worth mentioning here that at both temperatures, the overall conversion is kept less than 10% which is less than the equilibrium conversion barrier for the formation of C_4 aldehydes from C_2 as shown in Figure 13.

While no Guerbet products were formed from the reaction of pure ethanol at 633 K on Al_2O_3, the reaction of acetaldehyde-ethanol mixture at 483 K on the same material lead to the formation of Guerbet products as shown in Figure 14a. The selectivity to Guerbet products on Al_2O_3 was less

than 50% due to the competing rapid alcohol dehydration reaction. At 483 K, dehydration was more selective towards diethyl ether opposite to the high selectivity to ethylene at 633 K on the same material. In addition to ethyl ether and Guerbet products, traces amounts of ethyl ester were also detected possibly formed by the mechanism described in Figure 11.

By examining the C_4 products distribution shown in Figure 14b, it can be concluded that butanol is a secondary product while both crotonaldehyde and butyraldehyde appear as primary products. This suggests that butanol is not directly formed from ethanol reaction on Al_2O_3 but it is resulting from the hydrogenation of the primarily formed C_4 aldehydes. It is possible that crotonaldehyde is the main primary product in this case but because of it high thermodynamic instability and the rapid crotonaldehyde hydrogenation on the Al_2O_3 surface described in the next chapter, butyraldehyde gets formed at very low conversions making it appear as another primary product.

It is important to point out that co-feeding acetaldehyde with ethanol reduced the catalyst activity towards the unimolecular dehydration to olefins and increased the ratio of ether to olefins in the product distribution. This behavior can be explained by the difference in activation energy of these two reactions[87] or the inhibition effect of the aldehyde on the surface strong acidic functionality due to the stronger adsorption of the aldehyde to the acid sites. In addition to ethylene, C_4 hydrocarbons were also detected including butane, butenes, and butadiene. Due to the inhibited ethanol dehydration to ethylene at the reaction conditions and the presence of C_4 oxygenates in the product pool, it is reasonable to assume that these hydrocarbons are formed from dehydration of the C_4 Guerbet oxygenates not from the ethylene oligomerization as proposed in the case of feeding pure ethanol at higher temperature.

2.3.3.2. Basic MgO

The reaction of the ethanol-acetaldehyde mixture at 633 K lead to rapid formation of C_{4+} oxygenates on MgO. Reducing temperature less than 633 K lead to rapid catalyst deactivation due to catalyst hydrolysis to magnesium hydroxide as shown in the next chapter. As shown in Figure 15a, about 90% selectivity towards C_{4+} Guerbet oxygenates was achieved in this case with trace amounts of ethylene, ethyl ether, and ethyl acetate being formed. Ethylene can be formed from

ethanol on strong basic surfaces through the E_{1CB} mechanism as described earlier, while ethyl ether requires the act of both acid and base sites which are available on MgO surface. Ethyl acetate is expected to be formed on the strong basic surface through Tishchenko reaction as described earlier.

The main difference between the reaction of pure ethanol and ethanol-acetaldehyde mixture on MgO can be seen on the formed C_4 oxygenates identity and products distribution. While butanol was formed as the main and only Guerbet product from the reaction of pure ethanol on MgO, crotonaldehyde, butyraldehyde, butanol, and crotyl alcohols were all formed in the case of acetaldehyde co-feed. By examining the C_4 oxygenates product distribution at variable conversion as shown in Figure 15b, it can be concluded that crotonaldehyde is the primary product in this case while the other Guerbet products appear as secondary products. This suggests that acetaldehyde self-coupling is the major C-C bond formation pathway in this case. However, the fact that butanol was formed from the reaction of pure ethanol on MgO without measurable presence of crotonaldehyde or butyraldehyde suggests that there is a parallel mechanism that involves ethanol direct reaction with acetaldehyde to from butanol in addition to the acetaldehyde self coupling. From these findings, it is reasonable to hypothesize that which of the two mechanisms is the prevailing on MgO depends mainly on the ratio of acetaldehyde to ethanol pressure. Further investigation on the effect of these components pressures on the C-C formation rate is described in the next chapter.

2.3.3.3. Amphoteric TiO_2

Similar to Al_2O_3, high conversion was achieved on TiO_2 when co-feeding acetaldehyde so reaction temperature was lowered to 503 K to minimize the effect of conversion on the reactant pressure at variable flow rates. As shown in Figure 16, C_4 Guerbet products were formed in high selectivity (>80%) when Co-feeding acetaldehyde at 503 K on the amphoteric TiO_2, opposite to the very low selectivity towards Guerbet products that was obtained from reaction of pure ethanol at 633 K on the same material. This suggests that acetaldehyde is the reactive component in making new C-C bonds on TiO_2.

It can be seen from product selectivity against conversion shown in Figure 16 that crotonaldehyde is the primary product in this case while butyraldehyde is secondary with no butanol being formed at reaction conditions. Crotonaldehyde to butyraldehyde ratio is higher than the ratio between these two components at equilibrium at the reaction hydrogen pressure and temperature as shown in Figure 17. The facts that C_4 oxygenates are formed only when acetaldehyde is presented along with the observation that crotonaldehyde being a primary product presented at a ratio higher than equilibrium ratio to other C_4 oxygenates suggest that the main mechanism of the C-C formation is through bimolecular acetaldehyde condensation reaction which is also known as aldol condensation while ethanol does not contribute directly to this reaction through parallel mechanisms on TiO_2 which is in agreement with the findings from studying Guerbet chemistry on other acid-base catalysts.[21,28,33,45,58,88]

Unlike Al_2O_3 where it shows as a primary product, butyraldehyde clearly appears as a secondary product on TiO_2. This can be explained by the fact that the obtained conversion on Al_2O_3 was higher than that of TiO_2 at the testing reaction conditions. Also crotonaldehyde hydrogenation to butyraldehyde can be more difficult to occur on TiO_2 compared to Al_2O_3 due to the difference between the two surfaces in basicity strength as further discussed in the next chapter.

It was also observed that traces amounts of higher than C_4 aldehydes (n-hexanal and 2-ethyl-butyraldehyde) were formed possibly from the reaction of acetaldehyde with the formed crotonaldehyde and butyraldehyde as shown in Figure 16. In addition to Guerbet products, small amount of ethyl ester (selectivity <10%) was also detected on TiO_2.

Based on these findings, it is reasonable to propose that the alcohol dehydrogenation is the rate limiting step in formation of Guerbet product from ethanol on mild and weak basic oxides. This step is catalyzed by strong basic sites which are not abundant on the amphoteric TiO_2 or acidic Al_2O_3. Alcohols are known to dissociatively adsorb on oxides surfaces to form the corresponding alkoxide and an adsorbed proton as shown in Figure 8 at lower temperatures than that of the reaction as discussed earlier so it is possible that the abstraction of the β proton from the adsorbed alkoxide is the step with the highest activation barrier that requires both high temperature and

strong basic site. Bypassing this step by co-feeding acetaldehyde makes the subsequent C-C formation steps down the hill on the energy-reaction coordinate plot on the three oxides.

2.4. Conclusion

Metal oxides are heterogeneous catalysts with acid-base properties that can be applied to upgrade bioethanol through the formation of new C-C bonds via Guerbet reaction. The acid-base properties of the oxides can be tuned by changing the cation size where larger cations yield more basic catalysts. From literature review it can be concluded that early transition metal oxides and rare earth oxides are suitable catalysts for this chemistry. At 633 K, the highly acidic Al_2O_3 selectivity catalyzes ethanol dehydration to ethylene which becomes hydrogenated to ethane or oligomerized to longer chain hydrocarbons. The mildly acidic TiO_2 selectively catalyzes ethanol dehydration to diethyl ether in addition to other higher oxygenates formation through forming new C-C bonds. Basic MgO selectively catalyzes ethanol dehydrogenation to acetaldehyde in addition to forming butanol and ethyl ester.

Lower reaction temperature shifts the ethanol dehydrogenation selectivity from ethylene to diethyl ether while co-feeding acetaldehyde significantly shifts selectivity towards Guerbet products. Guerbet product selectivity was the lowest on Al_2O_3 due to the competing alcohol etherification at 483 K while MgO rapidly lost its activity at temperatures less than 633 K. Amphoteric TiO_2 was able to selectively catalyze C-C formation at 503 K while maintaining its activity during operation. It can be concluded that both strong surface acidity and basicity are undesired catalyst properties that need to be minimized to minimize alcohol dehydration and esterification respectively. Attenuating the catalyst basicity can hinder the alcohol dehydrogenation to aldehydes, which were found to be the reactive intermediate in the C-C bond formation reaction. The C_4 product distribution along with the need for acetaldehyde to form Guerbet products on both Al_2O_3 and TiO_2 suggest that there is no direct ethanol coupling occurring on these two surfaces and the formation of the higher oxygenates is mainly through acetaldehyde aldol condensation. Only MgO exhibits two parallel mechanisms for the formation of C-C bonds either through acetaldehyde self-coupling or through ethanol reaction with acetaldehyde. To validate this mechanism versus other proposed mechanisms for Guerbet reaction, mechanistic studies are done on the three oxides by

varying acetaldehyde, ethanol, hydrogen, and water pressure, keeping all the other reaction conditions constant. The results of these studies are reported in the next chapter.

2.5. Figures and Tables

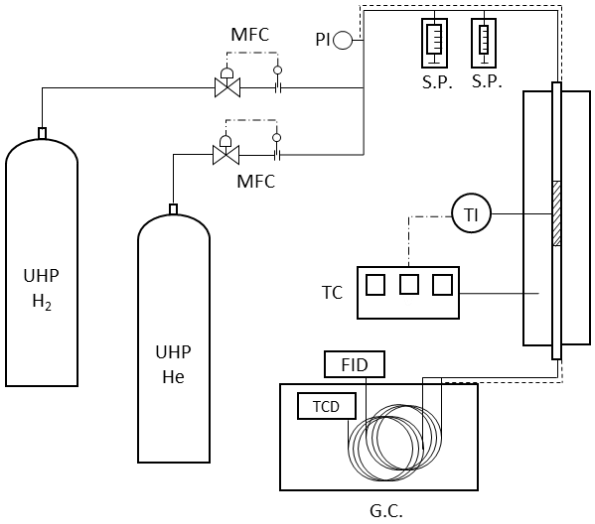

Figure 2. Reactor setup for catalytic formation of new C-C bonds via the Guerbet reaction. MFC: Mass Flow Controller, PI: Pressure Indicator, S.P.: Syringe Pump, TC: Temperature Controller, TI: Temperature Indicator, FID: Flame Ionization Detector, TCD: Thermal Conductivity Detector, GC: Gas Chromatography. Dashed line: heat traced tubes, dotted line: electronic signal

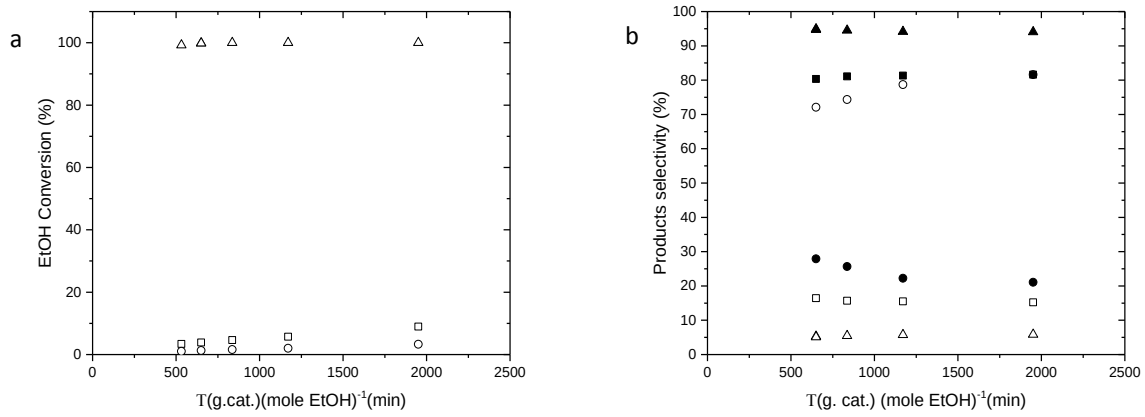

Figure 3 (a). Ethanol conversion at variable residence time on MgO (○), TiO_2 (□), and Al_2O_3 (Δ) at 3 kPa EtOH, 60 kPa H_2, bal. He, and 633 K reaction temperature. **(b).** Dehydrogenation + C-C coupling products selectivity (empty symbols) and dehydration products selectivity (filled symbols) as function of residence time on MgO (○), TiO_2 (□), and Al_2O_3 (Δ) at 3 kPa EtOH, 60 kPa H_2, bal. He, and 633 K reaction temperature

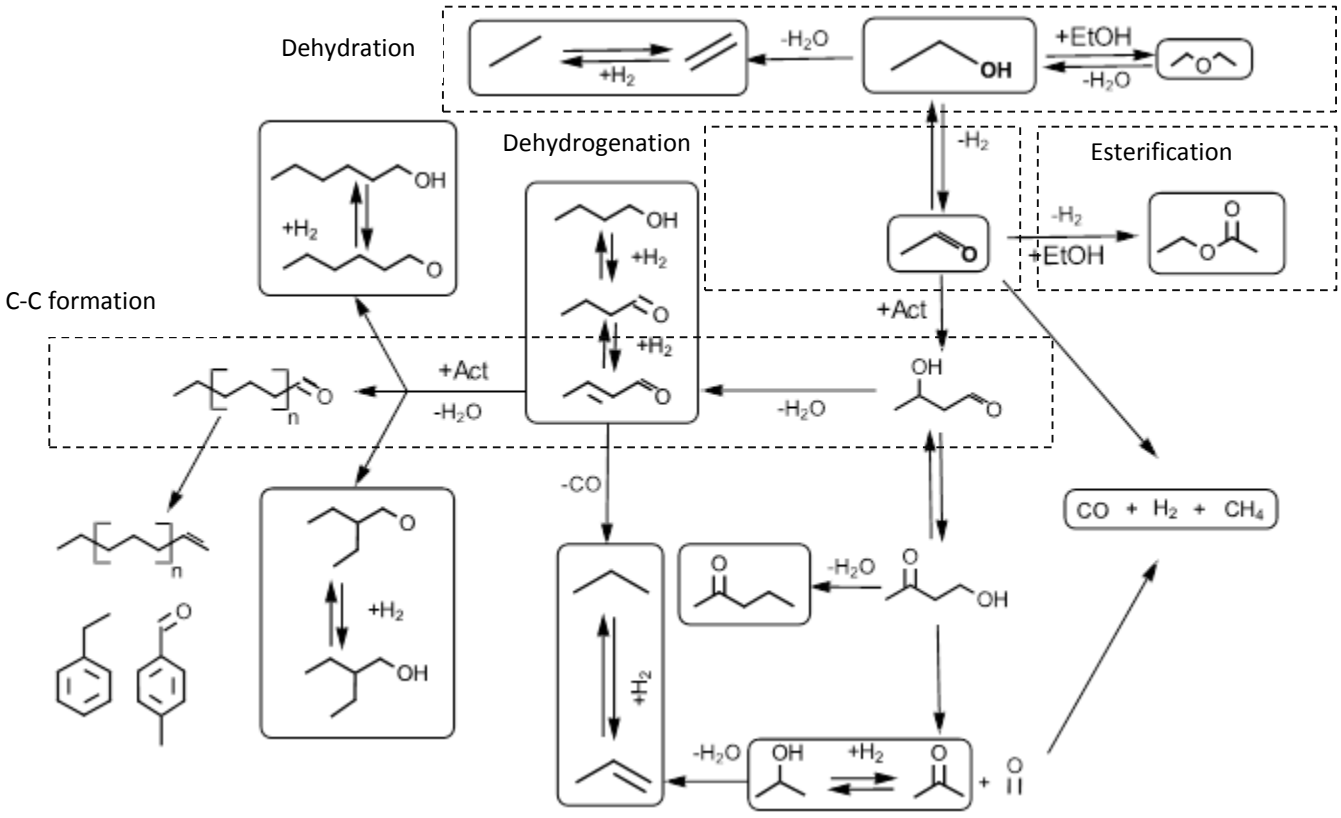

Figure 4. Ethanol reaction pathways on metal oxide surfaces

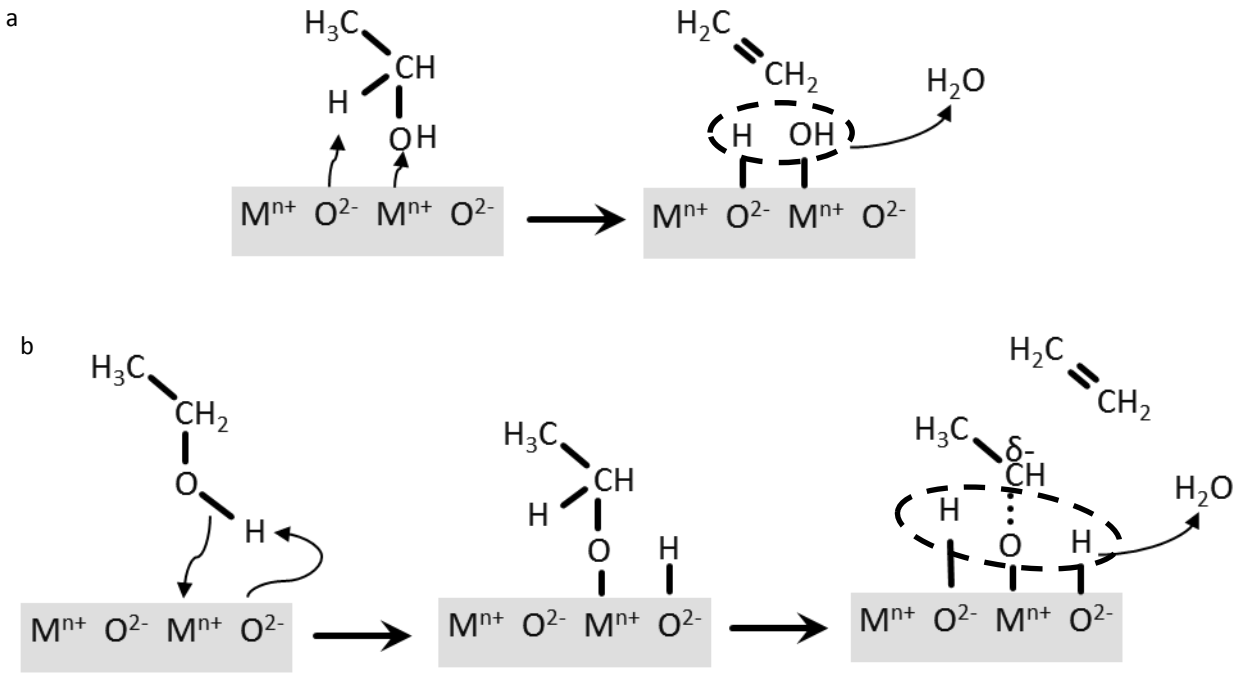

Figure 5 (a). Alcohol dehydration to olefin on metal oxides through E_2 elimination**. (b).** Alcohol dehydration to olefin on metal oxides through E_{1CB} elimination

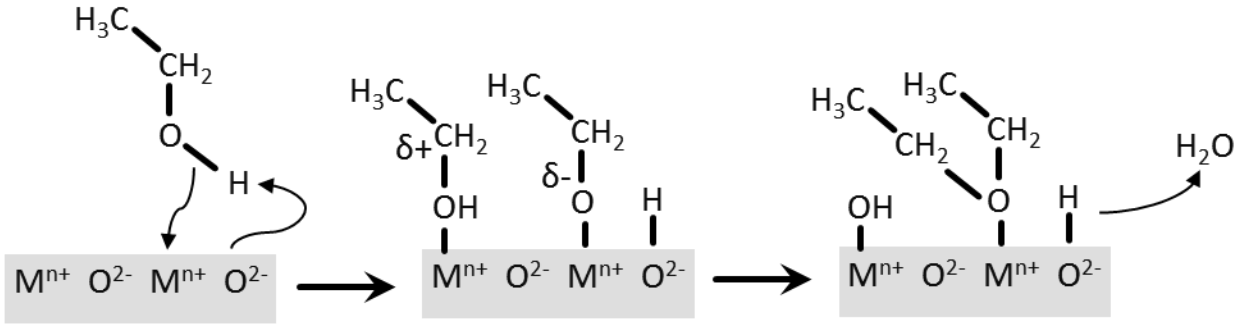

Figure 6. Alcohol bimolecular dehydration to ether on metal oxides

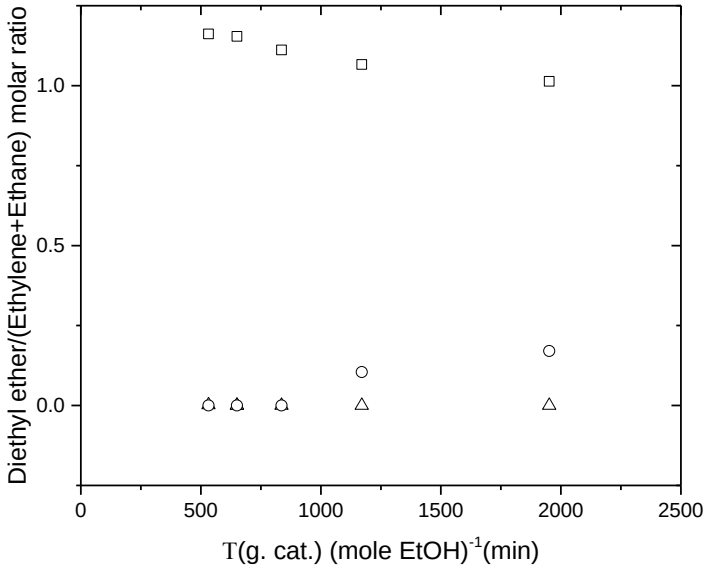

Figure 7. Diethyl ether to ethane + ethylene ratio on MgO (○), TiO_2 (□), and Al_2O_3 (Δ) at 3 kPa EtOH, 60 kPa H_2, bal. He, and 633 K reaction temperature

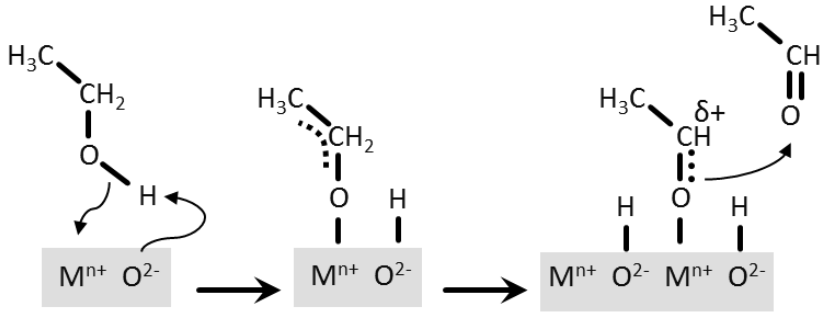

Figure 8. Alcohol dehydrogenation to aldehyde on metal oxides

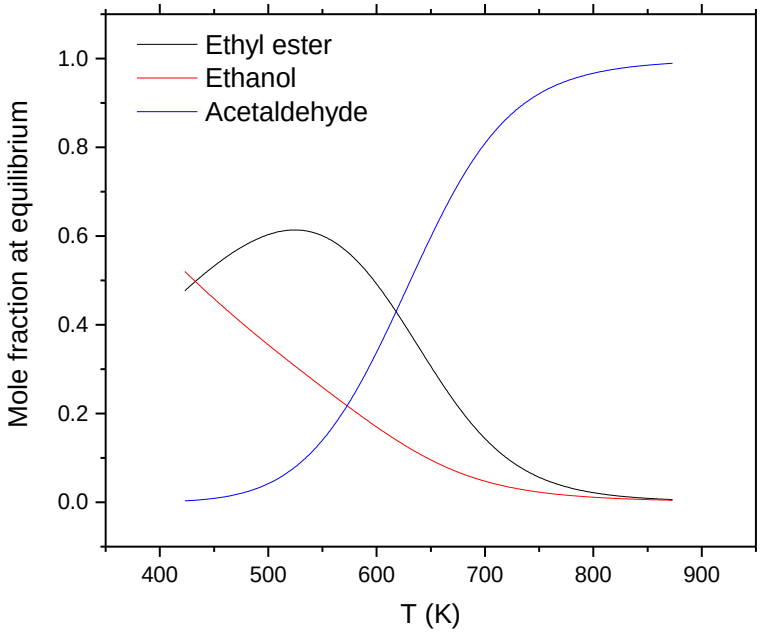

Figure 9. Ethanol dehydrogenation equilibrium products mole fraction at 101.3 kPa

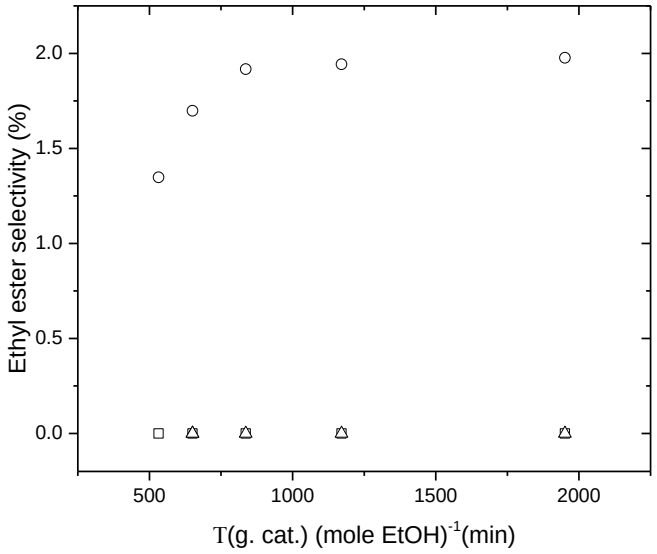

Figure 10. Ethanol esterification selectivity on MgO (○), TiO_2 (□), and Al_2O_3 (Δ) at 3 kPa EtOH, 60 kPa H_2, bal. He, and 633 K reaction temperature

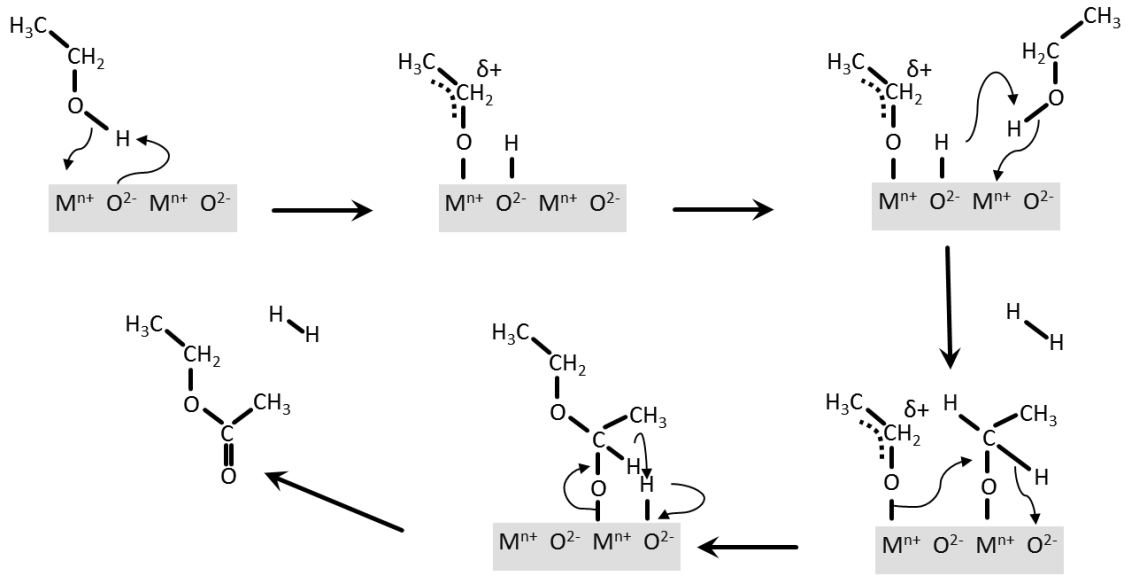

Figure 11. Alcohol bimolecular dehydrogenation to ester on metal oxides

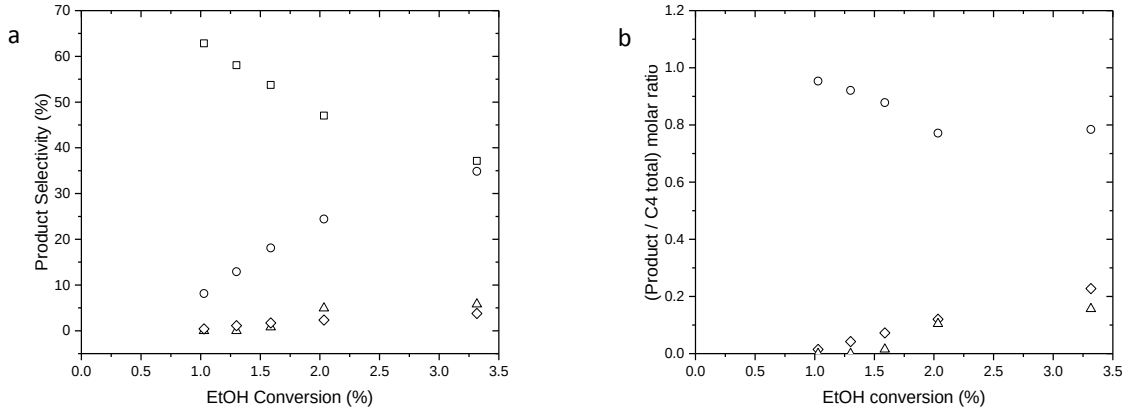

Figure 12 (a). Acetaldehyde (□), n-butanol (○), C_4 aldehydes (Δ), and C_4 hydrocarbons (◊) selectivity on 100 mg MgO as function of conversion at 3 kPa EtOH, 60 kPa H_2, bal. He, and 633 K reaction temperature. **(b).** n-butanol (○), C_4 aldehydes (Δ), and C_4 hydrocarbons (◊) Guerbet products relative mole ratio on 100 mg MgO as function of conversion at 3 kPa EtOH, 60 kPa H_2, bal. He, and 633 K reaction temperature

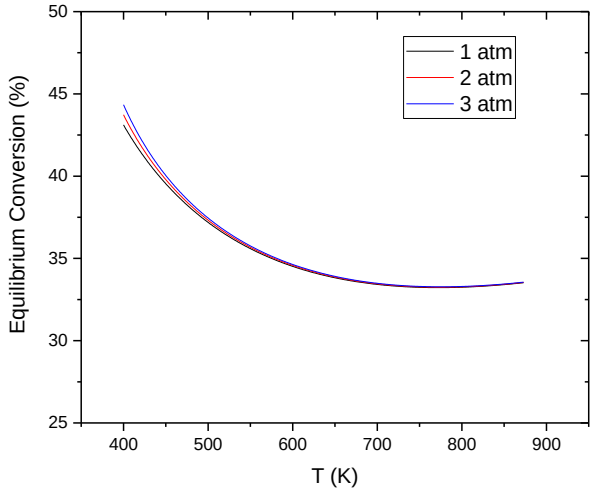

Figure 13. Acetaldehyde equilibrium molar conversion to crotonaldehyde at different pressures

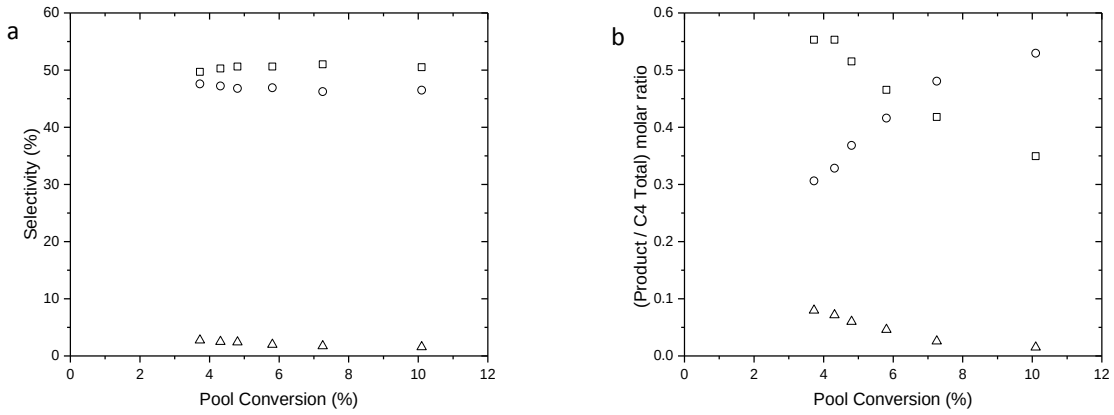

Figure 14 (a). Diethyl ether (□), ethyl ester (Δ), C-C coupling products (○) on 100 mg Al_2O_3 as function of feed pool conversion at 3 kPa EtOH, 0.4 kPa acetaldehyde, 60 kPa H_2, bal. He, and 483 K. **(b).** Butyraldehyde (□), crotonaldehyde (Δ), and n-butanol (○) Guerbet products relative mole ratio on 100 mg Al_2O_3 as function of feed pool conversion at 3 kPa EtOH, 0.4 kPa acetaldehyde, 60 kPa H_2, bal. He, and 483 K reaction temperature

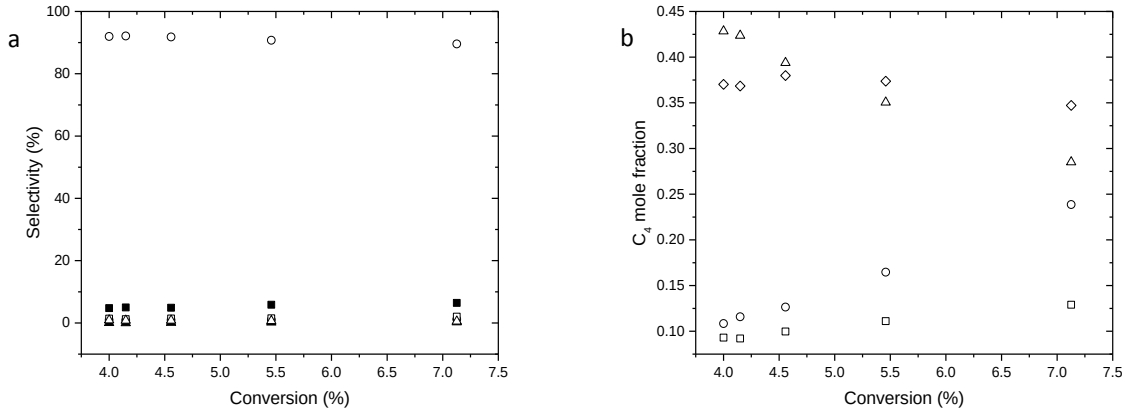

Figure 15 (a). Methane (▲), ketones(■), ethylene + ethane (●), diethyl ether (□), ethyl ester (Δ), C-C coupling products (○) on 100 mg MgO as function of feed pool conversion at 3 kPa EtOH, 0.4 kPa acetaldehyde, 60 kPa H_2, bal. He, and 633 K reaction temperature. **(b).** Crotyl alcohol (◊), butyraldehyde (□), crotonaldehyde (Δ), n-butanol (○) on 100 mg MgO as function of feed pool conversion at 3 kPa EtOH, 0.4 kPa acetaldehyde, 60 kPa H_2, bal. He, and 633 K reaction temperature

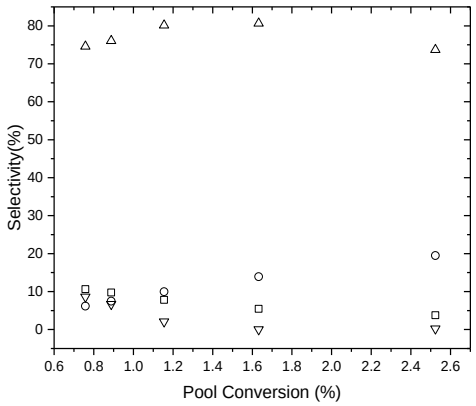

Figure 16. Crotonaldehyde (Δ), butyraldehyde (○), ethyl acetate (□), and C_{6+} aldehydes (◊) on 200 mg TiO_2 as function of feed pool conversion at 3 kPa EtOH, 0.4 kPa acetaldehyde, 60 kPa H_2, bal. He, and 503 K reaction temperature

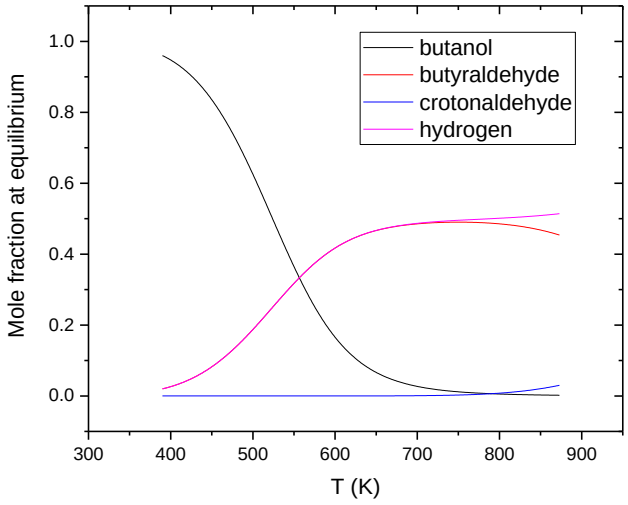

Figure 17. C_4 oxygenates thermodynamic equilibrium molar distribution

Table 2. Catalysts BET surface area and crystalline phase

Catalyst	BET surface area (m^2g^{-1})	Crystalline phase
Al_2O_3	125	gamma
TiO_2	11	anatase
MgO	140	periclase

Chapter 3: Mechanistic Study of C-C Bonds Formation via the Guerbet Reaction

3.1. Introduction

Formation of long chain branched alcohols through Guerbet reaction is widely applied as a pathway for synthesizing specialty chemicals with certain liquidity and hydrophobicity properties.[20,21] The plasticizer 2-ethyl-hexanol, for example, is produced through the Guerbet reaction of butanol. Guerbet alcohols in the range of C_{12} to C_{30} are also lubricants and raw materials in the personal care products industry. In recent years, Guerbet reaction received increased attention due to its potential usage as a pathway for upgrading the short chain oxygenates produced from the biomass fermentation.[121,124]

Ethanol is the simplest alcohol that can undergo self-coupling in Guerbet reaction due to harboring acidic hydrogen in the α position and at the same time can be efficiently produced from the biological depolymerization of biomass containing lignocellulose. These ethanol characteristics make ethanol a promising intermediate in biomass conversion to liquid fuels such as gasoline, kerosene and jet fuel in addition to other commodity chemicals such as butadiene, benzene, and xylenes.

Several studies investigated the ethanol Guerbet reaction mechanism and required catalyst properties. Through intermediate species identification and isotopic labelled experiments, it is widely believed that Guerbet reaction is a multi-step reaction[22,59] in which the reactant primary alcohol is first dehydrogenated to the corresponding aldehyde which couples with another aldehyde in a C-C bond formation aldol condensation reaction (route I in Figure 18) to form the aldol intermediate.[16,21,28,33,45,58,125] Under typical reaction conditions, the formed aldol is readily dehydrated to the unsaturated longer chain aldehyde that can be hydrogenated to the saturated aldehyde and alcohols. Alternative mechanisms were also proposed that involve the direct bimolecular condensation of two alcohol molecules[57,60,88,113,115,126,127] (route II in Figure 18) or one alcohol molecule with an aldehyde molecule[44,60,127] (route III in Figure 18). Some studies reported that it is possible to have more than one of these mechanisms occurring at the same time but it is still not clear how changing catalyst acid-base properties affects the identity of the prevailing

mechanism leading to C-C formation on a catalyst. Moreover, the rate determining step in the C-C bond formation through Guerbet chemistry on heterogeneous catalysts is not well defined either.[88]

In this chapter, we investigate the reaction of ethanol-acetaldehyde mixture on the highly basic MgO, the highly acidic gamma Al_2O_3, and the amphoteric anatase TiO_2 to elucidate the effect of changing acid-base properties on the prevailing mechanism(s) that leads to the formation of the new C-C bonds on metal oxides. Two parallel mechanisms are found to lead to new C-C formation on MgO through acetaldehyde self aldolization and acetaldehyde reaction with ethanol. A second order dependence on acetaldehyde pressure and a negative order on ethanol pressure were measured on the three oxides at acetaldehyde pressure > 0.3 kPa suggesting the C-C bonds are formed between two aldehydes in aldol condensation mechanism while ethanol act as inhibitor blocking the active sites for this reaction on Al_2O_3 and TiO_2.

Ethanol dehydrogenation to acetaldehyde is the rate limiting when started from ethanol on weakly or mildly basic oxides while product desorption is the rate limiting when starting from acetaldehyde. Strong basic sites are required for alcohols dehydrogenation while moderate strength acid-base sites are required for aldol condensation to proceed. Strong basic sites favor the cross aldolization of products, increase the product degree of branching, and harm catalyst stability.

Increasing acetaldehyde to ethanol ratio increases the Guerbet products selectivity on the three oxides in expense of dehydration and esterification products selectivity. Hydrogen pressure was found to have no direct effect on Guerbet activity on MgO and Al_2O_3 but decreases reaction rate on TiO_2 due to surface reduction. Water was found to deactivate MgO at temperatures lower than 663 K due to surface hydration but enhances catalyst activity at higher temperatures possibly due to the formation of surface hydroxyl groups. A similar enhancement in rate was also observed on TiO_2 either due to the formation of surface hydroxyl groups or healing oxygen vacancies. Water was found to reversibly inhibit Guerbet reaction and dehydration on Al_2O_3 where the inhibiting effect on dehydration was more significant leading to an increase in Guerbet products selectivity on this material.

The findings from this chapter provide better understanding of the optimum catalyst acid-base properties for selective Guerbet reaction and give guidance on how to optimize process conditions as well. It also poses new questions for future research regarding interaction of oxygenates with acid-base surfaces where expertise in DFT, in situ surface characterization, and kinetic measurements are needed.

3.2. Materials and Methods

3.2.1. Catalysts Preparation

Magnesium oxide (MgO, Aldrich, 99.995%), titanium oxide (TiO_2, Aldrich, 99.8%), aluminum oxide (Al_2O_3, Aldrich, >99.9%) were washed with deionized water (17.9 MΩ resistivity), dried in static air at 343 K overnight, then treated in flowing dry air (S.J. Smith, Ultra Zero) by heating to 773 K at 3 K min^{-1} and holding for 8 h. Samples were cooled down to room temperature, pelletized, and sieved to size range of 35-60 mesh.

3.2.2. Catalysts Characterization

BET surface area was measured by Micromeritics® using multipoint N_2 physisorption at 77 K. Prior to experiment, samples were outgassed at 673 K for 2 h in helium. Measured surface areas are reported in Table 2. The crystal phase of catalysts was determined using X-ray diffraction XRD (Bruker D-5000, Cu K- α radiation) and data is reported in Table 2.

3.2.3. Conversion, Selectivity, and Turnover Rate Measurements

Reaction rates were measured using a quartz tubular reactor (0.5 in. o.d.) with plug flow hydrodynamics, which is contained within a three-zone electrically heated furnace (Applied Test Systems) controlled using an electronic PID controller (Watlow, EZ-Zone®) as described in Figure 2. The bed temperature was measured with a type K thermocouple touching the outer surface of the tube at the catalyst bed position. Catalysts were mixed with additional quartz (SiO_2,

Supelco, analytical grade) to optimize reactant mixing with catalyst. Inertness of the quartz powder was tested at 633 K and no measurable reactions were observed.

Prior to the experiment, catalyst was in-situ treated in 30 kPa H_2 (S.J. Smith, 99.99%), 71 kPa He (S.J. Smith, 99.99%) flowing at 200 cm^3 min^{-1} for 1 h at 773 K then cooled down to the experiment temperature. All pretreatments and experiments were done at ambient pressure. The volumetric flow rates of gaseous feed components were controlled using calibrated mass flow controllers (Parker, MFC 600) while liquid components; ethanol (Decon, 200 Proof), acetaldehyde (Sigma Aldrich, 99.5%), acetaldol (Fisher), and deionized water were injected using two programmable syringe pumps (KD Scientific, Legato 110). Liquid feeds were injected to heated transfer lines by means of heat tape set at 393 K while reactor effluent lines were kept heated at 473 K to prevent high boiling point components condensation.

Reactor effluent was cooled and bubbled in ethanol to capture liquid products and injected to an offline gas chromatography coupled with a mass spectrometer (Shimadzu, 2010 GC-MS) to identify the formed products. The quantitative analysis was determined using an online gas chromatography (Agilent, HP 6890) equipped with a capillary column (Agilent, J&W HP-PLOT Q, L = 30 m, ID = 0.32 mm, film thickness = 20µm) connected to a flame ionization detector (FID) to detect hydrocarbons and oxygenates and a packed column (Restek, HayeSep Q, L = 2m, ID = 2 mm) connected to a thermal conductivity detector (TCD) to detect H_2, CO, CO_2, and H_2O.

The retention time for each component was determined by injecting prepared standard solutions of the following liquid chemicals in ethanol; 2-butanone (Supelco, analytical standard), 2-ethyl-1-hexanol (Fluka, analytical standard), 2-ethyl-1-butanol (Aldrich, 98%), 2-ethyl-2-hexenal (Aldrich^{CPR}), butyraldehyde (Fluka, 99%), butanol (Fisher, ACS grade), octanol (Alfa Aesar, 99%), hexanol (Sigma Aldrich, 98%), crotyl alcohol (Aldrich, 96%), hexanal (Aldrich, 98%), crotonaldehyde (Aldrich, 99%), acetone (Macron, ACS grade), Acetic acid (J.T. Baker, ACS grade). Retention time calibration for gaseous products were done by injecting gas mixture standards (Supelco, analytical standard) containing carbon monoxide, carbon dioxide, methane, ethane, ethylene, acetylene (1w/w% in N_2), propane, propylene, and butane (15 ppm in N_2).

Turnover rates were measured under differential conditions (<10% reactant conversion) to minimize the effect of reactant depletion on measured rates. Turnover rates are reported as moles of ethanol converted per minute per meter square surface area of the catalyst while selectivity is defined as following:

$$Product\ Selectivity(\%) = \frac{mole\ ethanol\ converted\ to\ product}{moles\ ethanol\ converted} X\ 100$$

3.3. Results and Discussion

3.3.1. Effect of Acetaldehyde Pressure on C-C Formation Rate

To investigate the effect of changing acetaldehyde partial pressure on C-C formation rates, the feed acetaldehyde pressure was varied while keeping ethanol pressure constant. The C-C formation rate was observed to be proportional to the acetaldehyde partial pressure on Al_2O_3, MgO, and, TiO_2 as shown in Figure 19. Nonlinear data regression reveals that the overall C-C formation rate reflects a second order dependence on acetaldehyde pressure on the three materials as indicated in Table 3.

Only route I in Figure 18 matches with a second order power on acetaldehyde pressure and hence it is proposed to be the predominant mechanism for C-C formation on the three oxides in presence of acetaldehyde at the experiment reaction conditions. Acidic and amphoteric oxides show poor activity towards ethanol dehydrogenation to acetaldehyde which explains why these oxides are inactive towards Guerbet reaction when acetaldehyde is not co-fed as shown in the previous chapter while basic oxides, on the other hand, can catalyze both reaction as described in section 2.3.1.3. The reported overall C-C formation rate includes crotonaldehyde, butyraldehyde, crotyl alcohols, butanol and other C_{6+} oxygenates. The presence of crotonaldehyde in the reaction products from the three oxides is an additional evidence that route I is the prevailing pathway for this reaction as explained in the proposed reaction elementary steps scheme for formation of butanol from ethanol in Figure 20. The following section discusses each of the elementary steps proposed in Figure 20.

Step (1) is the dissociative adsorption of ethanol which occurs easily on metal oxides at low temperatures[90,91,97,128,129] as demonstrated by the formation of alkoxides of several alcohols including ethanol. Step (2) is the deprotonation of ethoxide to from acetaldehyde which occurs at much higher temperatures compared to step (1)[91] due to its high activation barrier.[31] Step (2) requires strong basic sites to allow the abstraction of a proton from the stable ethoxide.[59,111] This explains why this step appears to be slow on Al_2O_3 and TiO_2 since no acetaldehyde is formed from ethanol on these surfaces at their reaction temperatures while MgO is only oxide able to form acetaldehyde at much higher temperatures as shown in the previous chapter.

The adsorption of carbonyl containing components, including aldehydes, on metal oxides is mainly through the interaction between the basic carbonyl oxygen and surface Lewis acid site.[30,86,130] From this it can be concluded that the availability of the acid sites is critical for C-C formation reaction since they provide the adsorbing sites required to stabilize the reactive intermidiates.[131] The equilibrium position of step (3), which is acetaldehyde desorption, highly depends on the acid sites strength.[59] The adsorbed aldehyde carbonyl group becomes polarized on the surface were the oxygen atom harbors a partial negative charge due to the electron donation by the surface acid site while the carbon atom harbors a partial positive charge as shown in Figure 21.

Step (4) is the recombinative desorption of atomic hydrogen to form molecular gaseous hydrogen. Despite the fact that it is not directly related to the formation of the C-C bonds, the speed of this step can affect the C-C formation rate as it sets the rate at which the basic sites are regenerated[54,115] and hence their abundance at any time under reaction conditions. The necessity of the basic sites to C-C formation was proven by Rode et al.[63] and Zhang et al.[111] where a decrease in butyraldehyde aldol condensation was noticed when the acidic carbon dioxide was co-fed during reaction or pre-adsorbed on the catalyst respectively. The higher C-C formation activity of hydroxyapatite compared to MgO was attributed to the shorter distance between basic sites on hydroxyapatite which allowed adsorbed hydrogen to recombine and desorb to the gas phase instead of being trapped on the isolated basic sites on MgO.[132] Another route for how the stability of hydrogen adsorption on surface oxygen affects C-C formation rate can be derived from the mechanism proposed by Singh et al.[133] where the C-C bonds are formed between enolate adsorbed on Lewis

acid sites and aldehyde adsorbed on Brønsted acid sites. The higher the stability of the adsorbed proton on the surface oxygen, the higher the density of the active Brønsted acid sites in this case.

It is worth mentioning here that basic sites coverage should theoretically depend on the hydrogen pressure in the gas phase, a hypothesis that is studies in section 3.3.5 of this chapter. In addition to the proposed of hydrogen dissociation on basic oxygen sites, an alternative hydrogen adsorption configuration is possible on metal oxides through the heterolytic dissociation to form a metal hydride and a hydroxyl group as reported for MgO,[27] however, this configuration is excluded from the proposed mechanism for the sake of simplicity.

Step (5) is the deprotonation of the adsorbed aldehyde to form enolate (carbanion intermediate) which harbors a negative charge on the α carbon.[54,119,123,132,134,135] Step (5) is, in principle, similar to step (2) in terms of the need to strong basic sites, however, the enolate formation from aldehyde has less activation barrier than that of the aldehyde formation from the alkoxide[39,99,136] possibly due to the difference in transition state energy in these two steps. The formed enolate is expected to be more stable on the surface compared to the parent aldehyde due to the double bond resonance, a hypothesis that is verified by TPD of adsorbed acetaldehyde on CeOx.[119] In addition, the act of the acid-base pairs was found to lower the energy barrier for abstraction of α hydrogen from carbonyl components as well.[27,63,84,123,130,131,137]

Since C-C formation reaction was found to proceed on MgO as well as Al_2O_3 and TiO_2 when acetaldehyde is co-fed, it is reasonable to propose that it requires the act of both acid and base sites as indicated by other studies. Mg cations on MgO surface are weak acids though and are not expected to participate in this reaction so it is possible that the more acidic under-coordinated Mg^{2+} sites play an important role in this step and hence, maximizing their surface density through increasing surface defects can positively affect the C-C formation as demonstrated in other studies.[47,130,138] In general, it can be concluded that oxides with stronger acid sites, high reducibility, and easier acid sites accessibility are more active for step (5).[119]

Step (5) was proposed by Zhang et al.[111] and Tsuji et al.[106] as the rate determining step in butyraldehyde self-condensation on metal oxides at 273 K, a hypothesis that was merely based on

comparison of activity of catalysts towards aldehyde versus ketone aldol condensation without preforming detailed kinetics measurement. This hypothesis does not align with the second order power dependence reported in this study for acetaldehyde since having step (5) as the rate limiting should lead to a first order power dependence instead. Moreover, later studies that came after Zhang's using TPD reported that this step occurred spontaneously on metal oxides surfaces at lower temperatures than that at which the C-C bond was formed.[119] Another DFT study reported that the activation barrier for this step is as low as 8.7 kcal.mole^{-1} on MgO[130] which is expected to be lower than that of the desorption energy of the formed crotonaldehyde which suggests that this step is not the rate limiting. Another liquid phase, acid catalyzed, acetaldehyde aldol condensation study reported a first order dependence on acetaldehyde concentration, a conclusion that was found to be based on an artifact resulting from the formation of acetaldehyde oligomers and was corrected later to a second order power dependence.[139]

It is worth mentioning here that the formation of aldehydes oligomers is common[30,140] but rarely reported in aldehydes reactive studies. In this study, the oligomer paraldehyde was detected using the GC-MS in a very small quantities compared to other products. The concentration of this oligomer was found to increase with time during the acetaldehyde-ethanol co-feed experiments. To isolate the effect of spontaneous oligomerization in feed solution, the GC method was designed to separate the new C-O bonds containing oligomers from the new C-C bonds containing aldol condensation products and the measured rates of C-C bonds formation were found not be affected by the feed solution age. The effect of oligomers presence on the surface coverage is expected not to be significant anyway since these oligomers spontaneously dissociate on the surface to the acetaldehyde monomer as verified by DFT calculations.[140]

Step (6) is the actual C-C bond formation which occurs between the negatively charged α carbon of the enolate and an adjacent positively charged carbonyl carbon of an adsorbed aldehyde through columbic interaction as shown in Figure 21. Step (6) is expected to depend on the polarization power of the Lewis acid site,[76,141] the stronger the acid site, the stronger the positive charged formed on the carbonyl carbon. The rate of the C-C bond formation is also expected to depend on the proximity of the adsorbates on the surface,[119] and the ratio of the aldehydes to enolate. Further

research is required to elucidate the effect of these factors on the C-C formation on metal oxides where model surfaces with well-defined structures can play a vital role in this area of research.

Since a second order power is measured for the formation of C-C bonds on the tested oxides, it is reasonable to propose that when starting from acetaldehyde, the rate determining step is step (6) or a subsequent step in the proposed mechanism similar to that suggested by Stefanov et al.[140] on TiO_2, and Marcu et al.[142] on Cu-Mg-Al mixed oxide. FTIR study of aldol condensation on TiO_2[133] showed that the C-C bonds can be formed at sub-ambient temperatures suggesting that step (6) is not the rate determining leaving step (7) to (9) to be the possible rate determining.

Step (7) is the protonation of the bidentate adsorbing adduct formed from the C-C coupling reaction. It is, in principle, opposite to step (1) where a proton and a carbonyl oxygen recombine to form a hydroxyl group. The main difference in this case is that the surface bidentate reacting in step (7) is less stable than that of the alkoxide formed in step (1) as demonstrated by the formation of the acetaldol on TiO_2 at temperature as low as 250 K.[133] This high instability can be attributed to the effect of the other adsorbing carbonyl functional on the molecule which lowers the activation barrier for step (7). Computational methods can verify the difference in activation barrier between this step and other possible rate determining steps.

Step (8) is similar to alcohol dehydration by E_2 elimination mechanism described in section 2.3.1.1. Such a step is expected to proceed with higher rates on metal oxides with higher acidity but it can still proceed with weak acidity since the dehydration of the acetaldol is significantly easier than that of the primary alcohols. This ease of aldol dehydration is attributed to the large difference in energy between the aldol reactant and the α, β unsaturated aldehyde product which is stabilized by the act of the conjugate C=C and C=O double bonds. When Co-fed with ethanol in absence of acetaldehyde on the three materials at their reaction conditions, acetaldol completely decomposed to acetaldehyde and C_4 oxygenates confirming its rapid decomposition. A similar conclusion regarding the rapid decomposition of the acetaldol at temperature as low as 273 K was reported by Singh et al.[133] on TiO_2, and by Jeong et al.[61] on aluminiophosphates as detected by FTIR. This high instability of acetaldol explains why it does not show up as a primary product

when acetaldehyde is co-fed at reaction conditions on the three oxides and makes it less likely that step (8) is the rate limiting.

Steps (9 and 11) are desorption of the unsaturated and saturated aldehydes respectively. Both steps are similar to step (3) in terms of the dependence of adsorbate stability on the acid sites strength. The main difference between steps (9) and (11) is the strength of the bond formed between the basic carbonyl oxygen in the two aldehydes and the surface Lewis acid site. Stefanov et al.[140] reported a fairly high binding energy (-83 kJ.mole^{-1}) of crotonaldehyde on TiO_2 surface which is even higher than that reported for acetaldehyde (-78 kJ.mole^{-1}) on the same surface. TPD done by Rasko et al.[143] showed that acetaldehyde desorbed at lower temperature than that of crotonaldehyde as well. Variable temperature ^{13}C NMR done by Denmark et al.[144] revealed that the α,β unsaturated aldehyde is a stronger base compared to the corresponding saturated aldehyde with the same chain length.

This high stability of the crotonaldehyde is attributed to the stabilizing effect of the conjugation of the C=C and the C=O double bonds which is not the case in the saturated butyraldehyde or acetaldehyde both lacking C=C bonds. A similar increase in stability is expected for aldehydes containing aryl group in α positons such as p-tolualdehdye which can formed from the cyclization of C_8 aldehyde formed from the cross aldol reaction. In addition to the carbonyl basicity, aldehydes containing C=C bonds can bind to Lewis acid sites through C=C π* bonding as well, however, this binding strength is expected to be weaker than the carbonyl binding so its effect is thought not to be significant in adsorbate stability.

Based on the aforementioned arguments regarding acetaldehyde aldol condensation elementary steps, steps (3 to 9), it is reasonable to propose that step (9 or 11) is the rate limiting. To back this hypothesis, findings from different studies need to be put together. FTIR studies of acetaldehyde reaction on TiO_2 confirms the formation of surface crotonaldehyde at temperature as low as 273 K[133] while TPD of acetaldehyde on different facets of TiO_2 shows that crotonaldehyde is only detected at temperatures higher than 400 K[100,140,143] suggesting that the activation barrier of the crotonaldehyde desorption is higher than that of the earlier steps starting from the acetaldehyde and hence desorption is the rate determining step. Stefanov et al.[140] came to the same conclusion

regarding the reaction order and the rate determining step that we propose here when studied the reaction of acetaldehyde on TiO_2 using FTIR and DFT as well.

Hanspal et al.[59] reported that C-C formation activity was higher on stoichiometric hydroxyapatite compared to MgO which can be explained by the lower oxygenates desorption energy on the former material as reported in the same study. Additionally, aldol condensation of acetone, which is more difficult to be enolized compared to acetaldehyde, was found to be limited by product desorption not reactant enolization as demonstrated by studies of this reaction on Al_2O_3, TiO_2, ZrO_2 and CeO_2.[30,131] It is important to clarify here that step (9 or 11) is proposed as the rate determining step for acetaldehyde aldol condensation not ethanol Guerbet reaction to butanol since the later involves more steps that can potentially be higher in activation barrier than step (9). In fact findings from Chapter 1 of this study suggest that step (2) has higher activation barrier than step (9) on Al_2O_3, and TiO_2.

Step (10) is the hydrogenation of the crotonaldehyde to butyraldehyde and is expected to depend on the ability of the basic sites to donate the hydrogen required for saturation. It is worth mentioning here that the equilibrium position of this reaction is highly skewed towards butyraldehyde as shown in Figure 17 and should theoretically allow a complete hydrogenation of the crotonaldehyde to butyraldehyde. The fact that crotonaldehyde exists as a measurable product on the three oxides suggests that the rate of crotonaldehyde formation is faster than that of its C=C double bond hydrogenation on metal oxides.

An alternative pathway for butanol formation from crotonaldehyde involves the hydrogenation of crotonaldehyde C=O bond to form crotyl alcohol, however, this pathway was excluded since the hydrogenation of the C=C is more thermodynamically favored compared to the hydrogenation of the C=O bonds[145] and no crotyl alcohol was detected on Al_2O_3 or TiO_2. This being said, measurable quantities of both cis- and trans- crotyl alcohols were detected in the product pool of MgO. It can be assumed that this difference in hydrogenation pathways is either due to the difference in reaction temperature or catalyst acid-base properties. At higher temperature, selectivity towards C=O bonds hydrogenation increases[71] which backs the first assumption. The second assumption is also in good agreement with the findings reported by Aramednia et al.[71] where acidic and amphoteric oxides

showed to be completely selective towards C=C bond hydrogenation while basic oxides showed to be more selective towards C=O hydrogenation of unsaturated aldehydes when an alcohol is present as a hydrogen donor.

This difference in selectivity was attributed to the change in α, β unsaturated aldehyde adsorption configuration based on the acid-base surface properties. Six adsorption configurations were proposed using theoretical methods for the α, β unsaturated aldehyde adsorption by Delbecq et al.[146]; three via C=O bond, two via C=C bond, and one via both C=C and C=O bonds. Another study by Aramednia et al.[147] using DRIFT showed that acidic oxides favor the adsorption configuration through the C=C bond leading to the C=C hydrogenation while basic oxides favor the C=O adsorption configurations leading to the hydrogenation of the C=O in addition to the C=C to some degree as well. These findings are in agreement with the high selectivity towards crotyl alcohol from the hydrogenation of crotonaldehyde on the mildly basic MgO mixed with B_2O_3 as reported by Ueshima et al.[148]

Whether hydrogenated to butyraldehyde or crotyl alcohol, the ultimate hydrogenation product of the two pathways is butanol. Step (12) is the hydrogenation of butyraldehyde to butanol and presented as the resultant of two elementary steps each involves the addition of one proton to the molecule in the opposite sequence of steps (1 and 2). The difference between step (12) and step (1 and 2) is the difference in activation barriers set by the relative stability of the alkoxide and the aldehyde on the surface. Since butanol was formed from butyraldehyde hydrogenation on Al_2O_3 but acetaldehyde was not formed from ethanol dehydrogenation on the same surface, it can be concluded that step (12) has lower activation barrier than that of step (2). Further computational studies are required to elucidate the relationship between the activation energy of alcohol hydrogenation - dehydrogenation and its carbon number on metal oxides.

It is worth mentioning here that out of the three main C_4 oxygenates (crotonaldehyde, butyraldehyde, and butanol), butyraldehyde is the only component that can undergo further C-C bond formation from both carbonyl and α carbon positions since it harbors both carbonyl functionality and acidic α hydrogen that can be abstracted to form the enolate. Crotonaldehyde, on the other hand, can only undergo aldol condensation with acetaldehyde to form C-C bond between

the crotonaldehyde carbonyl carbon and the acetaldehyde α carbon leading to the formation of sorbic aldehyde,[149,150] a highly unsaturated C_6 aldehyde that can further react to form benzene.[143,151-154] The degree of the polymerization and the product carbon number can possibly be controlled by setting the equilibrium conditions and catalyst hydrogenation activity to maximize or minimize the butyraldehyde pressure in the reaction medium depending on the desired products characteristics.

Assuming that the enolate formation, step (5), was really the rate limiting in the liquid phase reaction of butyraldehyde as proposed by Zhang et al[111], this does not directly contradict the conclusion from this study regarding step (9) being the rate limiting. Abstraction of α hydrogen from the adsorbed aliphatic aldehyde is expected to become more difficult as the aldehyde chain length increases[62] and hence it is possible that the activation barrier for formation of enolate from butyraldehyde is higher than that of the aldol condensation product desorption in this case, opposite to what is reported for acetaldehyde aldol condensation in this study. A separate study for the aldol condensation of butyraldehyde is required to verify this hypothesis where a first order dependence should be expected for the C-C formation versus butyraldehyde pressure in this case.

Despite that detailed investigation of the dependence of the rate determining step identity on the reactant chain length is not included in this study, a closer look on the trace amount of the C_6 aldehydes formed on TiO_2 at higher conversion (data not shown) shows that n-hexanal was formed at significantly higher ratio compared to 2-ethyl butyraldehyde (about 4:1 molar ratio). The former aldehyde is formed from the reaction of C_2 enolate with butyraldehyde while the later one is formed from the reaction of C_4 enolate with acetaldehyde. This difference in selectivity backs the hypothesis that the formation of enolate from butyraldehyde is more difficult than that from the acetaldehyde. This is also in agreement with the findings from Tichit et al.[62] where product selectivity from the longer chain aldehydes enolization was less than what is observed for the shorter chain aldehydes enolization.

This difference in enolization energy of aldehydes based on their chain length can be exploited to control the product degree of branching and carbon number by tuning the surface base properties. Qualitatively speaking, the ratio of the branched to linear C_{6+} aldehydes was generally higher on

MgO compared to that on TiO_2 which suggests that the discrimination in enolization of aldehydes based on their chain length diminishes as surface basicity increases. In case of acetaldehyde aldol condensation, products can potentially be kept selectively linear by reducing surface basicity of the catalyst and hence allow the step addition of C_2 enolates to the carbonyl carbon of the formed longer aldehydes. The advantage of forming linear products is that they are more resistant to dehydration and hence can undergo further C-C formation reactions. A similar argument was proposed by Tichit et al.[62] where the mildly basic Mg-Al mixed oxide was more selective to forming linear products from the reaction acetaldehyde with heptanal compared to the strongly basic MgO. Another study by Ordomsky et al.[30] suggested that stronger basic sites can make the enolization of butyraldehyde even easier than that of the acetaldehyde which can potential yield to a C-C formation rate run away as conversion goes on and a rapid increase in the product branching.

In addition to the difference in enolization-ability of aldehydes with different chain length, the surface coverage of the aldehydes is expected to change as aldehydes molecules get longer as well due to steric hindrance. While there is no detailed study that we are aware of that investigates how the adsorption configuration of aldehydes changes with surface acid-base properties, it is expected that a parallel or angled adsorption mode would be more favored due to the secondary interaction of the acid sites with the π^* bond of unsaturated aldehydes or due to the secondary interaction of the basic sites with the acidic α hydrogen of saturated aldehydes in addition to the primary interaction of the carbonyl oxygen with acid sites.[155] Such adsorption configurations can potentially hinder adsorption of other aldehydes on neighboring sites and hence lower the probability of C-C bonds formation. Rekoske et al.[90] reported that crotonaldehyde surface saturation coverage is 0.6 of that of acetaldehyde on TiO_2 which is in agreement with the proposed hypothesis regarding the hindered adsorption of long chain aldehydes.

3.3.2. Effect of Acetaldehyde Pressure on Side Reactions Rates

In addition to increasing the C-C formation rate, increasing the acetaldehyde pressure affected side reactions rates and hence the overall catalyst selectivity on the different oxides as shown in the next sections.

3.3.2.1. Al_2O_3

In addition to Guerbet products, diethyl ether and ethyl ester were also formed in measurable quantities from acetaldehyde-ethanol mixture reaction on Al_2O_3. As shown in Figure 22, the increase in acetaldehyde to ethanol ratio increased the catalyst selectivity to Guerbet products in expense of diethyl ether. This is in agreement with the etherification mechanism described in section 2.3.1.2 on Al_2O_3 where ethoxides, formed from ethanol dissociation on the surface, being the reactive intermediates while acetaldehyde does not play a positive role in the E_2 elimination reaction. Acetaldehyde can competitively adsorb on Al_2O_3 acid sites and decrease the surface coverage with ethoxides which explains the decrease in etherification rate and the negative power dependence shown for this reaction in Figure 22 and Table 4 respectively.

Unlike diethyl ether, ethyl ester formation selectivity increased with increasing acetaldehyde pressure on Al_2O_3 which is in agreement with the Tishchenko esterification reaction mechanism described in section 2.3.1.4 where ethanol dehydrogenation to acetaldehyde is the first step in this reaction followed by the formation of C-O bond between an adsorbed acetaldehyde and an ethoxide. At 483 K, no ethylene or C_4 hydrocarbons were formed, however, it is expected that at higher conversions, the dehydration of the formed higher alcohols and aldehydes through E_2 elimination mechanism will become more noticeable.

3.3.2.2. MgO

As discussed in section 2.3.1, feeding pure ethanol on MgO lead to butanol formation while Co-feeding acetaldehyde lead to the formation of other newly formed C-C bonds containing oxygenates including crotyl alcohols, crotonaldehyde, butyraldehyde, and C_{6+} aldehydes. It is worth mentioning here that once acetaldehyde was co-fed with ethanol, the rate of formation of butanol sharply increased and then decreased due to deactivation as shown in Figure 23. Upon cutting down the acetaldehyde feed pressure back to zero, no butanol was formed anymore as the surface strong sites were completely deactivated possibly by heavies formed from acetaldehyde reaction. In addition to the decrease in butanol formation rate, ethyl ester formation was also stopped due to deactivation suggesting that both reactions occur on the same sites. This

deactivation can be explained by the increase in conversion at high acetaldehyde pressure accompanied by the formation of non-volatile carbonaceous materials that deactivated the surface active sites.

This sort of rapid deactivation of MgO was reported under similar reaction conditions.[44-46] and explains why the C-C formation rate on this material is not significantly higher than that on the acidic or amphoteric oxides despite being tested at higher temperature and harboring stronger basic sites. Kinetics measurements under high acetaldehyde co-feed pressure were performed after reaching a new steady state during which deactivation effect became less obvious on the measured rates.

The proportional increase in the C-C formation rate with increasing acetaldehyde pressure was accompanied by a decrease in the ethanol dehydration rate to ethylene on MgO and an increase in ketonization rates as shown in Figure 24a. While acetaldehyde is the reactive intermediate in the C-C formation reactions, ethoxide, formed from ethanol dissociation on the surface, is the reactive intermediate in the ethanol dehydration by E_{1CB} elimination reaction on basic surfaces as shown in section 2.3.1.1. Since ethanol pressure was kept constant during the experiment, the decrease in dehydration rate, and the negative power dependence of dehydration rate on acetaldehyde pressure shown in Table 5, can be explained by the decrease in acid sites coverage by ethoxides due to the increase in the competitively adsorbing acetaldehyde pressure. Unlike dehydration, ketonization, involves acetaldehyde as a reactive intermediate as described in section 2.3.1.5 similar to Guerbet reaction. The main difference between ketonization and Guerbet reaction is that the increase in the ketonization rate reflects a semi first order dependence which explains why ketones selectivity was decreased in favor of Guerbet upon increasing acetaldehyde pressure as shown in Figure 24b.

3.3.2.3. TiO_2

The rate of formation and selectivity of Guerbet products on TiO_2 followed a similar increasing trend to that on MgO and Al_2O_3 with increasing acetaldehyde pressure as shown in Figure 25a and 25b. As in the case of Al_2O_3, selectivity to ethers was decreased at higher acetaldehyde pressure, however, unlike Al_2O_3, selectivity to esters was decreased as well. It is worth mentioning here that

while diethyl ether forms a significant portion of the product in the case of Al_2O_3, it forms a negligible portion of the product in case of TiO_2 when co-feeding acetaldehyde. The disappearance of diethyl ether from the product pool when co-feeding acetaldehyde can be explained by the decrease in surface coverage with ethoxides due to the competitive adsorption of the acetaldehyde and other formed aldehydes on the acid sites.

The increase in esterification selectivity was in expense of the decrease in etherification selectivity on Al_2O_3 while only Guerbet and esterification products are observed in quantitative amounts on TiO_2, increasing the acetaldehyde pressure increased the Guerbet selectivity in expense of the selectivity towards ethyl ester. Both Guerbet and esterification, involve acetaldehyde as a reactive intermediate as discussed in sections 2.3.1.4 and 2.3.3, however, their sensitivities towards the increase in acetaldehyde pressure is different. While Guerbet C-C formation rate showed a second order dependence on acetaldehyde pressure, esterification showed a first order dependence as shown in Table 6 since it involves the reaction of an adsorbed aldehydes with a surface ethoxide.

3.3.3. Effect of Ethanol Pressure on C-C Formation Rate

To investigate the role of ethanol in the reactions occurring on metal oxides and whether it participates directly in the formation of Guerbet products via parallel mechanisms to acetaldehyde aldolization or not, the C-C formation rate was measured at varying ethanol pressure keeping acetaldehyde pressure constant. To the best of our knowledge, this is the first experiment to study the effect of ethanol pressure independently from acetaldehyde on Guerbet reaction on metal oxides.

Interestingly, ethanol had an inhibiting effect on the formation of Guerbet products on the three oxides as shown in Figure 26. This can be explained by the strong adsorption of the stable ethoxides on the surface blocking the access of the aldehydes to the active sites and limiting their abundance at any time during the reaction. This inhibiting behavior by ethanol is an additional evidence that step (2) is the rate limiting in C-C formation from ethanol. As shown in Table 7, the degree of inhibition differs based on the catalyst used where TiO_2 exhibited the highest sensitivity towards inhibition by ethanol followed by Al_2O_3 and then MgO. The value of the measured

negative order is expected to change with reaction temperature, pressures of acetaldehyde and ethanol, and catalyst acid-base strength.

The effect of the acid-base properties on favoring the adsorption of the ethoxides versus the aldehyde is not well studied and further research is required including computational studies and TPD coupled with surface characterization techniques such as FTIR. It is expected that the stronger the acid sites become, the less discrimination in adsorption between acetaldehyde and alkoxide occurs which could explain why the inhibiting effect was higher on the less acidic TiO_2 compared to Al_2O_3. The low inhibition effect of ethanol on MgO can be explained by the presence of the direct C-C formation mechanism that involves the reaction of ethanol, or ethoxide, in addition to the acetaldehyde aldol addition. Taking a closer look at the individual components rates of formation at variable ethanol pressure and constant acetaldehyde pressure verifies the two parallel mechanisms explanation for the low inhibition effect of ethanol on MgO compared to the other two oxides.

As shown in Figure 27, rates of formation of C_4 aldehydes and higher oxygenates mainly formed by the aldol condensation pathway decreased with increasing ethanol pressure while the rate of formation of C_4 alcohols increased with ethanol pressure due to the promotion of the direct coupling route. At increasing ethanol pressure, the alcohols rate of formation reaches a maximum and then decreases due to the decrease in the overall rate of formation including both aldol condensation and direct condensation. The reason why alcohols rates are decreased at higher ethanol pressures is that the measured alcohols formation rate are the resultants of the two pathways, the direct condensation of ethanol and the hydrogenation of the aldehydes produced by the aldol condensation route. Ethanol pressure has opposite effect on the two routes and hence it is expected to see a maximal behavior of the alcohols rate of formation versus ethanol pressure.

To validate this hypothesis, the effect of ethanol pressure on C-C formation rate was measured in absence of acetaldehyde co-feed where the measured acetaldehyde pressure in the reactor effluent increased monotonically with increasing ethanol pressure in a first order manner. Since acetaldehyde pressure in the feed was kept as zero and the effluent acetaldehyde pressure is far from the equilibrium pressure, it is reasonable to assume that the average acetaldehyde pressure

across the bed increased monotonically with ethanol pressure as well. This being said, the measured C-C formation rate showed a first order increase with increasing ethanol, or bed average acetaldehyde, pressures as shown in Figure 28. This first order dependency on acetaldehyde pressure, at low acetaldehyde pressure (<0.1 kPa), is an evidence of the existence of a different mechanism from the second order aldol condensation mechanism measured at higher acetaldehyde pressure (>0.3 kPa) and reported in section 3.3.1.

This parallel mechanism at low acetaldehyde pressure is probably the reason behind the first order dependence on acetaldehyde pressure reported by Birky et al. for C-C formation reaction.[17] Chieregato et al.[127] proposed that which mechanism is predominant on MgO at any time depends on the relative ratio of surface aldehydes to enolates versus aldehydes to carbanions formed from deprotonation of the ethoxides methyl group. The higher the later ratio, the more prevailing the first order direct mechanism becomes. The formation of these carbanions is less likely to occur on Al_2O_3 and TiO_2 since it requires strong basic sites and hence the first order, acetaldehyde-carbanion coupling, is not expected to occur on these oxides.

A similar pseudo first order reaction was measured on TiO_2 when both acetaldehyde and ethanol pressures were increased monotonically together as shown in Figure 29. Since the dehydrogenation activity of TiO_2 is too low to produce acetaldehyde at reaction conditions, acetaldehyde-ethanol mixture was fed at variable pressure while maintaining the ratio between the two components pressures constant. This Pseudo first order should not be confused with that reported on MgO due to the direct condensation pathway, in case of TiO_2, the simultaneous increase in both acetaldehyde and ethanol pressures lead to a decrease in C-C formation rate order as the resultant effect of the second order response to the acetaldehyde and the negative higher than unity response to ethanol pressure as explained earlier.

It is worth noticing here that the negative, higher than unity in magnitude, order measured for the C-C formation reaction on TiO_2 at variable ethanol pressure confirms the need to have two surface adsorbing species to form the new C-C bonds in a Langmuir-Hinshelwood mechanism as proposed in the following equation:

$$\frac{r}{[L]} = \frac{kK\,(P_{acetaldehyde})^2}{(1+K_1P_{ethanol}+K_2P_{hydrogen}+K_3P_{acetaldehyde}+\cdots)^2}$$

Which is opposite to the C-C formation reaction through Eley-Rideal mechanism proposed by Chang et al.[153] on acidic Zeolites where a gas phase aldehyde reacts directly with another adsorbed one without the need for having both aldehydes adsorbed on the surface.

3.3.4. Effect of Ethanol Pressure on Products Selectivity

Increasing ethanol pressure while keeping acetaldehyde pressure constant affected ethanol dehydration, C-C formation, etherification, esterification, and ketonization differently. The following section describes how changing the ethanol pressures affected the selectivity of the three oxides.

Increasing feed ethanol to acetaldehyde pressure ratio on Al_2O_3 increased selectivity towards diethyl ether and ethyl ester in expense of C-C formation as shown in Figure 30. Since ethanol does not directly contribute to the aldol condensation reaction leading to C-C formation on Al_2O_3, no increase in the rate of this reaction is expected at higher ethanol pressure. In fact, increasing ethanol pressure decreases the C-C formation rate and increases the etherification rate by increasing the surface population of ethoxides and decrease surface population of acetaldehydes. The decrease in Guerbet products selectivity shown in Figure 30 is due to the effect of both increasing etherification rate and decreasing C-C formation rate. Since esterification involves the reaction of ethoxide with acetaldehyde, no significant change in esterification rate is expected from increasing ethanol pressure and the observed increase in ethyl ester selectivity is mainly due to the decrease in etherification rate.

Since two reaction mechanisms lead to the formation of C-C bonds from ethanol on MgO, two experiments were performed to study the effect of ethanol pressure on products selectivity; the first experiment was done with no acetaldehyde co-feed in which the only acetaldehyde present in reaction medium is the product of ethanol dehydrogenation while the other experiment is done with Co-feeding acetaldehyde to maximize the effect of the aldol condensation route. As shown in Figure 31a, at increasing ethanol pressure in absence of acetaldehyde in the feed, the selectivity to

C-C formation increased while the selectivity to acetaldehyde and ethylene decreased. As ethanol pressure was increased, the average acetaldehyde pressure across the catalyst bed increased as well. This increase in both acetaldehyde and ethanol lead to an increase in the C-C formation rate as described earlier. The decrease in acetaldehyde intermediate pressure at higher ethanol pressure suggests that the reaction of acetaldehyde to form C-C products is faster than the dehydrogenation of ethanol to acetaldehyde while the decrease in ethylene selectivity is due to the decrease in surface coverage ratio of ethoxide to aldehyde which is translated to an increase in the ratio of C-C formation rate to dehydration rate.

When co-feeding acetaldehyde with ethanol, Figure 31b, the effect of ethanol dehydrogenation on MgO becomes less significant as proved by the minimal change in the measured acetaldehyde pressure at reactor effluent at variable ethanol pressure. At such high acetaldehyde pressure (>0.3 kPa), rapid deactivation occurs to the catalyst as described in section 3.3.2.2 which explains the decrease in alcohol dehydrogenation rates and the disappearance of ethylene and ethyl ester from the product pool. Only C-C products and ketones are formed in this case, both groups of products are possibly formed through aldol condensation and the increase in ethanol pressure at constant acetaldehyde pressure did not seem to affect the selectivity to either products since both reaction rates responded in a similar manner.

The effect of increasing ethanol pressure on products selectivity on TiO_2 is shown in Figure 32. As ethanol pressure increases, C-C Guerbet products selectivity decreases in favor of ketones, diethyl ether, and ethyl ester selectivities. This can be explained by the inhibiting effect of ethanol on C-C formation due to the blockage of active surface sites by ethoxides. Ethoxides, on the other hand, are the active species for etherification and hence increasing ethanol pressure increases diethyl ether selectivity.

3.3.5. Effect of Hydrogen Pressure on C-C Formation Rate

Hydrogen pressure can potentially affect the C-C formation rate on metal oxides through Guerbet reaction through five mechanisms. The first mechanism is through affecting the ratio of ethanol to acetaldehyde by shifting the thermodynamic equilibrium towards higher ethanol to acetaldehyde

ratio and hence decrease the C-C formation rate. This effect becomes practically effective when operating close to equilibrium conditions which can only be achieved at high conversion, or high hydrogen to ethanol ratio. The second mechanism is through affecting the C_4 aldehydes to alcohols ratio by favoring hydrogenating of aldehydes to alcohols. The higher the C_4 aldehydes pressure in reaction medium, the higher the probability of forming new C-C bonds leading to C_{6+} oxygenates.

The third effect is through changing the surface coverage of active sites through adsorption of molecular hydrogen on basic oxygen sites to form surface hydroxyl groups and metal hydrides. The formation of metal hydrides can be described as a hard-soft acid-base interaction[156] which is weaker than the hard-hard acid-base interaction occurring between surface Lewis acids and alkoxides or aldehydes and hence no blocking of acid sites by hydrogen is expected. The formation of hydroxyl groups can lead to a decrease in the abundance of surface acid-base pairs required to deprotonate the adsorbed aldehydes and form the reactive enolates as described earlier. This step was proved not to be the rate determining step as discussed in section 3.3.1 and hence the effect of hydrogen on C-C formation rate through this mechanism is less likely. Opposite to this hypothesis, the formation of surface hydroxyl groups can have a positive effect on C-C formation on surfaces with low acidity since the hydroxyl groups themselves can act as additional acid sites.[133,157]

The fourth effect is through changing the surface acid sites oxidation state due to surface reduction. This can lead to creation of oxygen vacancies on the surface and loss of oxygen basic sites as described in Figure 33. In addition, the decrease in the conjugate metal sites oxidation state increases its Lewis acidity strength which has direct effect on the stability and polarization of adsorbed aldehydes, and hence the C-C formation rate. The fifth and last mechanisms at which hydrogen can affect C-C formation rate is through minimizing the formation of highly dehydrogenated carbonaceous species that can lead to coke formation on active sites.[158] This effect was reported on ZrO_2.under acetaldehyde aldol condensation conditions.[157]

Figure 34 shows the effect of changing hydrogen pressure on C-C formation rate on the three oxides at constant acetaldehyde and ethanol feed pressure where hydrogen pressure was increased while helium pressure was decreased. Changing hydrogen pressure had no effect on C-C formation

rates on both MgO and Al_2O_3 while it negatively affected the C-C formation rate on TiO_2. Acetaldehyde and ethanol pressures were set to keep the system away from dehydrogenation equilibrium and hence the effect of hydrogen on the ratio of acetaldehyde to ethanol pressures is negligible as demonstrated by the constant ethanol and acetaldehyde pressures measured at reactor effluent along the experiment. At reaction conditions, conversion is kept low and hence the subsequent formation of C-C bonds leading to C_{6+} oxygenates is negligible due to the low pressure of C_4 aldehydes. Since the experiment was done in short time (7 hours for each material after reaching steady state) the effect of long term deactivation due to coke formation on C-C formation was not obvious either. These findings suggest that the effect of hydrogen pressure on the rates of C-C formation is less likely through the mechanisms 1, 2 and 5 described earlier.

MgO and Al_2O_3 are known to be non-reducible oxides at reaction conditions, hence the change in surface oxidation state as described by mechanism 4 is not expected. However, since TiO_2 is in the metastable anatase phase, it is expected that surface reduction can occur at lower temperatures[159,160] than the other two materials leading to the formation of oxygen vacancies and stronger Lewis acid sites.[119,161] Surface reduction can potentially lead to the loss of the acid-base pairs required for enolization or lead to an increase in the crotonaldehyde desorption energy. Based on the proposed mechanism in this study in which product desorption is the rate limiting step, we propose that the increase in surface Lewis acidity due to surface reduction is the reason for the decrease in C-C formation rate at increasing hydrogen pressure. This hypothesis is in good agreement with the higher stability of the adsorbed aldehydes reported on hydrogen pretreated metal oxides compared to the oxidized oxides.[143,155] Idriss et al.[162] also reported that crotonaldehyde desorption temperature increased from 420 K to 570 K as the average Ti cation oxidation state decreased on TiO_2 (001) surface. More in-depth in situ studies using UV or X-ray absorption are needed to verify this hypothesis.

The remaining possible explanation for the decrease in the C-C formation rate on TiO_2 at increasing hydrogen pressure is through the change in surface basic sites coverage. At higher hydrogen pressure, higher surface hydroxyl group density is expected in expense of lower basic surface oxygen sites. Decreasing basic active sites density required for the deprotonation of aldehydes can potentially make this step the rate limiting step and reduce the overall C-C formation

reaction.[111] This explanation is unlikely since a second order dependence on acetaldehyde pressure was measured on TiO_2 at high hydrogen pressure (60 kPa). If deprotonation of aldehydes was the rate limiting step, a first order should have been observed instead.

3.3.6. Effect of Water Pressure on C-C Formation Rate

Water is the byproduct of the C-C formation condensation reaction as shown in step (8) so the presence of water in the reaction medium is unavoidable. In addition to the produced water from the reaction, biologically produced ethanol is expected to be hydrous which brings additional water to the reaction medium so it is important to study the effect of water on catalyst performance. Water pressure was increased on the three materials while helium pressure was reduced keeping ethanol, acetaldehyde, and hydrogen pressures all constant.

The results in Figure 35 show that increasing water pressure decreased the C-C formation rate on Al_2O_3 and MgO (tested at 603 K) but increased it on TiO_2 and MgO (tested at 633 K). The inhibiting effect on Al_2O_3 was found to be reversible since C-C formation rate returned back to its initial value when water co-feed was cut while the deactivation was irreversible on MgO (tested at 603 K) as indicated by the drop in activity when water co-feed was cut. This difference in the deactivation reversibility can be explained by the difference in how these two materials respond to humidity in the reaction medium. Water adsorbs on Al_2O_3 dissociatively to form hydroxyl groups and protons which covers the acid and basic sites as described in Figure 36.[163]

On MgO, on the other hand, the surface reacts with water in a hydration reaction to form a layer of $Mg(OH)_2$[164] which is less active towards C-C formation. Moreover, the allotropic transition from oxide to the hydroxide is accompanied by a loss of surface area as well. This explains the need to operate under temperature equal or higher than 633 K to get C-C formation proceed on MgO and overcome the described exothermic surface hydration problem.[27] When tested at higher temperature, MgO (tested at 633 K) did not show the same deactivation pattern under increasing water pressure since the reaction temperature does not favor the catalyst hydration. Similar stabilization effect by higher temperature was reported by Shen et al.[47] on supported MgO but it

was attributed to less carboxylic acid formation at higher temperature while surface hydration was not considered.

The increase in the C-C formation rate on MgO (tested at 633 K) can be explained by the formation of surface hydroxyl groups that act as additional active sites for the reaction.[30,133,165,166] At such high temperatures, catalyst is expected to lose its activity due to the formation of undesirable, highly unsaturated, cyclic, carbonaceous materials (coking).[44-46,143] This instability under wide range of reaction conditions limits the MgO long-term use in this reaction.

The activity enhancement upon increasing the water pressure from 0 to 1 kPa on TiO_2 could be attributed to either formation of surface hydroxyl groups or change in surface oxidation state. The first explanation is less likely since an inhibition effect was observed on the stronger acidic Al_2O_3. The second explanation is more plausible since at increasing water pressure, the total pressure of oxygenates to hydrogen increases and hence, an increase in surface oxidation is expected by healing surface oxygen vacancies. This surface oxidation attenuates the strength of acid sites and facilitates desorption of the formed crotonaldehyde. Water binding energy on TiO_2 surface was calculated to be around 90 $kJ.mole^{-1}$ using DFT[140], a value that is higher than that calculated for acetaldehyde but similar to that of crotonaldehyde. The fact that water does not inhabit acetaldehyde aldol condensation on TiO_2 is an additional evidence that crotonaldehyde desorption is the rate limiting since water competitive adsorption does not harm reaction rates. This suggests that out of the three materials.

Since water adsorption lead to blocking of acid sites[87,167], the inhibiting effect of water is expected to be stronger on the acid-catalyzed ethanol dehydration compared to the less acid dependent C-C formation and esterification reactions. This hypothesis can be verified by reporting the decrease in dehydration to diethyl ether selectivity in favor of selectivity to C-C Guerbet products and esters on Al_2O_3 as shown in Figure 37. Since both C-C formation and etherification lead to the formation of water as a byproduct, it is expected that Al_2O_3 becomes more selective towards C-C formation at higher conversions. At increasing water pressure, the surface Brønsted acid sites density was found not to increase on Al_2O3.[86] And even if they were formed, they are less acidic than the Lewis acid Al^{3+} sites and their activity towards alcohol dehydration is lower.[87]

Similar enhancement in catalyst selectivity is not expected in the case of MgO or TiO_2 since the other two competing reactions with C-C formation are ketonization and esterification respectively on these oxides. Both ketonization and esterification are acid-base catalyzed and hence their response to blocking of acid sites or increase in surface hydroxyl groups is similar to that of the C-C formation reaction. This conclusion is confirmed by the null change in selectivity towards C-C formation on these two materials at variable water pressure as shown in Figures 38a and 38b.

3.3.7. Effect of Side Products Pressures on C-C Formation Rate

Since the C-C formation rate on metal oxides was found to be sensitive to acid-base sites coverage, side products such as ethers, ketones, and esters can potentially affect the C-C formation rate by competitively adsorbing on the active sites and blocking access of reactive acetaldehyde to these sites. To study this effect, diethyl ether, acetone, and ethyl ester were co-fed with ethanol and acetaldehyde at variable pressures while keeping acetaldehyde, ethanol, and hydrogen pressures constant on TiO_2 as an example. As shown in Figure 39, acetone and diethyl ether were found to have no effect on C-C formation rate while ethyl ester had an inhibiting effect on the reaction rate. This can be explained by the relative difference in basicity of these three components to acetaldehyde and hence their bond strengths with acid sites.

The absolute difference in basicity as indicated by gas phase proton affinity determined by geometry optimization[168] and reported in Table 8 does not explain the specifically high inhibiting effect of ester on TiO_2 since acetone, for example, also has higher proton affinity than acetaldehyde and should theoretically have some inhibition effect on acetaldehyde aldol condensation which is not observed in this experiment. In addition, if crotonaldehyde desorption is the rate determining step, crotonaldehyde has similar basicity to that of the ester and hence the effect of ester on inhibiting C-C formation should not be as significant.

A possible explanation for this strong inhibition by esters is that ester, harboring and additional oxygen to that of the carbonyl oxygen, can adsorb on Lewis acid sites through a stable bidentate structure that has higher adsorption energy than that predicted through the coordination of the carbonyl oxygen with the acid site. A similar inhibitory effect is expected for carboxylic acids due

to their strong adsorption on active sites as well, a hypothesis that was confirmed by Shen et al.[47] on supported basic metal oxides.

At higher conversion where ethyl ester pressure increases, the inhibiting effect of this side product on the C-C formation becomes more noticeable. Also sine both C-C formation and esterification occur on TiO_2 at low conversions when both acetaldehyde and ethanol are co-fed, it is difficult to measure the intrinsic value of the C-C formation rate on TiO_2 in absence of ethyl ester at these reaction conditions. Eliminating ethanol, the source of ethoxides, while maintaining acetaldehyde in the feed, can potentially enable high selective formation of C-C bonds without esterification.

3.4. Conclusion

The predominant mechanism for C-C bond formation through Guerbet reaction on metal oxides is through ethanol dehydrogenation to acetaldehyde followed by acetaldehyde aldol condensation to crotonaldehyde and hydrogenation of crotonaldehyde to butanol. Deprotonation of adsorbed ethoxide to form the acetaldehyde is the rate limiting step when starting from ethanol while crotonaldehyde desorption is the rate limiting step when starting from acetaldehyde. Strong basic sites are required to dehydrogenate ethanol, however, their presence leads to rapid catalyst deactivation either by surface hydration or coking. Mild acid-base sites are more active for C-C formation and selective towards linear products but have poor ethanol dehydrogenation activity.

Maximizing surface acetaldehyde to ethoxide density by increasing acetaldehyde to ethanol ratio in the gas phase leads to an increase in the C-C formation rate and selectivity. Hydrogen was found not to affect reaction rates on non-reducible surfaces but inhibits the reaction on reducible surfaces by increasing the surface acid strength and hence increasing the products desorption energy. Water was found to deactivate MgO at lower temperatures due to surface hydration and inhibits C-C formation on Al_2O_3 by blocking active sites. An enhancement in TiO_2 activity with water was observed possibly due to attenuating surface acid strength. Among the identified side products, esters were found to have the highest inhibiting effect on C-C formation on TiO_2.

The high activity, stability, and selectivity of mild acid-base sites make amphoteric oxides more advantageous than strong acidic or basic oxides for C-C formation through aldol condensation of acetaldehyde. Since amphoteric surfaces have low ethanol dehydrogenation activity, addition of a separate dehydrogenation catalyst is needed when starting from ethanol.

3.5. Figures and Tables

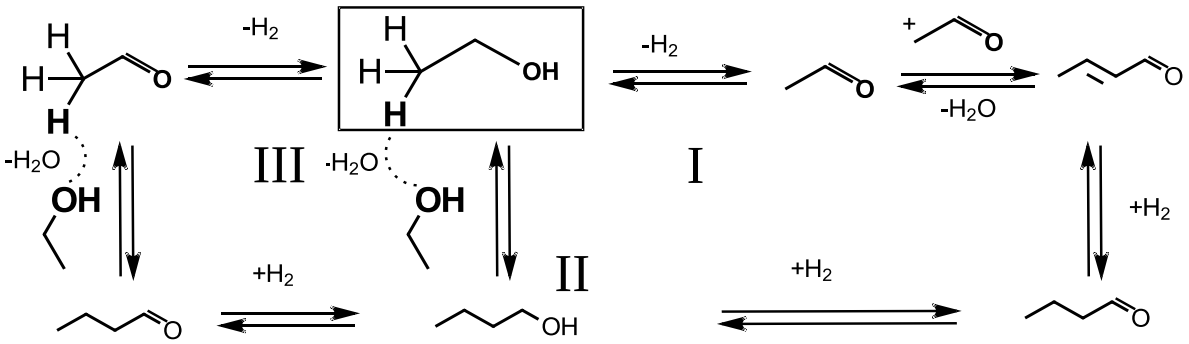

Figure 18. Alternative mechanisms for ethanol Guerbet reaction on metal oxides

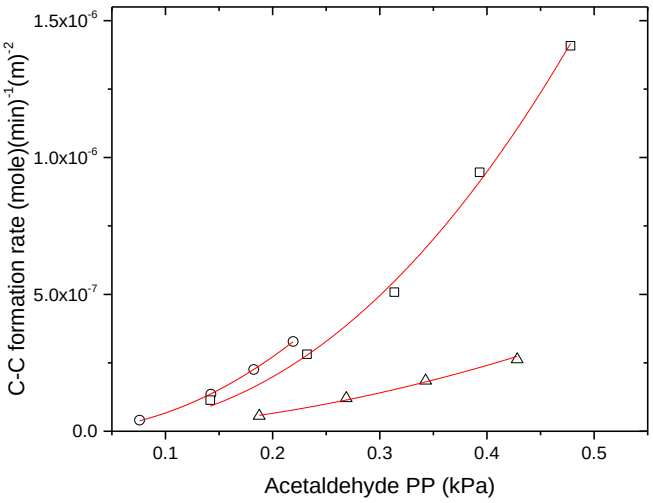

Figure 19. C-C formation turnover rate as function of acetaldehyde pressure on MgO (○) at 3 kPa EtOH, 60 kPa H_2, bal. He, and 633 K reaction temperature, TiO_2 (□) at 3 kPa EtOH, 60 kPa H_2, bal. He, and 483 K reaction temperature, and Al_2O_3 (Δ) at 3 kPa EtOH, 60 kPa H_2, bal. He, and 503 K reaction temperature

1. $C_2H_5OH_g + *_A*_B \rightleftharpoons C_2H_5O*_A + H*_B$
2. $C_2H_5O*_A + *_B \rightleftharpoons CH_3CHO*_A + H*_B$
3. $CH_3CHO*_A \rightleftharpoons CH_3CHO_g + *_A$
4. $2H*_B \rightleftharpoons H_2 + 2*_B$
5. $CH_3CHO*_A + *_B \rightleftharpoons {}^{-}CH_2CHO*_A + H*_B$
6. $CH_3CHO*_A + {}^{-}CH_2CHO*_A \rightleftharpoons *_A\,O\overset{CH_3}{\overset{|}{C}}HCH_2CHO*_A$
7. $*_AO\overset{CH_3}{\overset{|}{C}}HCH_2CHO*_A + H*_B \rightleftharpoons HO\overset{CH_3}{\overset{|}{C}}HCH_2CHO*_A + *_A*_B$
8. $HO\overset{CH_3}{\overset{|}{C}}HCH_2CHO*_A + H*_B \rightleftharpoons CH_3CH{=}CHCHO*_A + H_2O + *_B$
9. $CH_3CH{=}CHCHO*_A \rightleftharpoons CH_3CH{=}CHCHO_g + *_A$
10. $CH_3CH{=}CHCHO*_A + 2H*_B \rightleftharpoons CH_3CH_2CH_2CHO*_A + 2*_B$
11. $CH_3CH_2CH_2CHO*_A \rightleftharpoons CH_3CH_2CH_2CHO_g + *_A$
12. $CH_3CH_2CH_2CHO*_A + 2H*_B \rightleftharpoons CH_3CH_2CH_2CH_2OH_g + 2*_B$

Figure 20. Proposed elementary steps for formation of butanol from ethanol on metal oxide surfaces through aldol condensation. $*_A$ represents surface metal Lewis acid site while $*_B$ represents surface oxygen Brønsted base site

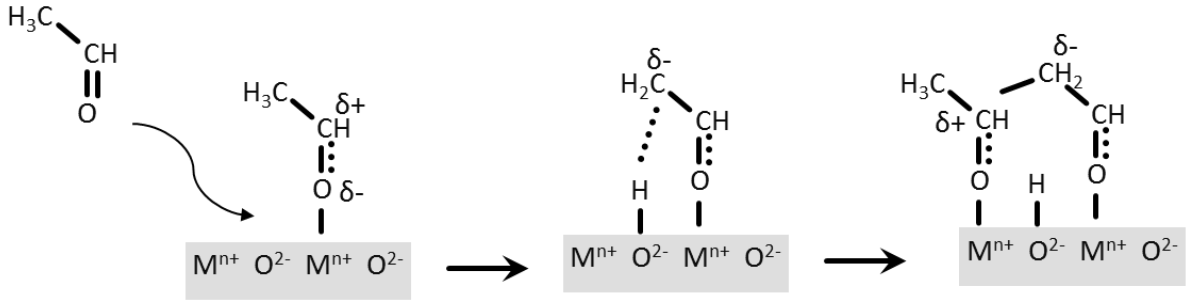

Figure 21. Formation of enolate and new C-C bond through aldehyde aldol condensation on metal oxides

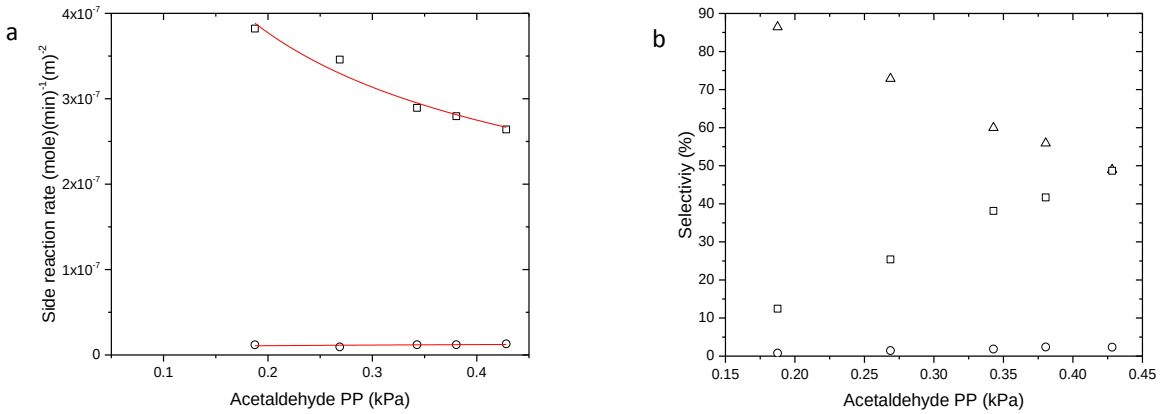

Figure 22 (a). Side reaction rates at variable acetaldehyde pressure on Al_2O_3 at 3 kPa EtOH, 60 kPa H_2, bal. helium at 483 K. (b) selectivity of diethyl ether (□), and ethyl acetate (○) at variable acetaldehyde pressure on Al_2O_3 at 3 kPa EtOH, 60 kPa H_2, bal. He at 483 K reaction temperature

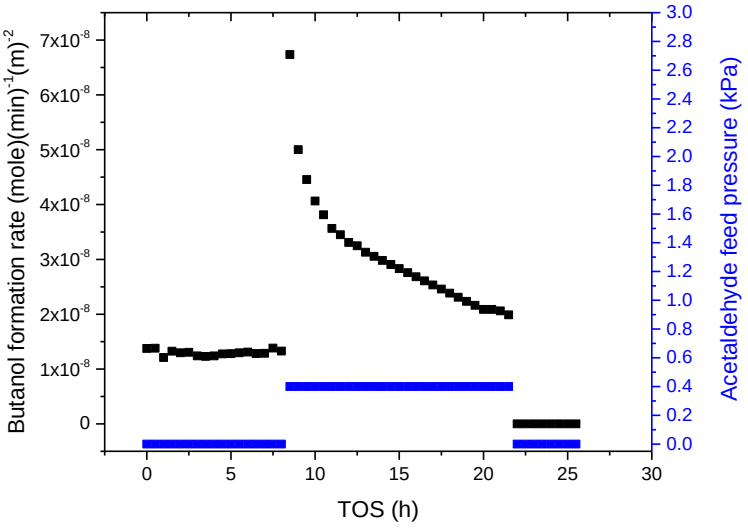

Figure 23. Effect of co-feeding acetaldehyde on butanol formation rate on MgO versus time on stream (TOS, h) at 3 kPa EtOH, 60 kPa H_2, bal. He, and 633 K reaction temperature

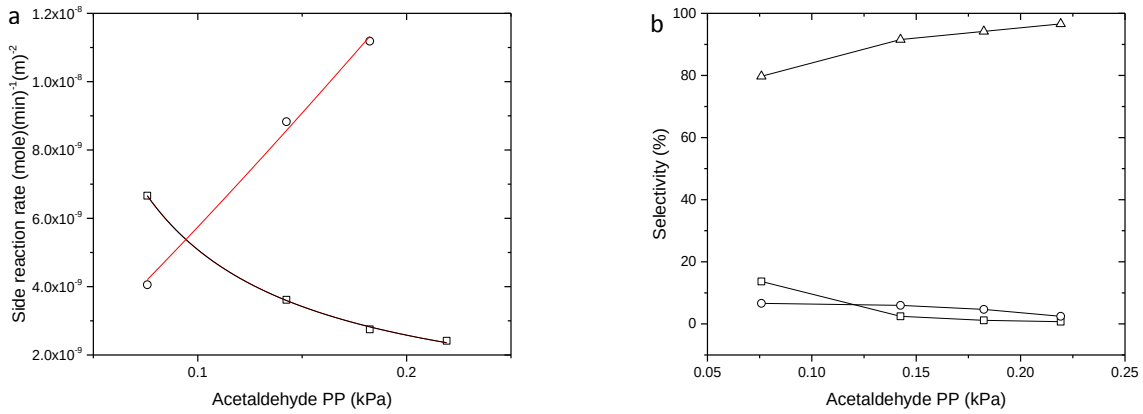

Figure 24 (a). Ketones (○), and ethylene (□) formation rates at variable acetaldehyde pressure on MgO at 3 kPa EtOH, 60 kPa H_2, bal. He, and 633 K reaction temperature **(b).** Guerbet C-C products (Δ), ethylene (□), and ketones (○) at variable acetaldehyde pressure on MgO at 3 kPa EtOH, 60 kPa H_2, bal. He, and 633 K reaction temperature

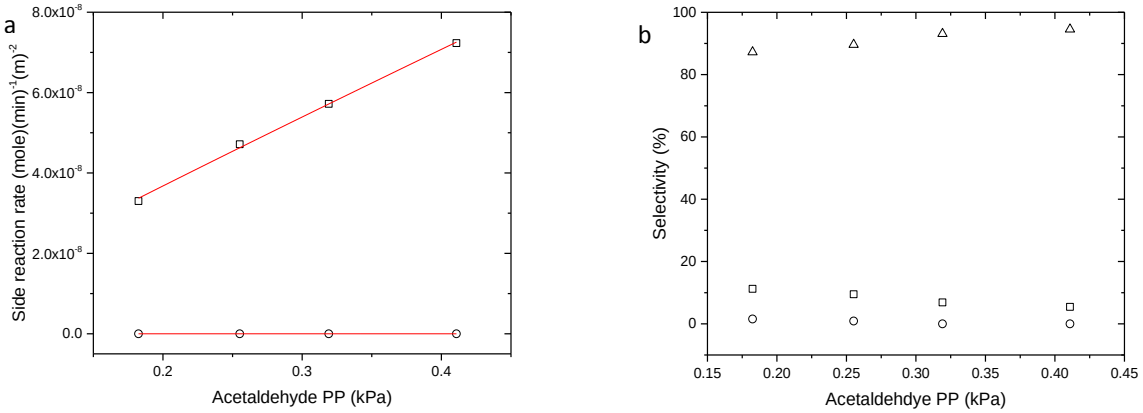

Figure 25 (a). Ethyl ester (□), and diethyl ether (○) formation rates at variable acetaldehyde pressure on TiO_2 at 3 kPa EtOH, 60 kPa H_2, bal. He, and 503 K. **(b).** Guerbet C-C products (Δ), ethyl ester (□), and diethyl ether (○) selectivity at variable acetaldehyde pressure on TiO_2 at 3 kPa EtOH, 60 kPa H_2, bal. He, and 503 K reaction temperature

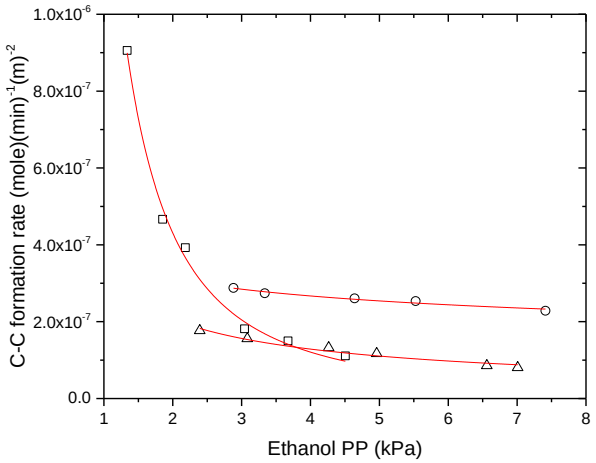

Figure 26. C-C formation turnover rate as function of ethanol pressure on MgO (○) at 0.3 kPa acetaldehyde, 60 kPa H_2, bal. He, and 633 K reaction temperature, TiO_2 (□) at 0.22 kPa acetaldehyde, 60 kPa H_2, bal. He, and 503 K reaction temperature, and Al_2O_3 (Δ) at 0.36 kPa acetaldehyde, 60 kPa H_2, bal. He, and 483 K reaction temperature

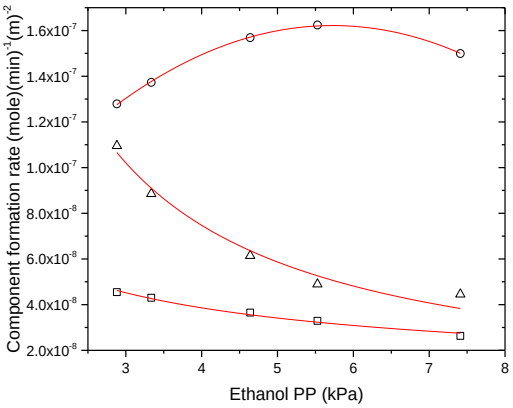

Figure 27. Turnover rate of formation of C_4 alcohols (○), C_4 aldehydes (□), and C_{6+} (Δ) oxygenates formed through C-C bond formation as function of ethanol pressure on MgO at 0 kPa acetaldehyde feed, 60 kPa H_2, bal. He, and 633 K reaction temperature

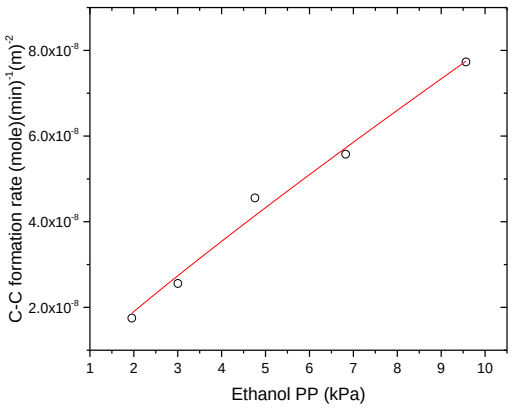

Figure 28. C-C formation turnover rate as function of ethanol pressure on MgO at 0 kPa acetaldehyde feed, 60 kPa H_2, bal. He, and 633 K reaction temperature

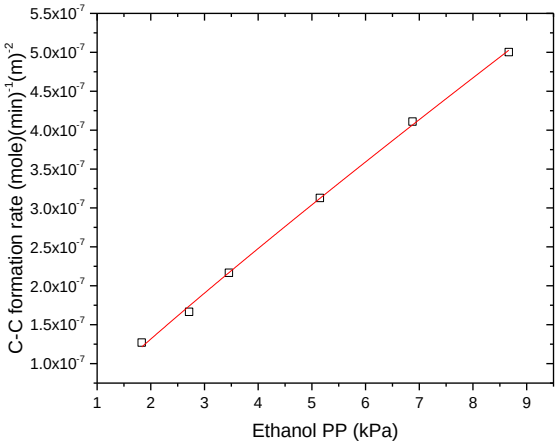

Figure 29. C-C formation turnover rate as function of ethanol pressure on TiO_2 at constant ethanol to acetaldehyde feed pressure ratio of 6:1, 60 kPa H_2, bal. He, and 503 K reaction temperature

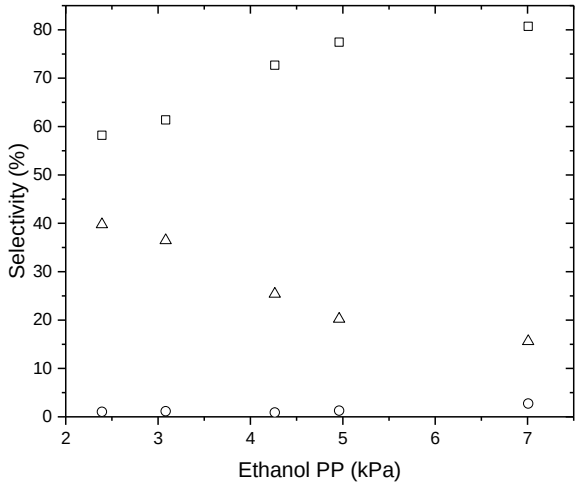

Figure 30. Diethyl ether (□), ethyl ester (○), and Guerbet C-C products (Δ) selectivity as function of EtOH pressure on Al_2O_3 at 0.36 kPa acetaldehyde pressure, 60 kPa H_2 and 483 K reaction temperature

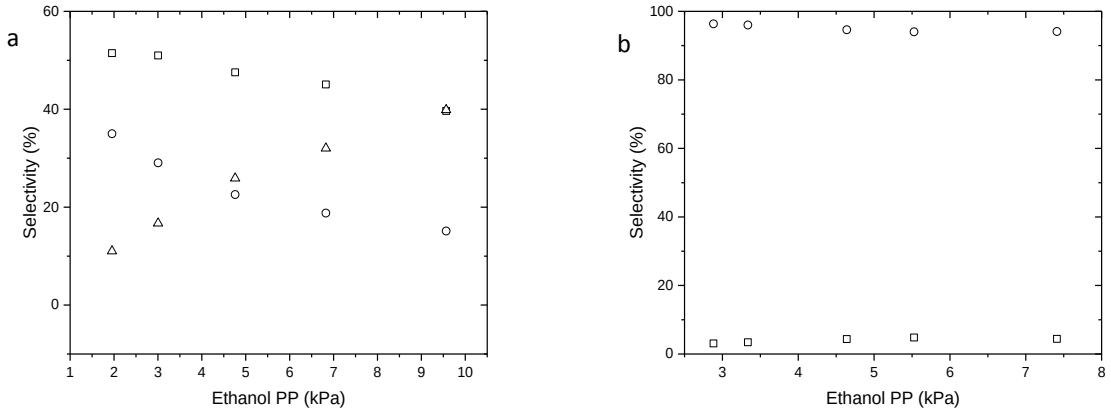

Figure 31 (a). Acetaldehyde (□), ethylene (○), and Guerbet C-C products (Δ) selectivity as function of ethanol pressure on MgO at 0 kPa acetaldehyde feed pressure, 60 kPa H_2 and 633 K reaction temperature**. (b).** Guerbet C-C products (○), and ketones (□) selectivity as function of ethanol pressure on MgO at 0.3 kPa acetaldehyde, 60 kPa H_2 and 633 K reaction temperature

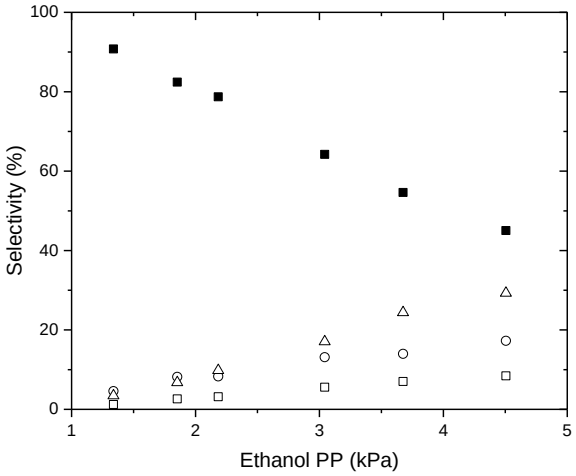

Figure 32. Diethyl ether (□), ethyl ester (○), ketones (Δ), and Guerbet C-C products (■) selectivity as function of ethanol pressure on TiO_2 at 0.22 kPa acetaldehyde, 60 kPa H_2, bal. He, and 503 K reaction temperature

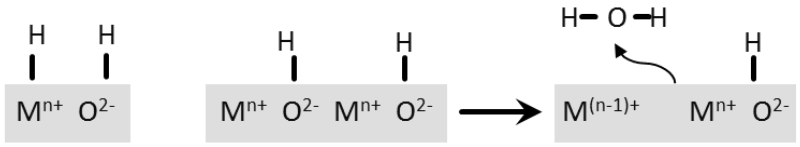

Figure 33. Hydrogen adsorption modes on metal oxides

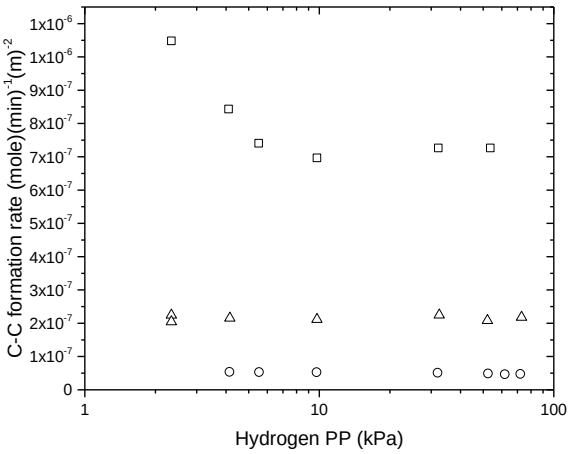

Figure 34. C-C formation turnover rate as function of hydrogen pressure on MgO (○) at 0.2 kPa acetaldehyde, 60 kPa H_2, bal. He, and 633 K reaction temperature, TiO_2 (□) at 0.36 kPa acetaldehyde, 60 kPa H_2, bal. He, and 503 K reaction temperature, and Al_2O_3 (Δ) at 0.36 kPa acetaldehyde, 60 kPa H_2, bal. He, and 483 K reaction temperature

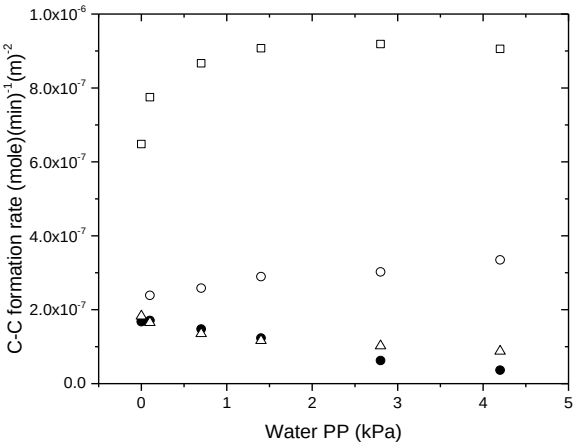

Figure 35. C-C formation turnover rate as function of water pressure on MgO (○) at 0.2 kPa acetaldehyde, 60 kPa H_2, bal. He, and 633 K reaction temperature, TiO_2 (□) at 0.36 kPa acetaldehyde, 60 kPa H_2, bal. He, and 503 K reaction temperature, Al_2O_3 (Δ) at 0.36 kPa acetaldehyde, 60 kPa H_2, bal. He, and 483 K reaction temperature, MgO (●) at 0.34 kPa acetaldehyde, 60 kPa H_2, bal. He, and 603 K reaction temperature

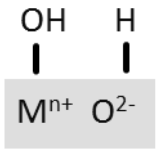

Figure 36. Water dissociative adsorption on metal oxides

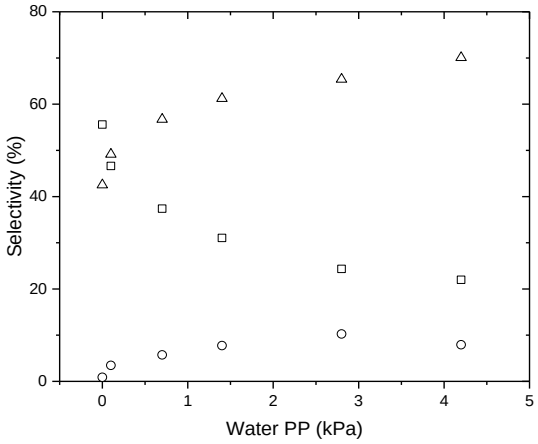

Figure 37. Diethyl ether (□), ethyl ester (○), and Guerbet C-C products (Δ) selectivity as function of water pressure on Al_2O_3 at 0.36 kPa acetaldehyde, 60 kPa H_2 and 483 K reaction temperature

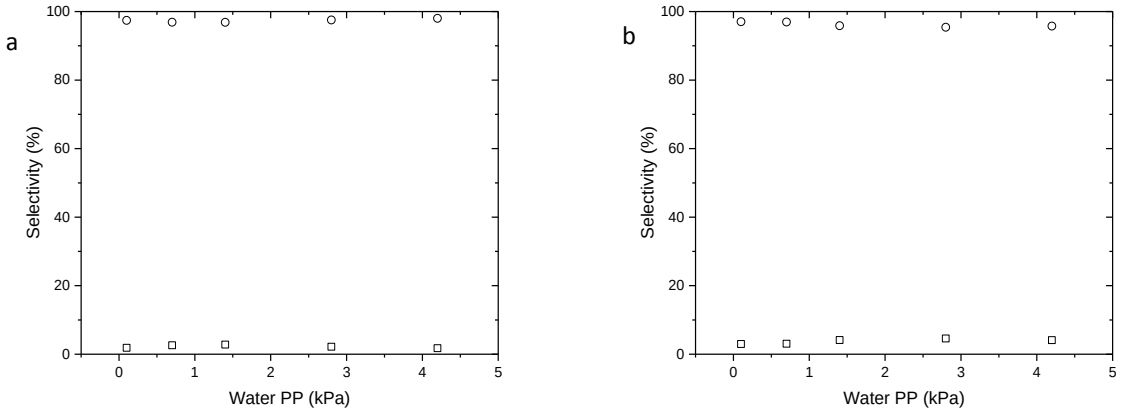

Figure 38 (a). Ketones (□), and Guerbet C-C products (○) selectivity as function of water pressure on MgO at 0.2 kPa acetaldehyde pressure, 60 kPa H_2 and 633 K reaction temperature. **(b).** Ethyl ester (□), and Guerbet C-C products (○) selectivity as function of water pressure on TiO_2 at 0.32 kPa acetaldehyde, 60 kPa H_2 and 503 K reaction temperature

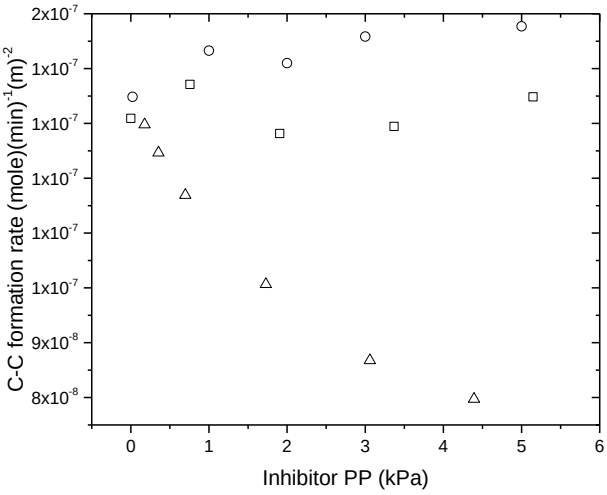

Figure 39. C-C formation turnover rate as function of diethyl ether (□), acetone (○), and ethyl ester (Δ) pressures on 100 mg TiO_2 at 7 $\mu l.min^{-1}$ liquid feed rate, 3 kPa EtOH, 0.3 kPa acetaldehyde, 60 kPa H_2, bal. He, and 493 K reaction temperature

Table 3. C-C formation rate best fit power dependency on acetaldehyde partial pressure

Catalyst	Best fit power	R^2
Al_2O_3	1.9	0.9943
TiO_2	2.1	0.9946
MgO	2.0	0.9996

Table 4. Side reactions rates best fit power dependency on acetaldehyde partial pressure on Al_2O_3 at 3 kPa EtOH, 60 kPa H_2, bal. He, and 483 K reaction temperature

Reaction	Best fit power	R^2
Esterification	0.75	0.9995
Etherification	-0.47	0.9689

Table 5. Side reactions rates best fit power dependency on acetaldehyde partial pressure on MgO at 3 kPa EtOH, 60 kPa H_2, bal. He, and 633 K reaction temperature

Reaction	Best fit power	R^2
Ketonization	1.17	0.9973
Dehydration	-0.97	0.9979

Table 6. Side reactions rates best fit power dependency on acetaldehyde partial pressure on TiO_2 at 3 kPa EtOH, 60 kPa H_2, bal. He, and 503 K reaction temperature

Reaction	Best fit power	R^2
Esterification	0.96	0.9979
Etherification	-	-

Table 7. C-C formation rate best fit power dependency on ethanol partial pressure

Reaction	Best fit power	R^2
MgO	-0.23	0.9648
Al_2O_3	-0.74	0.9639
TiO_2	-1.75	0.9908

Table 8. Gas phase proton affinity of carbonyl containing oxygenates[168]

Component	H^+ affinity (kJ)(mole)$^{-1}$
acetaldehyde	770
acetone	814
Methyl propionate	835
Dimethyl ether	798
Crotonaldehyde	835
Water	707

Chapter 4: Selective Alcohol Dehydrogenation Catalyst Design

4.1. Introduction

Aldehydes and ketones are widely used commodity chemicals and intermediates that can be produced by Wacker process, alcohols oxidative dehydrogenation, or hydroformylation.[169-175] Selective alcohol dehydrogenation to the corresponding aldehyde or ketone is a promising alternative pathway for producing these intermediates at high selectivity and milder reaction conditions. Acetaldehyde, for example, is used in acetic acid, acetic anhydride, ethyl acetate, pentaerythrit and other chemicals synthesis, and can be produced through the dehydrogenation of ethanol.[170] As demonstrated in Chapters 2 and 3 of this study, ethanol dehydrogenation to acetaldehyde is the first, and the rate determining, step in the formation of Guerbet products from ethanol.

In addition to acetaldehyde, other important intermediates can be produced from dehydrogenation of alcohols as well. Acetone, an important solvent and intermediate, can be produced from the dehydrogenation of isopropanol.[176] 2-butanone, an important solvent that has similar properties to acetone but boils at higher temperature, can be produced by the dehydrogenation of 2-butanol.[177] Isovaleraldehyde, an intermediate used in resin synthesis and isovaleric acid production which is widely used in medical application, can be produced from Isoamyl alcohol dehydrogenation.[169] Butyraldehyde, a solvent and an important intermediate in resins industry and rubber vulcanization, can be produced from Butanol dehydrogenation.[171] C_8 to C_{13} aldehydes are fine chemicals that can be produced from their corresponding alcohols by dehydrogenation. Octanone is another a long chain ketone that is widely used in perfumes, colognes, and artificial citric oils, and can be produced from octanol production.[178]

In addition to linear aldehydes and ketones, cyclic chemicals can be produced through the same route. Benzaldehyde, for example, is the second most important aromatic compound used in cosmetics and flavoring industry and can produced from the dehydrogenation of benzyl alcohol.[179] Cyclohexanone, another intermediate used in caproalctam synthesis, can be produced from the dehydrogenation of cylcohexanol.[180] Among these numerous examples, we selected ethanol

selective dehydrogenation as a model reaction for designing a selective catalyst for alcohol dehydrogenation.

Ethanol is difficult to be dehydrogenated compared to longer alcohols, since the thermodynamic equilibrium favors the alcohol formation as the alcohol chain length becomes shorter, making it necessary to go to high temperatures to allow appreciable conversion of ethanol as shown in Figure 9. Compared to the ketones produced from dehydrogenation of secondary alcohols, acetaldehyde produced from dehydrogenation of ethanol is more vulnerable to decarbonylation due to its stronger adsorption to metallic surface.[181,182] In addition to decarbonylation, acetaldehyde undergoes esterification reaction through its reaction with adsorbed ethanol or aldolization through its reaction with itself. These characteristics of ethanol dehydrogenation reaction make it necessary to design a selective catalyst that allows high acetaldehyde selectivity at appreciable ethanol conversion.

Church et al.[170] reported ethanol dehydrogenation to acetaldehyde selectivity as high as 88% on copper catalyst modified with chromium and cobalt at 95% ethanol conversion. However, the 10% selectivity loss to ethyl ester on this catalyst is expected to harm the dehydrogenation process economics since separation of ethyl ester can be costly. In ethanol Guerbet process, such a high carbon loss to ester can also be detrimental to process feasibility since esters are undesired in the product pool as explained in Chapter 2 of this study. Operation cost of the ethanol Guerbet process is also expected to increase due to esterification since esters were found to inhibit the Guerbet reaction as demonstrated in Chapter 3. In addition to the economic impact, chromium based catalyst can be harmful to the environment[183] and hence its usage makes the process less environmentally benign. Keeping these considerations in mind, it is reasonable to conclude that the feasibility of ethanol Guerbet process is highly dependent on the ethanol dehydrogenation catalyst performance and properties.

Basic oxides such as ZnO, MgO, and CuO showed to be active for alcohols dehydrogenation.[184] However, due to the oxides acid-base properties, other side products are formed on these surfaces as well reducing the desired product selectivity. Unlike metal oxides, metallic surfaces demonstrated high activity towards dehydrogenation reactions[172,178,185,186] without significant acid-

base activity due to the absence of metal oxygen bonds. Although that the alcohols are rapidly dehydrogenated on metal surfaces, other side reactions were found to occur including decarbonylation, etherification, and esterification too.

In this chapter we study the effect of changing metallic nanoparticles (NP) catalyst design parameters on ethanol dehydrogenation to acetaldehyde selectivity. These parameters include metal electronegativity, metal loading methods, alloying or promotion with a second element, heat treatment environment, support effects, and NP size effect. Copper was found to be the most selective metal among group 10 and 11 metals with ethyl ester as the main side product. Metal loading using Ion Exchange (IE) in high pH was found to yield more selective catalyst than Incipient Wetness (IW) with low pH solution while high temperature exposure in oxidizing environment was found to decrease Cu NP selectivity. Alloying Cu with other elements such as Au, Zn, or Cr had positive effect on catalyst selectivity. Support acidity was found to promote ester formation on supported Cu NP while support basicity promotes Guerbet products formation. Unsupported Cu powder was found to be the most selective catalyst towards acetaldehyde production from ethanol.

4.2. Materials and Methods

4.2.1. Catalysts Preparation

Cu, Ag, Au, Ni, Pt, and Pd supported NP were prepared on silica gel (Sigma-Aldrich, Davisil Grade 646) as following; prior to metal loading, silica was washed thoroughly with deionized water (17.9 MΩ resistivity), dried in static air at 343 K overnight, then treated in flowing dry air (S.J. Smith, Ultra Zero) by heating to 773 K at 3 K min^{-1} and holding for 12 h. Samples were cooled down to room temperature, pelletized, and sieved to size range 35-60 mesh to avoid mass transport and channeling effects.[187]

Cu, Ag, and Au aqueous solutions were prepared from $Cu(NO_3)_2.2.5H_2O$ (Aldrich, 99.99%), $AgNO_3$ (Aldrich, 99.9999%), and $AuCl_3$ (Aldrich, >99.99%) respectively. The metal precursors were loaded using IW where calculated amount of the solution was added dropwise to the support

just to fill the support open pores and result in a 2%wt metal loading. A calculated amount of $Ni(NO_3)_2 \cdot 6H_2O$ (Aldrich, 99.999%), $Pd(NH_3)_4Cl_2 \cdot H_2O$ (Aldrich, 99.99%), and $Pt(NH_3)_4Cl_2 \cdot xH_2O$ (Aldrich, 99.99%) were added to 1N NH_4OH (Macron, 28-30% NH_3) aqueous solution to form the metals amine precursors[188] required for Ni, Pd, and Pt NP formation respectively. The solution concentration was adjusted to obtain catalyst with 0.5%wt using IE method. The solution was added to the support in a ratio of 60 ml g^{-1} and stirred at room temperature for 24 h then filtered and washed with deionized water.

All catalysts made by IW and IE were dried in static air at 343 K overnight, then treated in flowing dry air by heating to 773 K at 3 K min^{-1} and holding for 6 h. Samples were cooled down to room temperature before being reduced in a 30 kPa H_2 (S.J. Smith, 99.99%), 71 kPa He (S.J. Smith, 99.99%) flowing at 350 cm^3 min^{-1} while heated to 573 K at 3 K min^{-1} and held for 6 h. Prior to exposure to atmospheric air, samples were cooled down and passivated with flowing 5% air, bal. He at 200 cm^3 min^{-1} for 30 min. Samples were labeled as ICu/SiO_2, Ag/SiO_2, Au/SiO_2, Ni/SiO_2, Pd/SiO_2, and Pt/SiO_2 as shown in Table 9.

Another 2%wt Cu supported on silica catalyst was prepared by IW as described above but instead of treating it in air after drying, catalyst was directly reduced in 30 kPa H_2, and 71 kPa flowing at 350 cm^3 min^{-1} while heated to 573 K at 3 K min^{-1} and held for 6 h. Catalyst was labelled as $IICu/SiO_2$. A third 2%wt Cu supported on silica catalyst was prepared by IE where $Cu(NO_3)_2.2.5H_2O$ was added to 1N NH_4OH aqueous solution before being mixed with the support in a ratio of 60 ml g^{-1} and stirred at room temperature for 24 h then filtered and washed with deionized water. The dry catalyst was oxidized at 773 K and then reduced at 573 K as described above. Catalyst was labeled $IIICu/SiO_2$ as shown in Table 9.

A series of Cu NP catalysts on different supports were prepared as following. Cu loading on anatase titania (Aldrich, 99.8%), and alumina (Aldrich, >99.9%) was done using IE as described above and the resulting catalysts were labelled Cu/TiO_2, and Cu/Al_2O_3 respectively. Cu loading on magnesia (Aldrich, 99.995%) and activated carbon (Fisher) was done using IW of $Cu(NO_3)_2.2.5H_2O$ solution and labeled Cu/MgO, and Cu/C respectively as shown in Table 9. Unsupported Cu was prepared by the degassing of $CuCO_3$ at 773 K for 6 h in air followed by

reduction as described above. $CuCO_3$ was prepared by the reaction of $Cu(NO_3)_2.2.5H_2O$ with Na_2CO_3 (Fisher, >99.5%).

Cu-Ag and Cu-Pd bimetallic NP on silica were prepared in the molar ratio 3 to 1 Cu to Ag or Pd with a total metal content of 2%wt using simultaneous IW. A solution containing the desired amounts of both metals precursors was added to the support dropwise followed by drying and reduction as described earlier, catalysts were labeled as Cu_3Ag_1/SiO_2 and Cu_3Pd_1/SiO_2. Cu-Au NP on silica was prepared by sequential loading. Cu was loaded on silica using IE as described above, catalyst was then dried and oxidized before being cooled down to room temperature. On the oxidized Cu containing catalyst, $AuCl_3$ solution was added using IW where the Cu to Au molar ratio was set to 10 to 1 then catalyst was dried again, oxidized, and then reduced. The resulting catalyst was labelled $Cu_{10}Au_1/SiO_2$ as shown in Table 9.

Zn and Cr promoted Cu NP on silica were prepared using sequential IW. Cu was loaded using IW as described earlier and catalyst was dried, oxidized then reduced. To the Cu containing catalyst, solutions of $Zn(NO_3)_2{\cdot}6H_2O$ (Sigma-Aldrich, 99%), and $Cr(NO_3)_3{\cdot}9H_2O$ (Sigma-Aldrich, 99%) were added dropwise to adjust the Cu to Zn or Cr ratio to 10 to 1 molar ratio. Following impregnation with the second metal, catalyst was dried, oxidized and reduced again. Resulting catalyst were labeled as $Cu_{10}Zn_1/SiO_2$, $Cu_{10}Cr_1/SiO_2$ as shown in Table 9. K modified catalyst were prepared by addition of KOH (Fisher, >85%) aqueous solution to the reduced Cu on silica and alumina using IW so that the Cu to K molar ratio is 10 to 1. Following K addition, catalyst was dried and reduced at 573 K as described earlier. Catalysts were labeled as K-Cu/SiO_2 and K-Cu/Al_2O_3.

4.2.2. Catalysts Characterization

The Cu content of the catalysts was verified using Inductively Coupled Plasma-Optical Emission Spectroscopy (ICP-OES, PerkinElmer 2000DV) while the NP size was measured using Transmission Electron Microscopy (TEM, JEOL 2010-LaB_6, 200 kV, bright field mode, single tilt holder) where samples were ground and sonicated in methanol before being dispersed on "holey carbon" Cu grids. Diameter of 500 particles was measured and the algebraic mean was determined

as the average particles size. Metals distribution in bimetallic NP was measured using Energy Dispersive X-ray Spectroscopy (EDS). JEOL 2010F STEM equipped with Oxford INCA 30 mm ATW detector was used while Samples were dispersed on "holey carbon" Cu grids as explained before. Spectra were collected along particles diameter for different elements. The crystalline phase of the formed catalyst was measured at room using X-ray diffraction XRD (Bruker D-5000, Cu K- α radiation, 40 kV).

CO chemisorption was used to quantify the number of exposed metallic sites and measure NP size at room temperature. Known amount of the catalyst was loaded in a U-tube glass cell and vacuumed overnight. Catalyst was in situ reduced for 1 h under the reduction conditions specified above then vacuumed at 573 K before being cooled down to room temperature under vacuum. The available cell volume for gas expansion was measured by the change in helium pressure due to expansion assuming that no helium adsorption occurs. Carbon monoxide (S.J. Smith, 99.99%) was dosed to the cell in known quantities using an in-house built dosing system where the pressure before and after adsorption was measured. From the difference in pressures and the measured expansion volume, the amount of CO adsorbed was calculated using ideal gas low.

Adsorption isotherm was developed for each catalyst sample and the surface saturation value was used to estimate the NP surface area. The adsorption ratio of CO molecule to metallic surface atom was assumed as 1:1 for Ni, Pd, and Pt while a ratio of 1:4[189] was assumed for Cu, and 0:1 ratio was assumed for Ag, Au, Zn, Cr, K, and metal oxides supports. The surface area of the Cu clusters was calculated assuming surface density of 1.47×10^{19} atoms m^{-2} which is the arithmetic mean value of the Cu(111), Cu(110), and Cu(100).[107] To measure the reversibility of CO adsorption on metal surface, following the first adsorption isotherm experiment, catalyst was vacuumed for at least 1 h at room temperature and another CO adsorption experiment was done.

To investigate the catalyst reducibility, Temperature Programmed Reduction (TPR) was performed. Known amount of the catalyst was loaded in a 0.5 in. o.d. quartz tube and purged with helium for 1 h at room temperature. 10% H_2, bal. Helium stream following at 100 cm^3 min^{-1} was fed to the system while temperature was increased in the rate of 5 K min^{-1} to 773 K. Gas effluent

was routed to a mass spectrometer (Pfeiffer, Thermostar^{TM}) where the M/Z 2 and 18 amu were online measured.

4.2.3. Conversion and Selectivity Measurements

Reactions rates were measured using a quartz tubular reactor (0.5 in. o.d.) with plug flow hydrodynamics, which is contained within a three-zone electrically heated furnace (Applied Test Systems) controlled using an electronic PID controller (Watlow, EZ-Zone®) as described in Figure 2. The bed temperature was measured with a type K thermocouple touching the outer surface of the tube at the catalyst bed position. Catalysts were mixed with additional quartz SiO_2 to optimize reactant mixing with catalyst. Inertness of the quartz powder was tested at 633 K and no measurable reactions were observed.

Prior to the experiment, catalyst was in-situ reduced for 1 hr as described above then cooled down to the experiment temperature. All pretreatments and experiments were done at ambient pressure. The volumetric flow rates of gaseous feed components were controlled using calibrated mass flow controllers (Parker, MFC 600) while liquid components; ethanol (Decon, 200 Proof), and deionized water were injected using two programmable syringe pumps (KD Scientific, Legato 110). Liquid feeds were injected to heated transfer lines by means of heat tape set at 393 K while reactor effluent lines were kept heated at 473 K to prevent high boiling point components condensation.

Reactor effluent was cooled and bubbled in ethanol to capture liquid products and injected to an offline gas chromatography coupled with a mass spectrometer (Shimadzu, 2010 GC-MS) to identify the formed products. The quantitative analysis was determined using an online gas chromatography (Agilent, HP 6890) equipped with a capillary column (Agilent, J&W HP-PLOT Q, L = 30 m, ID = 0.32 mm, film thickness = 20μm) connected to a flame ionization detector (FID) to detect hydrocarbons and oxygenates and a packed column (Restek, HayeSep Q, L = 2m, ID = 2 mm) connected to a thermal conductivity detector (TCD) to detect H_2, CO, CO_2, and H_2O.

The retention time for each component was determined by injecting prepared standard solutions of the following liquid chemicals in ethanol; acetaldehyde (Sigma Aldrich, 99.5%), 2-butanone (Supelco, analytical standard), 2-ethyl-1-hexanol (Fluka, analytical standard), 2-ethyl-1-butanol (Aldrich, 98%), 2-ethyl-2-hexenal (Aldrich^{CPR}), butyraldehyde (Fluka, 99%), butanol (Fisher, ACS grade), octanol (Alfa Aesar, 99%), hexanol (Sigma Aldrich, 98%), crotyl alcohol (Aldrich, 96%), hexanal (Aldrich, 98%), crotonaldehyde (Aldrich, 99%), acetone (Macron, ACS grade), Acetic acid (J.T.Baker, ACS grade). Retention time calibration for gaseous products were done by injecting gas mixture standards (Supelco, analytical standard) containing carbon monoxide, carbon dioxide, methane, ethane, ethylene, acetylene (1w/w% in N_2), propane, propylene, and butane (15 ppm in N_2). Reported conversion and selectivity are defined as following:

$$Conversion(\%) = \frac{mole\ ethanol\ in - mole\ ethanol\ out}{mole\ ethanol\ in} X\ 100$$

$$Product\ Selectivity(\%) = \frac{mole\ ethanol\ converted\ to\ product}{moles\ ethanol\ converted} X\ 100$$

4.3. Results and Discussion

4.3.1. Selectivity of Group 10 and 11 Metals NP Supported on Silica

ICP-OES measurements verified the metal contents of the catalysts except that for Ag possibly due to error in instrument calibration. XRD peaks for ICu/SiO2 catalyst didn't show strong copper peak due to the low metal content. High metal content (28%wt) Cu/SiO2 catalyst was prepared for XRD measurements instead. Oxidization of the high metal content Cu/SiO_2 catalyst at 773 K lead to the formation of CuO as demonstrated by peaks at 35, 39 and 48 degree corresponding to (111), ($\bar{1}$11), and ($\bar{2}$02) respectively as shown in Figure 40 in addition to the amorphous silica peak at 23 degree while catalyst reduction at 573 K lead to the formation of metallic Cu as demonstration by peaks at 43 and 52 degrees corresponding to (111) and (200) respectively. TPR of oxidized catalyst showed the hydrogen consumption feature around 480 K as shown in Figure 41. This is in agreement with TPR results reported for similar catalysts where CuO reduction to Cu_2O occurs at 420 K while Cu_2O reduction to Cu occurs at 460 K.[172]

Group 10 metals supported on silica generally had higher dispersion and smaller NP size compared to group 11 metals. This can be explained by the difference in Tammann temperature[190] and hence their mobility on the surface at high temperature. Both Ag and Au didn't show any significant CO adsorption as shown in Table 9 possibly due to the very low adsorption energy of CO on these two metals.[191,192] Cu NP size measured by TEM and CO adsorption generally matches for ICu/SiO_2 as shown in Table 9.

The reaction of ethanol at 503 K on different metals NP supported on silica lead to the formation of acetaldehyde and other side products including methane, carbon monoxide, ethylene, ethane, diethyl ether, ethyl ester, acetone, 2-butanone, butanol, and butyraldehyde as shown in Figures 42a and 42b. Selectivity to acetaldehyde was higher than 80% on group 11 metals but it was as low as 30% on Group 10 metals. The selectivity loss on group 10 metals was mainly due to the high decarbonylation reaction resulting in the formation of carbon monoxide, hydrogen, and methane. This decarbonylation reaction was found to be minimal on group 11 metals which is the reason for the high selectivity on this group of metals.

This difference in decarbonylation activity can be attributed to the difference in the aldehyde adsorption configuration. Group 10 metals adsorb the aldehyde in η^2 mode[193] due to the high electron back donation of the surface to the adsorbed molecule. The parallel η^2 mode facilitates further decomposition of the formed aldehyde[194-196] through breaking C-H and C-C bonds leads to the formation of carbon monoxide, hydrogen, and hydrocarbons.[181] This is not the case in group 11 metals where the aldehydes adsorb mainly in the perpendicular η^1 mode as shown in Figure 43.[197-199] The later adsorption is weaker[200] and allows aldehyde desorption to the gas phase before further decomposition.

It is worth mentioning here that the smaller amounts of group 10 metals were required compared to those required of group 11 metals catalysts to achieve the same conversion indicating that the former group metals is more active for dehydrogenation. This conclusion is not surprising since group 10 metals have higher density of state close to the Fermi level resulting in stronger interaction with surface species and higher ability to break bonds. This difference in activity was reported in other alcohol dehydrogenation studies where isopropanol dehydrogenation rate was

found to be 5 times higher on Pt compared to Cu[201] while ethanol dehydrogenation was found to be significantly higher on Pd compared to Cu when both metals are supported on alumina.[202]

Group 10 metals activity is expected to decrease at increasing conversion due to inhibition by CO. Group 11 metals, despite being less active, do not suffer this inhibition effect and hence allow high selectivity at high conversion. Among group 11 metals, Cu was found to be the most active and selective which can be explained by the increase in the support amount in case of Ag and Au. As the metal dispersion or specific activity decrease, the required amount of catalyst increases, for example, 2.5 g of Au/SiO_2 catalyst was required to achieve conversion similar to that of 15 mg ICu/SiO_2. Van der Burg et al.[185] also reported very low alcohol dehydrogenation rate on Au compared to other transition metals while another study reported that Au NP rapidly agglomerated under reaction conditions.[179]

By examining side products distribution on group 11 metals, it can be seen that C-O and C-C formation are the two main side reactions. The first leads to the formation of ethers and esters while the later leads to the formation of aldehydes, alcohols and ketones. These reactions can be metal or support catalyzed since they require acid-base interaction. For example, Au surfaces were found to be active for esterification reaction[203] while other studies including Chapter 2 and 3 of this study showed that these reactions can be catalyzed on metal oxide surfaces.

This high required support surface area in reaction medium in the case of Au can lead to promotion of other side reactions. Co-feeding acetaldehyde and ethanol on blank silica lead to the formation of small amounts of ethers, esters, and aldehydes verifying that high support surface area can lead to selectivity loss even when using an inert support such as silica. This being said, the support activity can't explain the high ethyl ester formation rate on ICu/SiO_2 catalyst suggesting that this reaction is metal catalyzed or that the metal loading procedure modifies the support surface in a way that makes it more active towards this reaction which requires more investigation as shown in the following sections of this chapter.

From data shown in Figure 42a, it can be concluded that Cu is the most appropriate metal for this reaction. In fact, copper is widely studied as a selective catalyst for alcohols dehydrogenation[204]

due to its high activity, stability, and low price compared to Ag, and Au. Dehydrogenation kinetics of ethanol to acetaldehyde on copper based catalyst was studied by Franckaert et al. and the rate limiting step was found to be the surface reaction on dual site[205] while Doca et al. reported that the desorption of the formed acetaldehyde is the rate limiting. Regardless of the rate limiting step identity of the ethanol dehydrogenation, esterification is commonly reported in Cu catalyzed alcohol dehydrogenation and hence it is required to minimize this side reaction selectivity.

4.3.2. Effect of Cu NP Loading Method on Catalyst Selectivity

Different methods can be used to form supported Cu NP and the method used has an effect on catalyst performance as demonstrated by the enhanced activity towards butanol dehydrogenation of Cu supported on silica prepared by Electroless Deposition compared to that prepared by IW.[206] Catalyst made by IE also showed different properties from that prepared by IW as Toupance et al.[207] reported the formation of copper phyllosilicate $[Cu(NH_3)_4(H_2O)_2]^{2+}$ complex during Cu loading on silica using IE, while using IW does not form this complex. The Cu phyllosilicate complex can lead to the formation of the difficult to reduce Cu-O-Si bonds during the catalyst reduction resulting in the formation of Cu^+ species on the reduced copper surface.[208]

These Cu^+ species can act as Lewis acid sites and potentially catalyze esterification reaction. The relation between the phyllosilicate formation and the esterification activity was demonstrated by Yu et al.[209] and was attributed to the increased ratio of Cu^+/Cu^0 sites as indicated by XPS, ammonia TPD, and pyridine adsorption FTIR. Similar conclusion was reached by Sato et al.[210] using CO adsorption FTIR and XANES on reduced Cu supported on silica where both Cu^0 and Cu^+ were detected. From these findings, it is reasonable to concluded that the method of loading affects the Cu^+/Cu^0 ratio on the surface and hence esterification activity. Catalyst made by IW was found to have less Cu^+ sites compared to that synthesized by ammonia evaporation[208] while catalyst prepared by solution-gelation was found to have even higher Cu^+ ratio than that prepared by ammonia evaporation.[211] In addition to the metal loading method, the initial precipitation temperature used in ammonia evaporation method was found to affect the Cu^+ sites abundance as measured by XPS.[212]

In the present study, we show the esterification selectivity of two catalysts ICu/SiO_2 and IIICu/SiO_2 made by IW and IE respectively. The catalyst made by IE showed less selectivity to ethyl ester compared to that of acetaldehyde and products resulting from its coupling as shown in Figure 44. This enhanced selectivity could be explained by the lower acidity of the support or the lower abundance of the Cu^+ acidic sites. The pH of the synthesis solution is around 11 for the catalyst made by IE but it is much lower for that prepared by IW. Acidification of support is expected for catalyst made by IW due to the presence of the acidic nitrate groups. In addition to the support acidity, catalyst made by IE had smaller NP size as demonstrated by TEM and CO adsorption as shown in Table 9.

In addition to NP size, the reversibility of CO adsorption on the catalyst made by IE is higher than that made by IW as shown in Table 9. The non-reversible CO adsorption on Cu surface at room temperature can be used as an indication for the presence of Cu^+ sites since the adsorption energy of CO on these sites is higher than that on the Cu^0 sites due to the stronger σ-component of the Cu^+-CO bond, and low stability of the Cu^0-CO π-bond.[208,210,213] This difference in reversibility between the two catalysts suggests that the there is less Cu^+/Cu^0 sites on the catalyst made by IE which may explain its lower selectivity to esterification.

4.3.3. Effect of Cu NP Thermal Treatment on Catalyst Selectivity

Decomposition of Cu precursors of catalysts made by IW in air at 773 K and hydrogen at 573 K led to different catalyst properties. Catalyst oxidized at 773 K (ICu/SiO2) showed significantly higher CO adsorption (almost twice as shown in Table 9) compared to catalyst IICu/SiO_2 which was only reduced at 573 K. Since TEM measurements on both catalysts did not show a noticeable difference in NP size of these two catalysts, it is reasonable to assume that the difference in the CO adsorption capacity is due to the change in either catalyst morphology or oxidation state.

By examining the CO adsorption reversibility on these two catalysts, we can see that the oxidized then reduced catalyst, ICu/SiO_2 showed higher non-reversibility compared to the directly reduced IICu/SiO_2. This is an additional indication that catalyst oxidation at high temperature lead to an increase in the Cu^+ sites relative abundance. In fact, an increase in Cu^+/Cu^0 ratio was observed on

oxidized then reduced Cu NP supported on titania as demonstrated by CO adsorption FTIR in a separate study.[214] XRD of the reduced forms of ICu/SiO_2 and $IICu/SiO_2$ showed only metallic copper peaks, however, this does not eliminate the possibility of the presence of highly dispersed oxidized species not detected by XRD.

Upon testing these two catalyst for ethanol dehydrogenation, it was noticed that catalyst oxidation lead to an increase in overall catalyst activity and ethyl ester yield at the same acetaldehyde yield as shown in Figure 45. The increased esterification activity and CO adsorption upon oxidation can be due to the increase in surface roughness[215] and the increase in the density of under coordinated Cu sites that are able to adsorb CO more strongly. In addition to stronger CO adsorption, it is possible to hypothesize that stronger acetaldehyde adsorption occurs on these sites leading to the acetaldehyde esterification instead of its desorption to the gas phase. Another possible explanation is the formation Cu silicate at higher temperature in oxidizing environment which may favor that formation of positively charged Cu^+ sites as well.

4.3.4. Effect of Cu NP Alloying with Another Metal on Catalyst Selectivity

Since the main side reaction on Cu surface is esterification, it is possible to suppress Cu esterification activity by alloying it with another metal that exhibits different electronegativity from Cu. The degree of alloying of copper with other metals can be predicted from the degree of charge transfer and hence the formed Cu-metal bond strength as explained by Rodriguez and Goodman.[216] In the same review, it was shown that the adsorption energy of CO on Cu on Pt, Rh, and Ru was higher than that of CO adsorption on Cu monometallic surface as indicated by the higher CO desorption temperature.

Doca et al.[217] reported that aliphatic alcohol dehydrogenation activation barrier decreases with increasing catalyst paramagnetisim through alloying Cu with other transition metals with Cu-Fe having the lowest activation barrier followed by Cu- Mn, Cu-Ni, then Cu-Cr. Yin et al.[218] showed that addition of Ni to Cu supported on silica formed a more sintering resident, homogeneous alloy with a lower reduction temperature compared to that of the monometallic catalyst as demonstrated by TPR, however, Ni enrichment occurred after reduction as detected by XPS. Requies et al.[172]

showed a similar decrease in reduction temperature when alloying Cu with Ru, however, NP sintering was more rapid, possibly due to the weakening effect of the Ru on the Cu-support interaction. The performance of the bimetallic NP was found to be affected by the sequence of the two metals loading as well where sequential Pd-Cu metal loading led to a catalyst with different properties from that prepared by simultaneous loading.[202]

From this brief review, it can be concluded that careful selection of the second metal identity, ratio, and loading method are required to optimize catalyst performance. Here we show the performance of three bimetallic NP supported on silica, namely Cu_3Ag_1/SiO_2, Cu_3Pd_1/SiO_2, and $Cu_{10}Au_1/SiO_2$. The first two alloys were made by IW and reduced directly, while the last one was made by IE. Low CO adsorption was observed on these alloys as shown in Table 9.

Despite not being oxidized at high temperature, the CO adsorption was not fully reversible (only 82%) on Cu_3Pd_1/SiO_2 indicating the presence of strongly adsorbing sites on the surface, possibly these of Pd since monometallic Pd showed very high non-reversibility as shown in Table 9. Assuming that all the non-reversibly adsorbing sites on this alloy are Pd sites and Pd reversible adsorption is 25% as shown in Table 9, we can calculate that the Pd/Cu ratio on the surface is 25.7% which is identical to the bulk ratio of these two metals as measured by ICP-OES. This is an indication of high miscibility and strong alloying effect of these two metals together in the nanoscale unlike what is expected from their bulk miscibility.[219] EDS on one NP of this catalyst confirmed the alloying effect where both signals of Pd and Cu changed monotonically across the particle diameter as shown in Figure 46 with no enrichment signs across the diameter. Similar alloying effect between Pd and Cu NP on alumina was reported using CO adsorption FTIR.[202]

Ag and Cu, on the other hand, are completely immiscible[220] at synthesis temperatures and a high charge transfer is unlikely in this bimetallic system and hence alloy formation is difficult. EXAFS study of Ag-Cu bimetallic supported NP showed the formation of Ag nanoclusters supported on the Cu NP under similar reaction conditions.[221] A complete reversibility of CO adsorption on this alloy was measured which is not surprising since Ag does not adsorb CO and the presence of Cu^+ is minimal because catalyst was reduced directly without oxidation. Au, on the other hand, has better miscibility with Cu than Ag.[222] Della Pina et al. [179] reported the disappearance of Cu peak

on XRD of the reduced samples of supported Au-Cu catalyst as an indication of the formation of AuCu alloy which was found to be more selective and active towards benzyl alcohol oxidative dehydrogenation to benzaldehyde compared to the monometallic NP.

Ethanol dehydrogenation selectivity of the bimetallic NP catalysts is shown in Figure 47 where the ratio of ethyl ester to acetaldehyde and its coupling products is reported at various ethanol conversions. The three alloys were found to yield less ethyl ester to acetaldehyde and its coupling products including butyraldehyde and butanol compared to monometallic Cu, however, the addition of foreign metals to the catalyst leads to promotion of other side reactions in addition to esterification as shown in Table 10. For example, addition of Ag and Au was found to favor the formation of C-C bonds through acetaldehyde aldol condensation leading to the formation of butyraldehyde which gets hydrogenated on the metal surface to butanol. The reason for why the activity of C-C formation increases relative to the esterification C-O bond formation going from Cu to Ag and Au could be due to the difference in atomic radii of these three elements. The distance between Cu atoms is shorter than that of Ag and Au and hence the energy of the transition state of the C-C and C-O bonds are expected to be different on these surfaces. No explicit study that we are aware of tackles this hypothesis and hence further investigation is required.

Pd-Cu alloy, on the other hand, was found to catalyze decarbonylation of the formed aldehyde resulting in a decrease in the acetaldehyde selectivity even below that achieved on the monometallic Cu NP. This decarbonylation activity can be attributed to the presence of Pd surface sites able to adsorb acetaldehyde in the η^2 mode as described above. In addition to decarbonylation, the Pd-Cu alloy was found to catalyze diethyl ether formation. Etherification was also catalyzed on large NP size monometallic Pd/SiO_2 (data not shown) where large ensembles were found to have higher selectivity to this reaction due to their ability to accommodate an adsorbed alkoxide adjacent to η^2 adsorbing aldehyde as proposed by Pham et al.[197] The fact that ethers apparently do not form on the 1 nm Pd/SiO_2 catalyst made by IE is probably because they are too small to accommodate required species or that the presence of highly coordinated Pd sites is low. The formation of ethers on Cu-Pd alloy but not on Cu or Pd can be explained by the ability of the alloys surface to accommodate both species required for etherification. Etherification was also detected

on Ag-Cu and Au-Cu alloys possibly due to the increase in NP size of the alloys compared to the Cu monometallic NP and the higher electronegativity of Ag and Au compared to Cu.

From these results it can be concluded that the Cu-Au alloy is the only alloy that shows an additional advantage to the monometallic Cu NP on silica. Other possible alloys that are not tested here are Cu-Ni and Pt-Au. Both alloys were tested for butanol dehydrogenation by Van der Burg et al. [185] and the fist was found to be still active for decarbonylation at high Cu content while the latter was active for etherification at high Au content. This is not surprising since CO FTIR showed that the electronic effect of Ni alloying with Cu is almost negligible[223] suggesting that the metallic sites behavior in these alloys is not be very different from that of the sites on their monometallic surfaces defeating the purpose of alloying.

In addition to alloying Cu with group 10 and 11 metals, addition of Zn or Cr to supported Cu NP is frequently attempted to overcome Cu NP sintering,[169,180,224,225] a problem that is commonly reported for Cu based catalysts.[226] Zn and Cr are selected due to their ability to form solid solution with Cu since their electronegativity and atomic radii are close to Cu as demonstrated by their position in the Darken-Gurry domain of copper alloys.[227] In addition to its stabilizing effect, increasing Zn content in Cu NP supported catalyst was found to lower the Cu reduction peak as demonstrated by TPD[169] but also increased the Cu^{+}/Cu^{0} ratio.[180] Besides Zn and Cr, doping with other metals was attempted to modify Cu NP properties. Acidic boric oxide, for example, was found to have a stabilizing effect on Cu/SiO_2 catalyst but due to its high electron affinity it tends to make Cu reducibility more difficult and increases the presence of Cu^{+} sites as well[226] from which, an increase in esterification would be expected in this case. Basic MgO, on the other hand, was found to have a positive effect on catalyst activity[228] which can be attributed to the stabilizing effect of MgO on Cu NP. Interestingly, it was reported in the same study that promotion with oxides of higher basicity than MgO such as CaO, SrO, or BaO had a negative effect on catalyst stability. This later conclusion contradicts the enhancement in n-butanol dehydrogenation selectivity and activity that was reported for Cu NP promoted with Ba[171] making it difficult to predict the effect of addition of these metals on catalyst performance.

Here we show the effect of addition of both Zn and Cr to Cu NP catalysts in catalysts $Cu_{10}Zn_1/SiO_2$ and $Cu_{10}Cr_1/SiO_2$ respectively. As shown in Figure 48, addition of these elements reduced ethyl ester selectivity versus acetaldehyde selectivity and its coupling products compared to monometallic Cu NP. Despite this suppression in the relative ethyl ester selectivity, the acetaldehyde absolute selectivity did not change significantly by addition of these two elements as shown in Table 11. This can be attributed to the promotion of other acid-base catalyzed reactions such as etherification, ketonization and C-C coupling formed on the nano size particles of Zn and Cr oxides formed from addition of these two elements. From the shown data it can be concluded that while addition of Zn or Cr may have stabilizing effect on the Cu NP, addition of these two metals is not expected to enhance the overall acetaldehyde selectivity of the catalyst. In fact, over promotion of the catalyst with these two elements can lead to a decrease in acetaldehyde selectivity due to the promotion of the Zn and Cr oxides to acid-base catalyzed reactions. Similar conclusion regarding the detrimental effect of the over promotion of Cu catalyst with Cr was reported by Tu et al.[225]

4.3.5. Effect of Cu NP Support Properties on Catalyst Selectivity

The catalytic properties of Cu NP depends on the support acid-base properties as well as its reducibility, for example, Cu supported on MgO was found to be more selective towards dehydrogenation of 2-butanol to 2-butanone compared to Cu supported on silica, where dehydration to butenes was the main side reaction.[187] Cu supported on Cr and Mg oxides were found to have slower dehydrogenation rate compared to that supported on silica which was attributed to the stronger interaction of the former oxides with the metallic catalyst. Cu supported on highly reducible CeO_2 showed lower reduction peak temperature compared to that supported on less reducible TiO_2 or ZrO_2.[172] Also the formation of Cu^+ sites on catalysts made by ammonia evaporation was found to be affected by the support where the ratio of Cu^+/Cu^0 was found to follow this order $SiO_2>>Al_2O_3>ZrO_2>TiO_2$.[208] Also XPS on Cu supported on MgO showed that the presence of Cu^+ species was minimal compared to that supported on silica which lead to higher selectivity towards 1-octanol dehydrogenation to 1-octanal.[173]

In addition to affecting the Cu sites oxidation state and reducibility, nonmetallic active sites on the support itself can catalyze other reactions as discussed earlier. For example, despite the fact that the presence of Cu^+ sites is low on ZrO_2 as demonstrated by CO adsorption reversibility[208] and XANES,[210] esterification was found to be high on Cu NP supported on ZrO_2 due to the high support acidity.[112,210] From this brief review, it can be concluded that using different support than silica to suppress the Cu^+ formation does not always lead to a decrease in esterification activity, and careful selection of the support is required in this case. Here we show the performance of Cu NP supported on supports with different acid-base properties including amorphous silica, magnesia, anatase titania, activated carbon, γ alumina, and unsupported Cu powder as reported in Figure 49.

Cu NP supported on alumina showed the highest relative esterification selectivity followed by silica while NP supported on magnesia, titania, and carbon did not show any significant esterification. This is in agreement with the acid catalyzed esterification mechanism where high Lewis acidity of Al^{3+} sites or Cu^+ sites act as the active sites in synergy with the metallic Cu^0 sites. This conclusion is in agreement with that reported by Santacesaria et al. on chromia and alumina.[229] It is worth mentioning here that the supports that showed high esterification are the same supports that showed high non-reversibility in CO adsorption at room temperature as shown in Table 9 indicating that Cu^+ abundance and esterification are linked together. An in situ XANES experiment is planned for Cu NP supported on different supports to verify the effect of support on the Cu^+ formation.

It is necessary to mention here that on the supports that didn't form esters, high acetaldehyde aldol condensation selectivity was detected such as in the case of TiO_2, MgO, and carbon, as shown in Table 12, which reduced the absolute acetaldehyde selectivity on these oxides. As conversion increases, higher molecular weight, non-volatile, aldehydes and alcohols formed through this reaction cause catalyst deactivation. Also Cu sintering is more rapid on these supports compared to silica and alumina as demonstrated by CO adsorption and reported in other studies as well.[187] One the other hand, the fact that unsupported Cu powder was the most selective for acetaldehyde is an additional proof that supports in general have negative effect on the acetaldehyde selectivity no matter how inert they are.

Unsupported Cu catalysts are possible to be used, however, their stability is lower than supported NP due to rapid deactivation. Other studies reported comparable methanol dehydrogenation initial rates on Cu supported on silica and Raney Cu.[230] However, a more rapid deactivation occurred on Raney Cu which was attributed to the aldehyde polymerization on the surface. The reason for why large Cu surface with high average coordination number, such as in the case of Raney Cu, is more active towards aldehyde polymerization compared to dispersed Cu NP is not clear, however, it is possible that the coverage density of the aldehyde is larger on Raney Cu and hence the polymerization probability is higher. Another study for ethanol dehydrogenation on Cu catalyst promoted with Cr indicated that while ethanol dehydrogenation was a first order reaction, deactivation was second order[225] which is an additional evidence of deactivation due to dimerization of aldehyde products. In a different study,[215] Cu foam was used as catalyst for ethanol dehydrogenation and its performance was compared to supported Cu catalysts. It was found out that pre-oxidation is required to activate the copper foam by increasing surface roughness but rapid deactivation was again reported on this type of catalyst which was attributed to surface reconstruction due to reduction under reaction conditions. Unsupported Raney nickel coated with copper was found to catalyze ethanol dehydrogenation to acetaldehyde but also acetaldehyde decarbonylation to methane and carbon monoxide.[231] Despite the high Cu content of this catalyst coating (28%), nickel core had a strong effect on the product selectivity since decarbonylation is known to be catalyzed by nickel not copper. More efforts are needed to develop a stable unsupported Cu that does not rapidly lose its activity during operation.

4.3.6. Effect of K Doping on Catalyst Selectivity

Addition of K was found to block Lewis acid sites and reduce the esterification reaction as shown in Table 12. Similar effect was reported by the reduction in etherification rate on metal surfaces by alkali metal additoion.[185] It can also be seen that the selectivity towards other acid catalyzed reaction such as dehydration and etherification was decreased by K addition, however, an increase in C-C formation products was seen possibly due to the formation of basic sites by K addition. Addition of high amount of K to catalyst can reduce acetaldehyde selectivity by increasing aldol products selectivity and hence an optimization of K/support ratio is required.

4.3.7. Effect of Cu NP Size on Catalyst Selectivity

In addition to oxidation state and support effect, NP size is known to affect catalyst properties. It is important to notice that oxidation state, support effect, and NP size are all linked properties[232] and it is difficult to separate one factor from the others during catalytic testing experiments. Sad et al.[101] reported that increasing Cu NP size increased specific esterification turnover rate, however, in this study, the Cu^{+}/Cu^{0} ratio was not reported and hence, it is not possible to link the particle size to the Cu^{+} abundance. It is worth mentioning here that Cu surface area is frequently measured by N_2O dissociation,[233] however, this method only counts for Cu^{0} metallic sites and hence it can give a faulty low dispersion in case of high Cu^{+}/Cu^{0} ratio which can be the case in the aforementioned study.

In this study we show the effect of changing silica supported Cu NP size, as measured by CO adsorption, on ethanol dehydrogenation selectivity. Similar conclusion to that of Sad et al was observed as shown in Figure 50, the larger the Cu NP, the higher the esterification relative selectivity. This increase in esterification activity on larger Cu NP was attributed to the lower activation barrier of the C-O bond formation on the highly coordinated Cu sites on large NP. This contradicts the findings from this study where almost no esterification at all is reported on the unsupported Cu powder, which if the coordination number-activation barrier argument was valid, should show the highest esterification selectivity.

This difference in selectivity between the unsupported Cu powder and the supported Cu NP suggests that the reported increase in esterification activity is mainly due to the change in Cu oxidation state more than the change in Cu average coordination number. Since the larger Cu NP were optioned by increase the thermal treatment temperature, it can be assumed that the high temperature favored the formation of the copper silicate, or the Cu-O-Si bonds, which results in the formation of partially charged Cu species. It is difficult to prove this theory without more in deep analysis including in situ XANES on different size Cu NP measured by TEM, an experiment that is planned to be conducted.

4.3.8. Cu^{+}/Cu^{0} REDOX Formation Cycle

Despite being proved that Cu^{+} species are responsible for ester formation, it is not clear why increasing reduction temperature does not eliminate esterification. One possible explanation for this is the back oxidation of a portion of the surface Cu sites under reaction conditions where oxygenates like ethanol, acetaldehyde, and ester can potentially oxidize the reduced Cu sites on the Cu NP surface. A similar hypothesis was proposed for ester hydrogenation on Cu by Ma at al.[234] where a dynamic redox cycle is thought to occur under reaction conditions where oxygenates act as oxidizing agents and hydrogen act as a reducing agent. At any time under these conditions, an equilibrium ratio of Cu^{+}/Cu^{0} is achieved as shown in Figure 51.

TPR done on reduced catalyst after exposure to ethyl ester and evacuation showed a reduction feature indicating catalyst oxidation by ester and confirming this hypothesis.[234] An in situ XANES experiment is planned to further investigate this redox effect under reaction conditions and show how the equilibrium position changes with support, particle size, and other catalyst parameters.

4.4. Conclusion

Cu is the most selective catalyst for ethanol dehydrogenation among group 10 and 11 metals. Increase in catalyst acidity, due to formation of oxidized Cu species or using acidic support, was found to increase esterification activity and reduce acetaldehyde selectivity. Cu loading on silica at high pH using IE method was found to give more selective catalyst than that made by IW. Oxidation of Cu at high temperature was found to increase its CO adsorption strength and esterification activity. Alloying Cu with Pd or Ag reduced esterification activity but increased decarbonylation, etherification, and aldolization activity. Au-Cu alloy prepared by sequential loading was found to surpass monometallic Cu NP in terms of acetaldehyde selectivity. Addition of Cr or Zn reduced esterification but oxides of these two metals can promote other acid-base reactions and reduce acetaldehyde selectivity. Replacing silica with more basic oxides lead to a decrease in esterification selectivity and an increase in aldolization selectivity. This catalyst was found to be less stable on basic supports due to more rapid sintering and coking. Addition of K to acidic supports reduced, but did not eliminate, esterification. Larger Cu NP were found to be less

selective to acetaldehyde formation while unsupported Cu powder was found to be the most selective catalyst out of all the catalysts tested in this study.

4.5. Figures and Tables

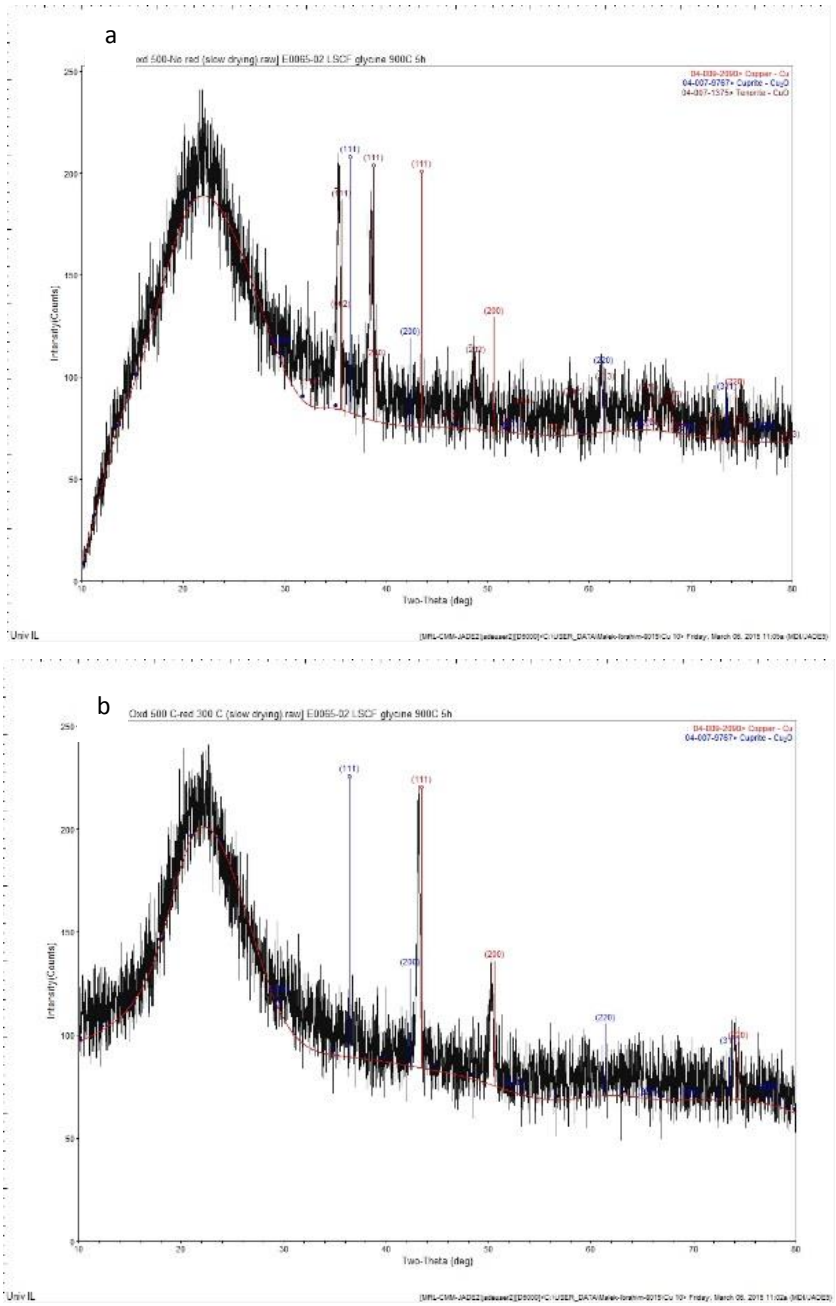

Figure 40 (a). XRD of 28%wt Cu/SiO_2 oxidized sample at 773 K. **(b).** XRD of 28%wt Cu/SiO_2 reduced sample at 553 K

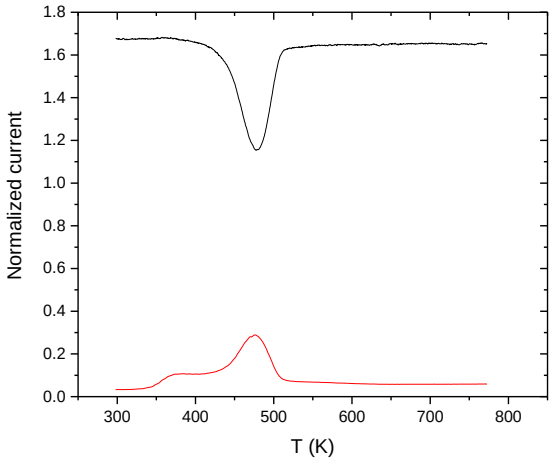

Figure 41. TPR of ICu/SiO_2 catalyst from room temperature to 773 K in 10%H_2 bal. He, ramp rate 5 K.min^{-1}. Black, M/Z=2, Red, 18=M/Z

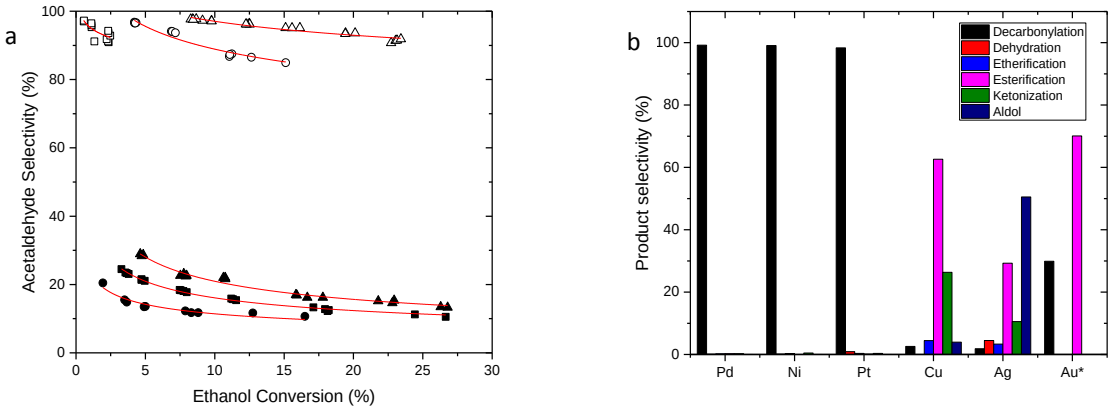

Figure 42 (a). Ethanol dehydrogenation selectivity to acetaldehyde on 15 mg ICu/SiO_2 (Δ), 1 g Ag/SiO_2 (○), 2.5 g Au/SiO_2 (□), 19 mg Ni/SiO_2 (■), 15 mg Pd/SiO_2 (▲), and 157 mg Pt/SiO_2 (●). **(b).** Side products distribution at 10% ethanol conversion at 3 kPa EtOH, 15 kPa H_2, bal. He, and 503 K reaction temperature. * Au selectivity data is at 8% conversion

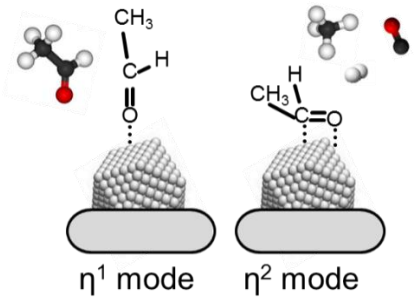

Figure 43. Different acetaldehyde adsorption configurations on metal surfaces

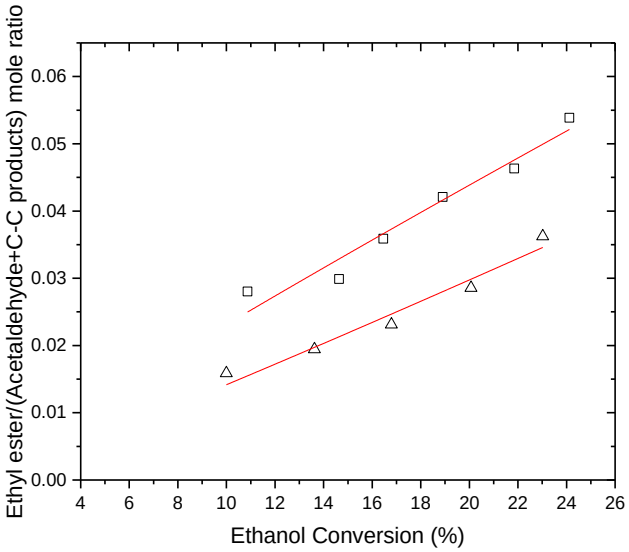

Figure 44. Ethyl ester relative selectivity on $ICuSiO_2$ (□), and $IIICu/SiO_2$ (Δ) at 3 kPa EtOH, 15 kPa H_2, bal. He, and 503 K reaction temperature

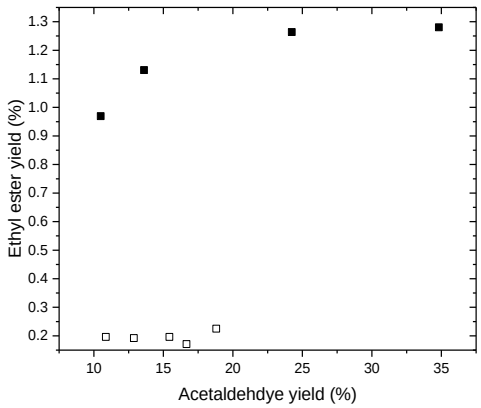

Figure 45. Ethyl ester relative selectivity on $ICuSiO_2$ (■), and $IICu/SiO_2$ (□) at 3 kPa EtOH, 15 kPa H_2, bal. He, and 503 K reaction temperature

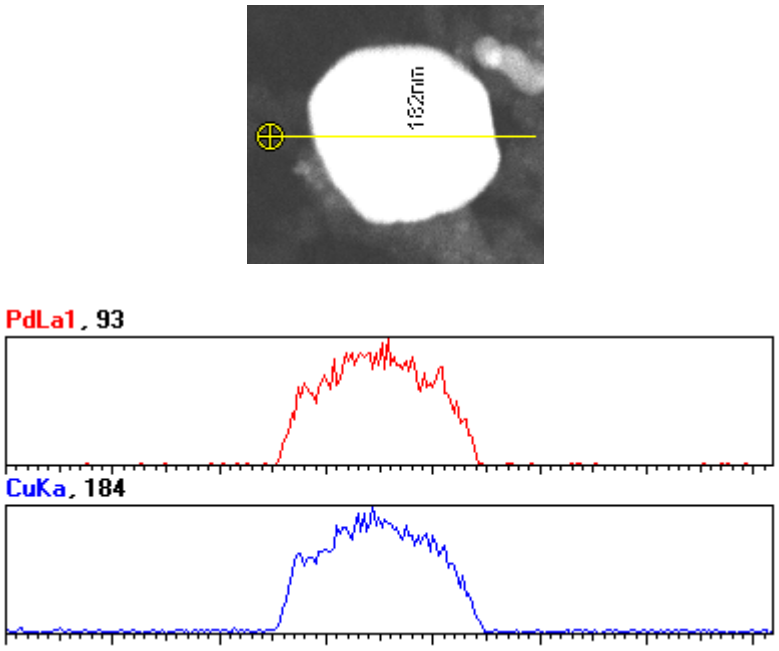

Figure 46. EDS of Pd and Cu signal across Cu_3Pd_1/SiO_2 NP diameter

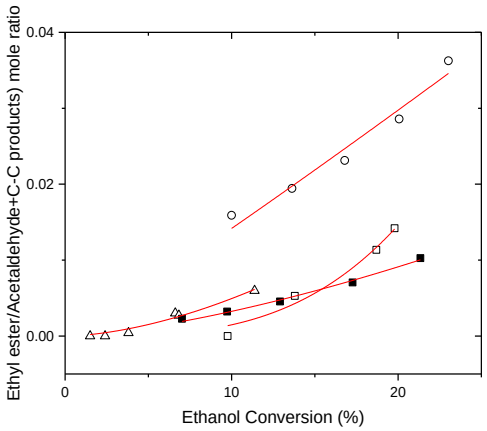

Figure 47. Ethyl ester relative selectivity on 70 mg Cu_3Ag_1/SiO_2 (Δ), 70 mg Pd_1Cu_3/SiO_2 (■), 15 mg $Cu_{10}Au_1/SiO_2$ (□), 47 mg ICu/SiO_2 (○) at 3 kPa EtOH, 15 kPa H_2, bal. He, and 503 K reaction temperature

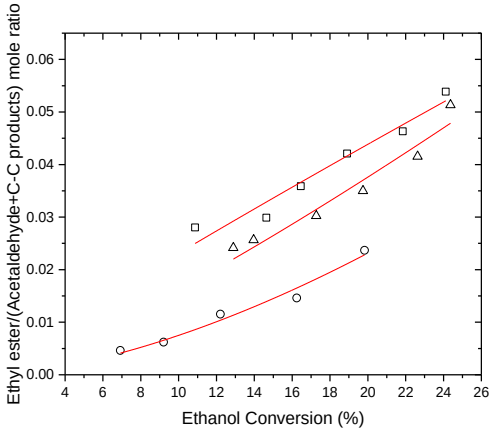

Figure 48. Ethyl ester relative selectivity on 52 mg $Cu_{10}Zn_1/SiO_2$ (Δ), 19.5 mg $Cu_{10}Cr_1/SiO_2$ (○), 47 mg ICu/SiO_2 (□) at at 3 kPa EtOH, 15 kPa H_2, bal. He, and 503 K reaction temperature

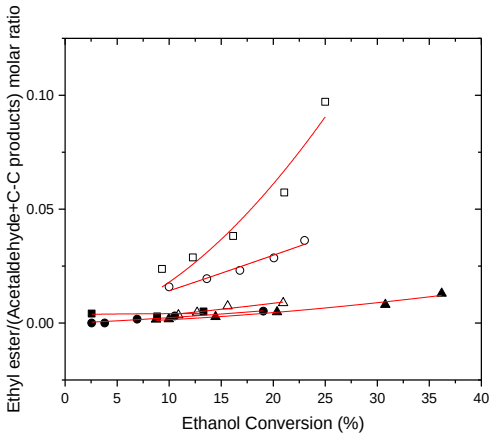

Figure 49. Ethyl ester relative selectivity on 13 mg Cu/Al_2O_3 (□), 35 mg Cu/MgO (●), 105 mg Cu/C (■), 15 mg IIICu/SiO_2 (○), 100 mg Cu/TiO_2 (▲), and 311 mg unsupported Cu powder (Δ) at 3 kPa EtOH, 15 kPa H_2, bal. He, and 503 K reaction temperature

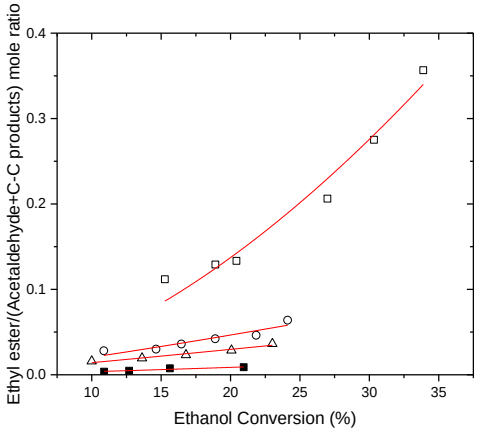

Figure 50. Ethyl ester relative selectivity on different size Cu NP supported on silica 20 nm, 4.6 nm, 3 nm, unsupported Cu powder at 3 kPa EtOH, 15 kPa H_2, bal. He, and 503 K reaction temperature

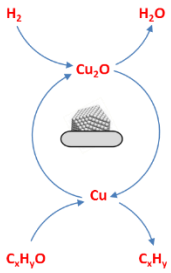

Figure 51. Scheme of Cu oxidation-reduction cycle under ethanol dehydrogenation reaction conditions

Table 9. Metal NP catalysts design parameters and properties

Catalyst	Metal (%wt)	Loading method	Oxidation T (K)	Reduction T (K)	d[a] nm	CO uptake µmol.mol^{-1}	d[b] nm	CO ads. Reversibility
ICu/SiO_2	2	IW	773	573	4.3	39,000	5.7	80
IICu/SiO_2	2	IW	--	573	4.7	22,000	10.3	100
IIICu/SiO_2	2	IE	773	573	2.8	86,000	2.6	96
Ag/SiO_2	2	IW	773	573	4.9	--	--	--
Au/SiO_2	2	IW	773	573	--	--	--	--
Ni/SiO_2	0.5	IE	773	573	--	466,00	1.9	--
Pd/SiO_2	0.5	IE	773	573	--	900,000	1	25
Pt/SiO_2	0.5	IE	773	573	--	117,000	7.7	--
Cu/Al_2O_3	2	IE	773	573	--	56,000	4.0	85
Cu/MgO	2	IW	773	573	--	--	--	--
Cu/TiO_2	0.28	IE	773	573	7.7	55,000	4.1	100
Cu/C	2	IW	773	573	--	--	--	--
Cu_3Pd_1/SiO_2	2	IW	--	573	25	9,000	42.6	82
Cu_3Ag_1/SiO_2	2	IW	--	573	--	23,000	9.71	100
$Cu_{10}Au_1/SiO_2$	2	IE	773	573	--	8,000	27	--
$Cu_{10}Zn_1/SiO_2$	2	IW	773	573	--	35,200	6.4	--
$Cu_{10}Cr_1/SiO_2$	2	IW	773	573	6.0	22,000	10.3	--

a: NP diameter measured by TEM, b: NP diameter measured by CO adsorption

Table 10. Ethanol dehydrogenation products selectivity on bimetallic NP supported on silica at 10% ethanol conversion

	Acetaldehyde	Methane	Ethane+ ethylene	Diethyl ether	Ethyl ester	Ketones	C-C products
Cu_3Ag_1	92.01	0.30	0.25	2.28	0.58	1.26	3.32
Cu_3Pd_1	94.73	4.32	0.00	0.22	0.30	0.20	0.23
$Cu_{10}Au_1$	100.00	0.00	0.00	0.00	0.00	0.00	0.00
Cu	97.09	0.00	0.00	0.13	1.94	0.75	0.09

Table 11. Ethanol dehydrogenation products selectivity on silica supported NP promoted with Zn and Cr

	Acetaldehyde	Methane	Ethane+ ethylene	Diethyl ether	Ethyl ester	Ketones	C-C products
$Cu_{10}Zn_1/SiO_2$	94.78	0.07	0.07	0.22	2.64	2.04	0.18
$Cu_{10}Cr_1/SiO_2$	95.15	0.14	0.06	0.97	1.41	1.22	1.07
ICu/SiO_2	93.98	0	0.05	0.22	3.42	2.00	0.34

Table 12. Ethanol dehydrogenation products selectivity on Cu NP supported on different supports and modified with K

	Acetaldehyde	Methane	Ethane+ ethylene	Diethyl ether	Ethyl ester	Ketones	C-C products
Cu/Al_2O_3	84.58	0.00	0.53	8.99	2.45	1.97	1.47
Cu/MgO	94.09	0.24	0.00	0.00	0.28	0.65	4.74
Cu/C	90.18	0.21	0.00	0.48	0.40	0.70	8.03
Cu powder*	98.36	0.08	0.00	0.10	0.33	1.13	0.00
$IIICu/SiO_2$	96.62	0.00	0.16	0.15	1.59	1.34	0.14
Cu/TiO_2	93.21	0.00	0.11	0.21	0.24	0.38	5.86
$K\text{-}Cu/Al_2O_3$	93.64	0.27	0.00	1.52	1.18	1.29	2.10
$K\text{-}Cu/SiO_2$	98.35	0.10	0.00	0.00	0.72	0.08	0.75

*Mixed with silica

Chapter 5: Ethanol Guerbet Reaction Engineering on Heterogeneous Bifunctional Catalysts

5.1. Introduction

Butanol and longer chain alcohols are more suitable as liquid fuels compared to ethanol due to their superior physical properties[16,235], however, it is more economic to produce ethanol from biomass fermentation.[236] Catalytic conversion of ethanol to butanol and longer chain alcohols allows high efficiency conversion of biomass feed and high quality of fuel product at the same time.

Ethanol, being an alcohol with a hydrogen atom attached to α carbon, can undergo the Guerbet reaction to from butanol through a multistep reaction that involves dehydrogenation to acetaldehyde, aldol condensation of acetaldehyde to crotonaldehyde, and hydrogenation of crotonaldehyde to butanol as described in chapter 3. This reaction can be catalyzed by either homogeneous or heterogeneous catalysts, however, the heterogeneous catalysts option provides additional advantages by reducing operation pressure, equipment cost, and eliminating the need for catalyst separation and product purification which are estimated to form around 30% of the Guerbet alcohols price produced by homogeneous catalysts.[23,237-239]

The need for renewable fuels production in a green and economically feasible way increased the interest in designing catalyst and process for catalytic conversion of ethanol to longer chain alcohol using heterogeneous catalysts.[237,240] This chapter incorporates the findings from the previous four chapters along with knowledge from traditional oil refining to engineer a catalyst and a process for ethanol catalytic conversion to butanol and longer alcohols with the ability to control product properties.

5.2. Materials and Methods

5.2.1. Catalysts Preparation

Anatase titanium oxide (TiO_2, Aldrich, 99.8%) was washed with deionized water (17.9 MΩ resistivity), dried in static air at 343 K overnight, then treated in flowing dry air (S.J. Smith, Ultra Zero) by heating to 773 K at 3 K min^{-1} and holding for 8 h. Samples were cooled down to room temperature, pelletized, and sieved to size range of 35-60 mesh. Cu supported NP were prepared on silica gel (Sigma-Aldrich, Davisil Grade 646) as following; prior to metal loading, silica was washed thoroughly with deionized water, dried in static air at 343 K overnight, then treated in flowing dry air (S.J. Smith, Ultra Zero) by heating to 773 K at 3 K min^{-1} and holding for 12 h. Samples were cooled down to room temperature, pelletized, and sieved to size range 35-60 mesh to avoid mass transport and channeling effects.[187]

Cu NP supported titania and silica were prepared by IE. Cu aqueous solutions was prepared from $Cu(NO_3)_2.2.5H_2O$ (Aldrich, 99.99%) dissolved in 1N NH_4OH (Macron, 28-30% NH_3) aqueous solution to form the copper amine precursors[188]. The solution was added to the support in a ratio of 60 ml g^{-1} and stirred at room temperature for 24 h then filtered and washed with deionized water. Catalyst was then dried overnight and oxidized in flowing dry air by heating to 773 K at 3 K min^{-1} and holding for 6 h. Samples were cooled down to room temperature before being reduced in a 30 kPa H_2 (S.J. Smith, 99.99%), 71 kPa He (S.J. Smith, 99.99%) flowing at 350 cm^3 min^{-1} while heated to 573 K at 3 K min^{-1} and held for 6 h. Prior to exposure to atmospheric air, samples were cooled down and passivated with flowing 5% air, bal. He at 200 cm^3 min^{-1} for 30 min. Samples were labeled as IIICu/SiO_2, and Cu/TiO_2, as shown in Table 9.

5.2.2. Catalysts Characterization

TiO_2 BET surface area was measured by Micromeritics Company using multipoint N_2 physisorption. Measured surface area is reported in Table 2. The Cu content of the catalysts was verified using Inductively Coupled Plasma-Optical Emission Spectroscopy (ICP-OES, PerkinElmer 2000DV) while the NP size was measured using Transmission Electron Microscopy

(TEM, JEOL 2010LaB_6, 200 kV, bright field mode, single tilt holder) where samples were ground and sonicated in methanol before being dispersed on "holey carbon" Cu grids. Diameter of 500 particles was measured and the algebraic mean was determined as the average particles size. The crystalline phases of the heat treated TiO_2 and reduced Cu NP catalysts were measured at room using X-ray diffraction XRD (Bruker D-5000, Cu K- α radiation, 40 kV).

CO chemisorption was used to quantify the number of exposed metallic sites and measure NP size at room temperature. Known amount of the catalyst was loaded in a U-tube glass cell and vacuumed overnight. Catalyst was in situ reduced for 1 hr under the reduction conditions specified above then vacuumed at 573 K before being cooled down to room temperature under vacuum. The available cell volume for gas expansion was measured by the change in helium pressure due to expansion assuming that no helium adsorption occurs. Carbon monoxide (S.J. Smith, 99.99%) was dosed to the cell in known quantities using an in-house built dosing system where the pressure before and after adsorption was measured. From the difference in pressures and the measured expansion volume, the amount of CO adsorbed was calculated using ideal gas low.

Adsorption isotherm was developed for each catalyst sample and the surface saturation value was used to estimate the NP surface area. The adsorption ratio of CO molecule to metallic surface atom was assumed as 1:4[189] CO:Cu, and 0:1 ratio was assumed for metal oxides supports. The surface area of the Cu clusters was calculated assuming surface density of 1.47×10^{19} atoms.m^{-2} which is the arithmetic mean value of the Cu(111), Cu(110), and Cu(100).[107]

5.2.3. Conversion, Selectivity, and Turnover Rate Measurements

Reaction rates were measured using a quartz tubular reactor (0.5 in. o.d.) with plug flow hydrodynamics, which is contained within a three-zone electrically heated furnace (Applied Test Systems) controlled using an electronic PID controller (Watlow, EZ-Zone®) as described in Figure 2. The bed temperature was measured with a type K thermocouple touching the outer surface of the tube at the catalyst bed position. Catalysts were mixed with additional quartz SiO_2 to optimize reactant mixing with catalyst. Inertness of the quartz powder was tested at 633 K and no measurable reactions were observed.

Prior to the experiment, catalyst was in-situ treated in 30 kPa H_2 (S.J. Smith, 99.99%), 71 kPa He (S.J. Smith, 99.99%) flowing at 200 cm^3 min^{-1} for 1 h at 773 K then cooled down to the experiment temperature. All pretreatments and experiments were done at ambient pressure. The volumetric flow rates of gaseous feed components were controlled using calibrated mass flow controllers (Parker, MFC 600) while liquid components; ethanol (Decon, 200 Proof), acetaldehyde (Sigma Aldrich, 99.5%), and deionized water were injected using two programmable syringe pumps (KD Scientific, Legato 110). Liquid feeds were injected to heated transfer lines by means of heat tape set at 393 K while reactor effluent lines were kept heated at 473 K to prevent high boiling point components condensation.

Reactor effluent was cooled and bubbled in ethanol to capture liquid products and injected to an offline gas chromatography coupled with a mass spectrometer (Shimadzu, 2010 GC-MS) to identify the formed products. The quantitative analysis was determined using an online gas chromatography (Agilent, HP 6890) equipped with a capillary column (Agilent, J&W HP-PLOT Q, L = 30 m, ID = 0.32 mm, film thickness = 20µm) connected to a flame ionization detector (FID) to detect hydrocarbons and oxygenates and a packed column (Restek, HayeSep Q, L = 2m, ID = 2 mm) connected to a thermal conductivity detector (TCD) to detect H_2, CO, CO_2, and H_2O.

The retention time for each component was determined by injecting prepared standard solutions of the following liquid chemicals in ethanol; 2-butanone (Supelco, analytical standard), 2-ethyl-1-hexanol (Fluka, analytical standard), 2-ethyl-1-butanol (Aldrich, 98%), 2-ethyl-2-hexenal (Aldrich^{CPR}), butyraldehyde (Fluka, 99%), butanol (Fisher, ACS grade), octanol (Alfa Aesar, 99%), hexanol (Sigma Aldrich, 98%), crotyl alcohol (Aldrich, 96%), hexanal (Aldrich, 98%), crotonaldehyde (Aldrich, 99%), acetone (Macron, ACS grade), Acetic acid (J.T. Baker, ACS grade). Retention time calibration for gaseous products were done by injecting gas mixture standards (Supelco, analytical standard) containing carbon monoxide, carbon dioxide, methane, ethane, ethylene, acetylene (1w/w% in N_2), propane, propylene, and butane (15 ppm in N_2).

Turnover rates were measured under differential conditions (<10% reactant conversion) to minimize the effect of reactant depletion on measured rates. Turnover rates are reported as moles

of ethanol converted per minute per meter square surface area of the catalyst while selectivity and conversion are defined as following:

$$Product\ Selectivity(\%) = \frac{mole\ ethanol\ converted\ to\ product}{moles\ ethanol\ converted} X\ 100$$

$$Conversion(\%) = \frac{mole\ ethanol\ in - mole\ ethanol\ out}{mole\ ethanol\ in} X\ 100$$

5.3. Results and Discussion

5.3.1. Bifunctional Catalyst Design

From the detailed mechanistic study of the ethanol Guerbet reaction described in Chapter 3, it can be concluded that the reaction proceeds through a multistep mechanism where the identity of the active sites required for the initial dehydrogenation and final hydrogenation steps is different from that required for the intermediate aldol condensation step. This difference in active sites identities lead to the development of bifunctional catalyst concept where a metal function catalyzes the dehydrogenation and hydrogenation reactions while a metal oxide catalyzes the aldol condensation reaction.

The findings from Chapter 2 and 3 can be used as guidance for selecting the suitable metal oxide function to achieve high aldol condensation selectivity. In general, a hydrothermally stable metal oxide with mild acid-base properties and low reducibility is more suitable as a catalyst for this chemistry. Catalysts with these properties include oxides of titanium, hafnium, scandium, yttrium, lanthanum and possibly other lanthanides such as praseodymium and neodymium. In addition to these metal oxides, mixed metal oxides in perovskite or spinel structure[16,241] can be also used since they allow more tunable acid-base properties by adjusting the ratio of the two metals in the oxide. The main drawback of mixed metal oxides is the potential formation of separate phase of mono-metal oxide that exposes strong acid or base sites that can harm product selectivity.

It was also concluded in Chapter 4 that copper based catalysts, either in the form of copper powder or copper NP supported on non-acidic supports and modified with gold, chromium, and potassium,

are good catalyst for alcohol dehydrogenation without excessive alcohol etherification, esterification, or aldehyde decarbonylation. It is proposed here that combining these two functions together allows low temperature, selective, and stable conversion of ethanol to longer chain alcohols.

In addition to optimizing catalyst individual functions, the way how these two functions are combined also needs to be optimized. One way for combining the two active functions is to perform simultaneous dehydrogenation, aldolization, and back hydrogenation all on one catalyst bed that contains both functions. Another way is to perform two or all of the reaction main steps sequentially on a dedicated monofunctional catalyst bed for each step. The following sections highlights the advantages and disadvantages of each option.

5.3.2. Simultaneous Reactions Configuration

Simultaneous ethanol dehydrogenation, aldol condensation, and produced aldehydes hydrogenation can be performed by passing ethanol vapor on a catalyst bed that consists of either copper based catalyst mechanically mixed with the aldolization metal oxide or through supporting the copper NP on the aldolization metal oxide where the metal oxide in the latter case acts as both Cu NP support and aldol condensation catalyst. To evaluate the performance of these two configurations, Cu NP supported on anatase titania was tested at the same conditions as Cu NP supported on silica mechanically mixed with titania. As shown in Figure 52a, changing reaction temperature changed the C-C products selectivity along with the acetaldehyde-ethanol pool conversion to other products. It can be seen from Figure 52a that Cu NP supported on titania gives better selectivity and high conversion at the same time.

As described in Chapter 3, C-C products selectivity increases as the ratio of acetaldehyde to ethanol pressure increases in the reaction medium. As shown in Figure 52b, the acetaldehyde to ethanol pressure ratio at reactor effluent was slightly higher for the Cu supported on titania catalyst which can be the reason for the increase in C-C products selectivity. To compare the intrinsic activity of both catalytic systems regardless of ethanol to acetaldehyde pressure ratio, the apparent rate constant was calculated for both catalytic systems based on the second order dependence of C-C

formation on acetaldehyde pressure and the Langmuir-Hinshelwood mechanism suggested in Chapter 3. From these two findings, reaction rate constant, k_{app}, was simplified as shown in the following equation:

$$k_{app} = \frac{r(P_{ethanol})^2}{(P_{acetaldehyde})^2}$$

Where r is the measured reaction rate in mole min^{-1} m^{-2}, while ethanol and acetaldehyde pressures are in bar. From plotting $ln(K_{app}/T)$ versus 1000/T, both activation energy and entropy can be estimated from linear fit slope and intercept respectivly.[242] A shown in Figure 53, the normalized rate constants values, $ln(K_{app}/T)$, for Cu/SiO_2 mixed with TiO_2, blank TiO_2 with acetaldehyde Co-feed, and Cu/TiO2 were measured. The measured values were close for Cu/SiO_2 mixed with TiO_2 and blank TiO_2 with similar measured activation barrier and slope as shown in Table 13. The measured normalized rate constant was slightly lower for Cu/SiO_2 mixed with TiO_2 than that of the blank TiO_2 possibly due to the inhibitory effect of the formed ethyl ester from the Cu NP supported on silica as described in Chapter 3. Interestingly, the measured normalized rate constant for Cu/TiO_2 was 2 to 3 times higher than those measured for blank TiO_2 with acetaldehyde co-feed or mixed with Cu/SiO_2. Also the calculated activation barrier was about 70% of that calculated for the other two systems while the slope was only 20% as shown in Table 13.

The matching values of activation barrier and slope for the mechanically mixed titania with copper and the blank titania with acetaldehyde co-feed should not be surprising since mechanical mixing does not alter titania surface properties and hence no change in adsorption, surface reaction, or desorption energy is expected for the C-C formation elementary steps described in Chapter 3. The two mixed catalytic functions are only affecting each other through changing the reactants and products pressures in the gas phase.

The increased activity in the case of the Cu/TiO_2 compared to the other two catalytic systems suggests that having the Cu NP supported on the titania surface changes the energetics of the C-C formation reaction. Based on the kinetics measurements described in Chapter 3, crotonaldehyde desorption was proposed to be the rate limiting step in acetaldehyde aldol condensation on titania. It is worth mentioning here that no crotonaldehyde was observed when Cu function was introduced either when mechanically mixed or supported on titania and only butyraldehyde or butanol were

detected due to the high hydrogenation activity of Cu compared to TiO_2 catalysts. Crotonaldehyde hydrogenation by itself can't not explain the difference between the mechanically mixed system and the Cu/TiO_2 system since in both cases it occurs as demonstrated by the absence of crotonaldehyde from products pool in both cases. The main difference between these two cases is that for crotonaldehyde to become hydrogenated on Cu surface in the case of the mechanically mixed functions, it needs to desorb from the TiO_2 surface and adsorb on the Cu/SiO_2 surface so the crotonaldehyde desorption step is still necessary. On Cu/TiO_2, on the other hand, adsorbed crotonaldehyde can be rapidly hydrogenated by the act of hydrogen spillover[214,243] from the adjacent Cu NP and hence it becomes hydrogenated to the easier to desorb molecules; butyraldehyde and butanol without going through the high activation barrier of crotonaldehyde desorption step.

This hypothesis is in agreement with the decrease in the desorption temperature of the C-C formation product when anatase titania was doped with gold as reported by Nadeem et al.[154] Facilitated product desorption by the addition of Cu can be the reason for the increase in pool conversion and the C-C products selectivity at the same acetaldehyde/ethanol ratio on the Cu/TiO_2 catalyst compared to the Cu/SiO_2+TiO_2 as shown in Figure 52a. It is also possibly that the transition state in case of Cu/TiO_2 involves hydrogenation and desorption (bonds formation, and breaking respectively) compared to desorption (bonds breaking only) on unmodified TiO_2 which can potentially explain the difference in the entropy gain represented by the slope values.

It is worth mentioning here that the change in TiO_2 specific surface area due to Cu NP deposition was negligible (less than 0.5%) as calculated from the measured Cu NP diameter by both TEM and CO adsorption, as shown in Table 9, and assuming a hemispherical NP, where the area covered by the Cu NP is the area of base circle of the hemisphere while the Cu surface area is the area of the dome. Also the TiO_2 phase was checked with XRD and found that the heat treated Cu promoted TiO_2 was still in the anatase phase with no rutile being formed.

While enhanced Guerbet activity by addition of transition metals to metal oxides was reported in different studies,[16,28,36,54,115,121,244] this phenomenon was explained by the ability of the metal to lower the activation barrier of alcohol dehydrogenation to aldehyde. Here it is proved that an

additional benefit is gained by having the metal function supported directly on the metal oxide where it facilitates product desorption and active site turnover as well.

While unsupported Cu powder showed higher selectivity to acetaldehyde compared to the supported Cu NP as found in Chapter 4, using Cu powder mechanically mixed with TiO_2 would sacrifice the additional benefit of having the Cu NP supported on TiO_2 described above. The tradeoff between these two effects requires a special optimization, however, the supported Cu NP on titania selectivity can potentially be enhanced by alloying Cu with Au, and addition of Cr and K as a stabilizer, and acidity attenuator respectively. Addition of these three elements was found to be beneficial to Cu NP dehydrogenation selectivity as described in Chapter 4 of this study.

An additional aspect of the simultaneous reaction configuration is the effect of each catalyst function by or side products on the performance of the other function. Ethyl ester, the main side product from the Cu function was found to inhibit the aldolization activity of the metal oxide as described in Chapter 3. In this chapter, the effect of aldolization byproduct, water, on the Cu dehydrogenation function performance was studied. As shown in Figure 54, co-feeding water with ethanol suppressed esterification selectivity and found to be advantageous in terms of acetaldehyde selectivity. The reason for this decrease in ethyl ester relative selectivity in presence of water could be explained by the ability of the hydroxyl groups, formed from dissociation of water on the metal surface, to block the Cu^+ Lewis acid species required for esterification as described earlier.

5.3.3. Sequential Reactions Configuration

The concept of preforming sequential alcohol dehydrogenation, aldehyde aldol condensation, and product hydrogenation is based on preforming each of these steps on a separate catalyst function that gives the highest selectivity. This concept utilizes the findings from Chapters 2 and 3 where the ratio of acetaldehyde to ethanol pressure was found to greatly affect the C-C bond formation rates and selectivity on the metal oxide and hence feeding the aldolization reactor with low, or no alcohol can increase he metal oxide C-C formation selectivity. Theoretically, an amphoteric oxide like anatase titania can give complete conversion of acetaldehyde to C-C aldol products in absence of alcohols. In addition to the higher C-C formation selectivity, separating catalytic steps allows

separate control and optimization of reaction conditions for each step. For example, ethanol dehydrogenation equilibrium conversion is increased by high temperature and low pressure while acetaldehyde aldolization equilibrium conversion is favored by low temperature and high pressure as shown in Chapter 2.

Performing ethanol dehydrogenation at increasing temperature on IIICu/SiO_2 catalyst increases acetaldehydes selectivity and decreases esterification selectivity as shown in Figure 55, however, the acetaldehyde selectivity was found to go through a maximum and then decrease at around 535 K as acetaldehyde aldol condensation starts to accelerate and consume part of the formed acetaldehyde.

Absence of metal function from the aldol condensation reactor allows a better control of product degree of saturation and chain length. Where butyraldehyde and butanol are easily formed in presence of metal function, crotonaldehyde is the main product in absence of it as described earlier. As mentioned before, crotonaldehyde is lacking the acidic hydrogen in the α position that can be abstracted to for enolate and hence its self aldolization is not possible which restricts formation of C_{8+} aldehydes and alcohols. This ability to control chain length can be of great importance if a specific product is required at high selectivity such as n-butanol, which can be produced by selective hydrogenation of crotonaldehyde in a separate reactor on Cu powder while butadiene can be produced from deoxygenation of crotonaldehyde with ethanol,[2,149,245] and benzene can be produced from reaction of acetaldehyde with crotonaldehyde on metal oxides with specific properties at higher temperature range.[143,150-152]

The main drawback in the sequential reactions configuration is that the achieved conversion in each step is limited by the thermodynamic equilibrium. Unlike simultaneous dehydrogenation, aldolization where the produced acetaldehyde becomes consumed in the aldol reaction, the dehydrogenation conversion in the sequential scheme is limited to that set by equilibrium at reaction conditions, an issue that can be solved by introducing intermediate separation between reactors with recycle of unreacted feed.

5.3.4. Hybrid Reactions Configuration

Since both simultaneous and sequential reaction configurations have their own advantages and disadvantages, a hybrid configuration is proposed that allows gaining benefits from both schemes. In the proposed hybrid scheme, ethanol is first dehydrogenated in the dehydrogenation unit where the catalyst is Cu powder and reaction temperature is set to allow maximum acetaldehyde selectivity (around 535 K at 101.3 kPa). As conversion increases and brings the system closer to dehydrogenation equilibrium conditions, the ratio of side reactions rates to that of dehydrogenation becomes higher and hence, it is preferred to keep conversion lower than that of equilibrium (possibly around 70% of equilibrium conversion). While oxidative dehydrogenation provides a way to overcome the equilibrium limited conversion, this option is excluded to maintain high product selectivity and allow hydrogen conservation as well. The ethanol feed to this unit does not need to be anhydrous. As part of the integration of the Guerbet process with the ethanol bio-refinery, it is proposed in Figure 56 to feed this unit with 15% water ethanol stream eliminating the need for the energy intensive ethanol azeotropic dehydration unit.[246] As shown in Figure 54, water presence in ethanol dehydrogenation medium on Cu based catalyst lead to an increase in acetaldehyde selectivity.

The effluent of this unit contains unreacted ethanol, acetaldehyde, hydrogen, water, and traces of ethyl ester, 2-butanone, butyraldehyde, and butanol as predicted from results in Chapter 4. Selectivity as high as 99% to acetaldehyde can be achieved from this reactor at 30% ethanol conversion. Separation of acetaldehyde and hydrogen from the other components is easy due to the large difference in boiling points between acetaldehyde and ethanol. Since acetaldehyde boiling point is less than that achieved by cooling water, operation under higher than atmospheric can be beneficial in this case, an economic optimization would be required to assess the effect of pressure on ethanol conversion per pass and separation cost.

The bottoms of the ethanol-acetaldehyde separation column contains water concentration higher than 15% and hence it can be recycled back to the main ethanol dehydration unit as shown in Figure 56. The tops of this column contain hydrogen and acetaldehyde in almost equimolar ratio and can be routed directly to the aldol condensation reactor. In case of using metal free, amphoteric

metal oxide as aldolization catalyst, no hydrogen separation is required since hydrogen was found not to have a significant impact on C-C formation rates or products selectivity on such catalyst as demonstrated in Chapter 3. Products formed in this case are C_4 and C_6 aldehydes in addition to benzene with crotonaldehyde being the main product.

In case of using metal doped metal oxide as catalyst, acetaldehyde back hydrogenation to ethanol is expected to occur on the metal surface and hence, reaction temperature and pressure should be set to favor acetaldehyde aldolization more than that of acetaldehyde hydrogenation. Unlike the case of blank amphoteric metal oxides, hydrogen partial pressure is expected to affect C-C formation rate on metal doped metal oxides due to the change in the acetaldehyde to ethanol ratio. As shown in Figure 57, C-C formation rate greatly decreased at increasing hydrogen pressure due to the back hydrogenation to ethanol. Reducing hydrogen to acetaldehyde pressure ratio in the feed to the aldolization reactor in this case is beneficial and can be achieved by acetaldehyde absorption or refrigerated distillation.

The temperature of this reactor should be less than that of the dehydrogenation reactor to mitigate catalyst deactivation by coking[150,158] while the amount of catalyst required is set by the catalyst surface area. The titania surface area used in this study was kept low (11 $m^2 g^{-1}$) to eliminate mass transfer issues but another anatase titania sample prepared by titanium butoxide hydrolysis and heat treated at 773 K had a surface are of 42 $m^2 g^{-1}$, while other more sophisticated synthesis methods[247,248] can achieve surface area higher than 100 $m^2 g^{-1}$.

Whether promoted with metal or not, aldolization catalyst produces significant amount of aldehydes that can be hydrogenated to alcohols on Cu based catalyst in a separate finishing reactor where additional hydrogen can be co-fed If needed. Theoretically, Guerbet is a hydrogen self-sufficient reaction going from the reactant to the product alcohols. Additional hydrogen may be needed If product hydro-deoxygenation is required. Additional hydrogen can be produced from ethanol steam reforming as discussed in other detailed studies.[249,250]

5.4. Conclusion

Ethanol Guerbet conversion to butanol and higher alcohols allows high biomass fermentation efficiency and fuel products quality at the same time. Copper based catalysts are selective for ethanol dehydrogenation while anatase titania is selective for acetaldehyde aldolization. Both catalysts are required to allow reasonable Guerbet conversion and selectivity. Simultaneous dehydrogenation and aldolization can be performed on a bifunctional system containing both catalysts where the produced acetaldehyde from ethanol dehydrogenation becomes continuously consumed in the aldol condensation elimination the thermodynamic limitation on ethanol conversion. Having Cu NP supported on titania increases titania aldolization activity and reduces the measured activation barrier possibly by facilitating products desorption. Sequential reactions, on the other hand, allow independent conditions optimization for each step including temperature and ethanol to acetaldehyde pressure. A hybrid process configuration with intermediate separation is proposed to allow better product properties control and higher selectivity. Water was found to enhance copper dehydrogenation selectivity and hence feeding the Guerbet unit with hydrous ethanol is possible eliminating the need for the expensive azeotropic distillation.

5.5. Figures and Tables

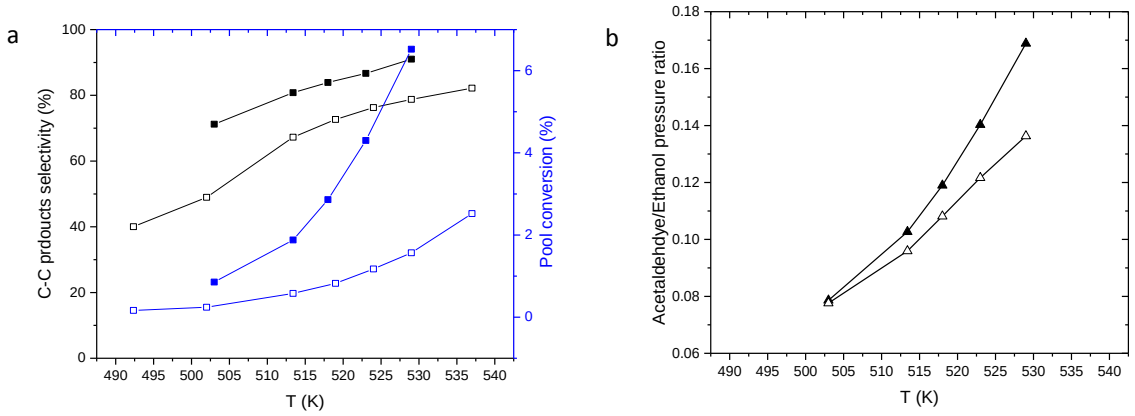

Figure 52 (a). Guerbet products selectivity and pool conversion **(b).** Acetaldehyde/ethanol pressure ratio measured at reactor effluent. 15 mg IIICu/SiO_2 +100 mg TiO_2 (open symbols) and 100 mg Cu/TiO2 (filled symbols) at different temperatures. Reaction conditions: 11 µl.min^{-1} liquid EtOH feed at 3 kPa vapor feed pressure, 60 kPa H_2, bal. He.

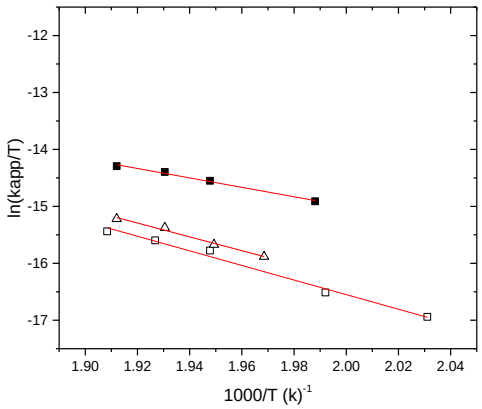

Figure 53. Normalized C-C formation rate constant versus reaction temperature inverse on 15 mg IIICu/SiO_2 +100 mg TiO_2 (□) and 100 mg Cu/TiO_2 (■) at 11 μl.min^{-1} liquid EtOH feed, 3 kPa EtOH vapor feed, 60 kPa H_2, bal. He, and 100 mg blank TiO_2 (Δ) at 11 μl.min^{-1} liquid ethanol-acetaldehyde feed, 2.78 kPa EtOH vapor feed, 0.22 kPa acetaldehyde, 60 kPa H_2, bal. He

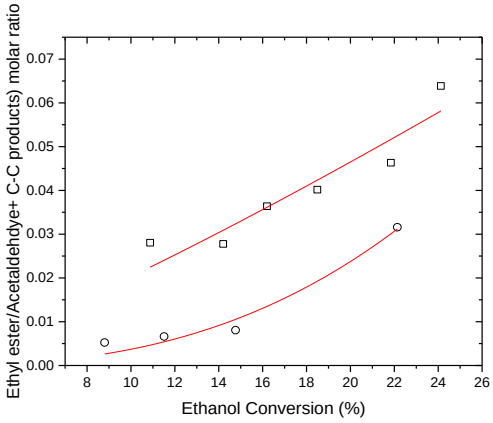

Figure 54. Ethyl ester relative selectivity on 15 mg IIICu/SiO_2 at 0 kPa water co-feed (□) and 5 kPa water co-feed (○) at 503 K, 3 kPa EtOH vapor feed, 60 kPa H_2, bal. He

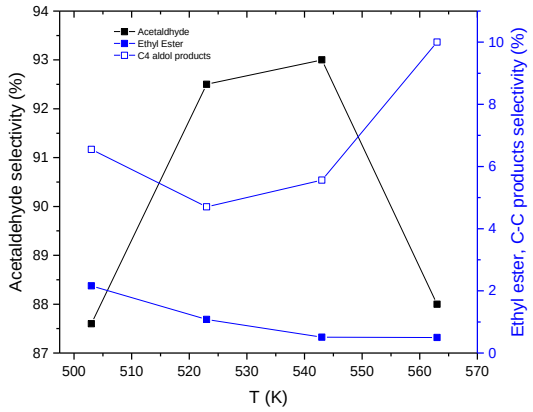

Figure 55. Acetaldehyde (■), ethyl ester (■), and C-C products (□) selectivity at 20% ethanol conversion on 15 mg IIICu/SiO_2 at variable temperature. Reaction conditions: 11 µl.min^{-1} liquid EtOH feed, 3 kPa EtOH vapor feed, 60 kPa H_2, bal. helium

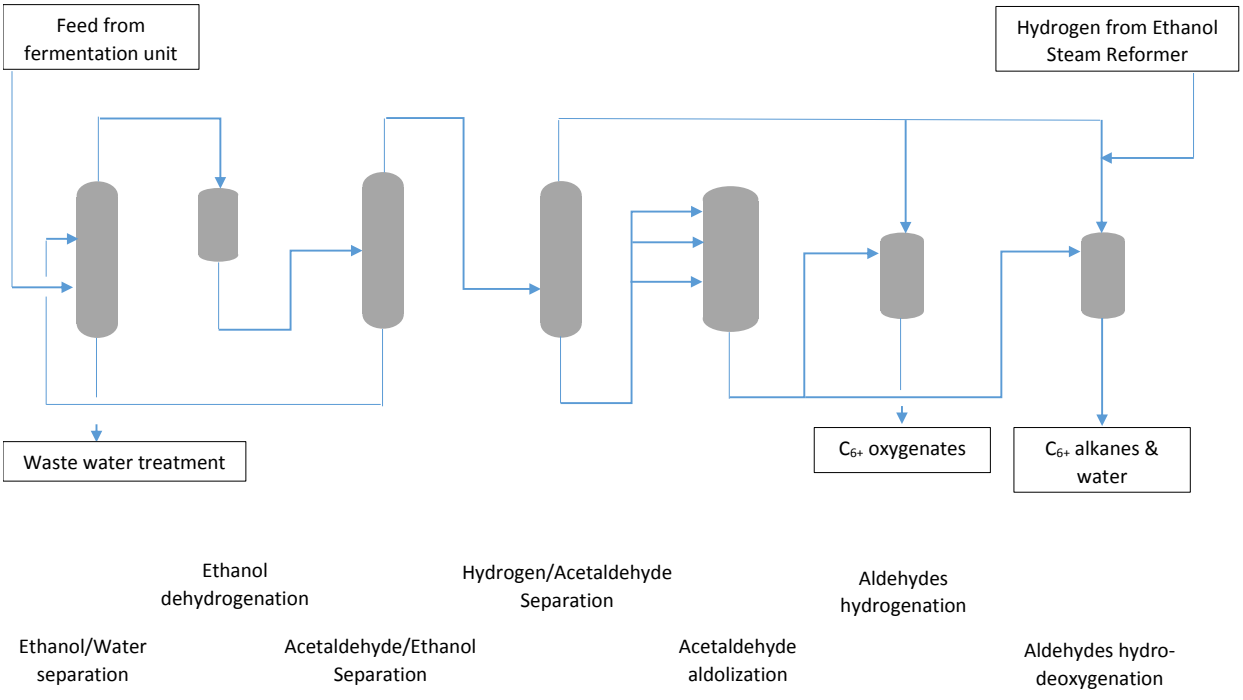

Figure 56. Guerbet process scheme for bioethanol conversion to higher alcohols and alkanes

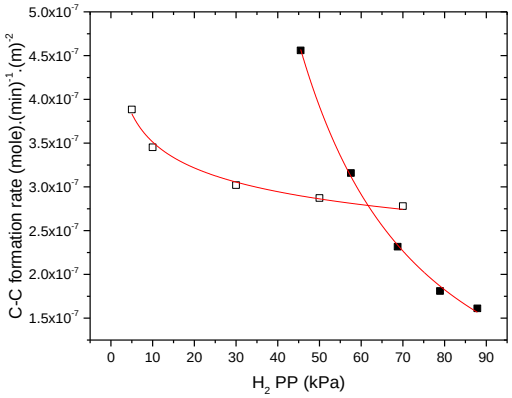

Figure 57. Effect of hydrogen feed pressure on C-C formation rate measured on 100 mg of Cu/TiO_2 with 0 kPa acetaldehyde, and 3 kPa EtOH vapor feed, bal. He, at 493 K reaction temperature (■), and 100 mg of TiO_2 with 0.25 kPa acetaldehyde and 3 kPa etOH vapor feed, bal. He, at 493 K reaction temperature (□)

Table 13. Measured activation barrier and slope from Figure 53

Catalyst system	**C-C formation activation barrier kJ.mole^{-1}**	**slope**
III$Cu/SiO_2 + TiO_2$	106.4	9
TiO_2	100.9	8
Cu/TiO_2	68.8	1.6

Chapter 6: Conclusion and Future Research

6.1. Conclusion

The accelerating growth in world energy demand and the limited energy resources represents a future challenge that needs to be addressed through finding alternative renewable sources of energy. Ethanol can be efficiently produced from biomass fermentation but its physical properties limit its usage to a small fraction of the automotive gasoline market. Catalytic conversion of ethanol to molecules with higher carbon number allows the use of biomass carbon in other forms of fuels and chemicals including aviation gasoline, diesel, aromatics, and olefins.

Ethanol Guerbet is a promising reactive route that converts ethanol to butanol and longer chain oxygenates but there is a need for highly selective and stable heterogeneous catalyst to make this process economically feasible. The reaction was found to proceed mainly through ethanol dehydrogenation to acetaldehyde followed by acetaldehyde aldol condensation and product hydrogenation. Based on this mechanism, it is proposed to use a bifunctional, heterogeneous, catalyst system where a metallic function facilitates dehydrogenation and hydrogenation reactions while a metal oxide catalyzes the aldol condensation reaction.

Copper was found to be highly selective for ethanol dehydrogenation to acetaldehyde when used as bulk powder or supported on non-acidic supports as nanoparticles. Esterification was found to be the main side reaction on copper surfaces and addition of gold, potassium, and chromium to the supported catalyst was found to enhance its selectivity and stability. The method of copper loading on the support and the heat treatment conditions were also found to affect the produced catalyst oxidation state and catalytic performance.

Amphoteric anatase titania was found to be more selective towards acetaldehyde aldolization compared to the highly acidic gamma alumina and more stable compared to the highly basic magnesia. In addition to acetaldehyde aldol condensation, ethanol dehydration to ethylene and diethyl ether and esterification to ethyl ester were found to occur on metal oxides as well. Increasing the acetaldehyde to ethanol pressure ratio was found to enhance selectivity towards

aldol products by increasing the ratio of surface acetaldehydes to ethoxides. Hydrogen pressure was found not to have a measurable effect on non-reducible metal oxides but had a slight inhibiting effect on reducible oxides possibly due to increasing surface acid sites strength and raising the activation barrier for product desorption and active sites regeneration.

Water is the main byproduct from aldol condensation and was found to inhibit aldol reaction on alumina by blocking active sites but not on titania. Water was also found to enhance copper nanoparticles ethanol dehydrogenation selectivity possibly by blocking active sites for undesired reactions. The design of water tolerant bifunctional catalyst allows high ethanol conversion and eliminates the need for feed expensive water separation.

Supporting the metallic function on the aldolization metal oxide function was found to promote the metal oxide aldolization activity possibly due to facilitating product hydrogenation and desorption allowing more rapid sites turnover. The Guerbet reaction main steps can be carried out either simultaneously or sequentially with both configurations having their advantages and disadvantages. A proposed hybrid process configuration with intermediate separation allows high conversion at reasonable selectivity with the ability to control products characteristics.

6.2. Outlook and Future Directions

After more than a century of its discovery, the formation of C-C bonds through Guerbet reaction is still an active area of research and further studies are required to allow economic valorization of ethanol through this reaction including acid-base properties optimization, product properties controlling, reaction conditions optimization, and catalyst stability tests.

The acid-base function required for aldolization can be further optimized to minimize side reactions that occur on this catalyst. In addition to mono metal oxides and mixed metal oxides discussed in this study, other acid-base heterogeneous catalysts can also be used such as nitradated metal oxides, functionalized metal oxides, and clays. While findings from this study can be used as guidelines to narrow down the selection pool for the aldolization function, further quantitate investigation is required to link the catalyst activity to an intrinsic property that can be measured

and predicted from theoretical calculations to minimize the number of trial and errors required to design a catalyst with the required characteristics. Intrinsic properties such as cation size, oxidation state, metal-oxygen bond strength, surface sites coordination, sites proximity, dielectric constant, isoelectric point, and surface reducibility are possible metrics that can be used to guide this type of research. In addition to the composition of the acid-base function, further research regarding the synthesis method and its effect on catalyst performance is also required.

The alcohol dehydrogenation function design also requires further investigation where a more stable, unsupported copper powder with high surface area is needed. While nanoparticles alloys were tested in this study, unsupported alloys should also be studied as dehydrogenation catalysts such as brass and bronze. Further in situ investigations of copper nanoparticles oxidation states is required to understand how the oxidation states change with support type, nanoparticle size, and reaction environment as well. While all the tested copper nanoparticles were loaded from aqueous solutions, non-aqueous loading such as impregnation with toluene or other hydrocarbons copper solutions can be beneficial to minimize catalyst acidity. Further investigation is required to elucidate the reason for why copper nanoparticles are more selective towards esterification while silver nanoparticles are more selective towards aldolization. Factors such as the effect of metal electronegativity and atomic radius on the transition state energy for these two reactions need to be studied.

While Guerbet reaction kinetics on metal oxides were tackled in this study, further investigation is required to validate some of the assumptions made, especially regarding the energetics of each of the elementary steps proposed and how changing acid-base properties affect the activation barrier of each step relative to the others which pose challenging questions for DFT techniques on semiconductors as catalysts. It is also important to further investigate oxides reducibility effect on their Guerbet reaction activity using both theoretical methods and in situ surface measurements to fully understand this effect. In addition to surface reducibility, it is desired to understand how the increase in surface basicity strength can promote esterification versus aldolization where both experimental and theoretical methods are needed to be applied on surfaces with different degree of basicity.

Since this study focuses on ethanol Guerbet, acetaldehyde was co-fed as an expected intermediate, however, it is required to study the kinetics of longer chain aldehydes reaction on the same metal oxides to understand how changes in the aldehyde chain length and branching affect its activity on the metal oxide. Such knowledge is needed to understand the reaction behavior at high conversion at which products secondary reactions become more effective. Understanding how increasing aldehyde chain length or branching affect its basicity, enolization-ability, and adsorption configuration can help tailor the catalyst to produce products with certain properties.

At uncontrolled high conversion, the product pool is expected to contain too many components to be described in terms of specific components concentration and hence collective properties such as octane number, pour point, flash point, calorific value, oxidation resistance, and iodine number need to be measured to better describe products from different catalysts or different process conditions. Process research is also required to optimize process scheme and reaction conditions to allow better insights into factors governing process economics such as energy consumption, feed consumption, fixed cost, products value, and waste generated where tools such as process simulation coupled with techno-economic analysis are mostly needed.

References

(1) Shafiee, S.; Topal, E. When will fossil fuel reserves be diminished? *Energy Policy* **2009**, *37*, 181-189.

(2) Angelici, C.; Weckhuysen, B. M.; Bruijnincx, P. C. A. Chemocatalytic Conversion of Ethanol into Butadiene and Other Bulk Chemicals. *ChemSusChem* **2013**, *6*, 1595-1614.

(3) Schlör, H.; Fischer, W.; Hake, J.-F. The meaning of energy systems for the genesis of the concept of sustainable development. *Applied Energy* **2012**, *97*, 192-200.

(4) Luo, L.; Voet, E. v. d.; Huppes, G. Energy and Environmental Performance of Bioethanol from Different Lignocelluloses. *International Journal of Chemical Engineering* **2010**.

(5) Anbarasan, P.; Baer, Z. C.; Sreekumar, S.; Gross, E.; Binder, J. B.; Blanch, H. W.; Clark, D. S.; Toste, F. D. Integration of chemical catalysis with extractive fermentation to produce fuels. *Nature* **2012**, *491*, 235-239.

(6) Bai, F. W.; Anderson, W. A.; Moo-Young, M. Ethanol fermentation technologies from sugar and starch feedstocks. *Biotechnol Adv* **2008**, *26*, 89-105.

(7) Atsumi, S.; Cann, A. F.; Connor, M. R.; Shen, C. R.; Smith, K. M.; Brynildsen, M. P.; Chou, K. J.; Hanai, T.; Liao, J. C. Metabolic engineering of Escherichia coli for 1-butanol production. *Metab Eng* **2008**, *10*, 305-311.

(8) Jones, D. T.; Woods, D. R. Acetone-butanol fermentation revisited. *Microbiol Rev* **1986**, *50*, 484-524.

(9) Goldemberg, J. Ethanol for a Sustainable Energy Future. *Science* **2007**, *315*, 808-810.

(10) Frolkova, A. K.; Raeva, V. M. Bioethanol dehydration: State of the art. *Theor Found Chem Eng* **2010**, *44*, 545-556.

(11) Blanch, H. W. Bioprocessing for biofuels. *Curr Opin Biotechnol* **2012**, *23*, 390-395.

(12) Buckeridge, M. S.; De Souza, A. P.; Arundale, R. A.; Anderson-Teixeira, K. J.; DeLucia, E. Ethanol from sugarcane in Brazil: a 'midway' strategy for increasing ethanol production while maximizing environmental benefits. *GCB Bioenergy* **2012**, *4*, 119-126.

(13) Zinoviev, S.; Muller-Langer, F.; Das, P.; Bertero, N.; Fornasiero, P.; Kaltschmitt, M.; Centi, G.; Miertus, S. Next-generation biofuels: Survey of emerging technologies and sustainability issues. *ChemSusChem* **2010**, *3*, 1106-1133.

(14) Yüksel, F.; Yüksel, B. The use of ethanol–gasoline blend as a fuel in an SI engine. *Renewable energy* **2004**, *29*, 1181-1191.

(15) Wu, C.-W.; Chen, R.-H.; Pu, J.-Y.; Lin, T.-H. The influence of air–fuel ratio on engine performance and pollutant emission of an SI engine using ethanol–gasoline-blended fuels. *Atmospheric Environment* **2004**, *38*, 7093-7100.

(16) Riittonen, T.; Eränen, K.; Mäki-Arvela, P.; Shchukarev, A.; Rautio, A.-R.; Kordas, K.; Kumar, N.; Salmi, T.; Mikkola, J.-P. Continuous liquid-phase valorization of bio-ethanol towards bio-butanol over metal modified alumina. *Renewable Energy* **2015**, *74*, 369-378.

(17) Birky, T. W.; Kozlowski, J. T.; Davis, R. J. Isotopic transient analysis of the ethanol coupling reaction over magnesia. *Journal of Catalysis* **2013**, *298*, 130-137.

(18) Merola, S.; Tornatore, C.; Marchitto, L.; Valentino, G.; Corcione, F. Experimental investigations of butanol-gasoline blends effects on the combustion process in a SI engine. *Int J Energy Environ Eng* **2012**, *3*, 1-14.

(19) M. Guerbet, C. R. *Acad. Sci. Paris* **1899**, *1002*.

(20) D.F. Cadogan, C. J. H., in: J.I. Kroschwitz, M. Howe-Grant: In *Kirk-Othmer Encyclopedia of Chemical Technology*; Wiley/Interscience, New York,, 1991; Vol. 19.

(21) O'Lenick, A., Jr. Guerbet chemistry. *Journal of Surfactants and Detergents* **2001**, *4*, 311-315.

(22) Kozlowski, J. T.; Davis, R. J. Heterogeneous Catalysts for the Guerbet Coupling of Alcohols. *ACS Catalysis* **2013**, *3*, 1588-1600.

(23) Kelly, G. J.; King, F.; Kett, M. Waste elimination in condensation reactions of industrial importance. *Green Chemistry* **2002**, *4*, 392-399.

(24) Burk, P. L.; Pruett, R. L.; Campo, K. S. The rhodium-promoted guerbet reaction: Part I. Higher alcohols from lower alcohols. *Journal of Molecular Catalysis* **1985**, *33*, 1-14.

(25) Gregorio, G.; Pregaglia, G. F.; Ugo, R. Condensation of alcohols catalysed by tertiary phosphine transition metal complexes. *Journal of Organometallic Chemistry* **1972**, *37*, 385-387.

(26) Tanabe, K.; Hölderich, W. F. Industrial application of solid acid–base catalysts. *Applied Catalysis A: General* **1999**, *181*, 399-434.

(27) Hattori, H. Heterogeneous Basic Catalysis. *Chemical Reviews* **1995**, *95*, 537-558.

(28) Carlini, C.; Marchionna, M.; Noviello, M.; Raspolli Galletti, A. M.; Sbrana, G.; Basile, F.; Vaccari, A. Guerbet condensation of methanol with n-propanol to isobutyl alcohol over heterogeneous bifunctional catalysts based on Mg–Al mixed oxides partially substituted by different metal components. *Journal of Molecular Catalysis A: Chemical* **2005**, *232*, 13-20.

(29) Hasni, M.; Prado, G.; Rouchaud, J.; Grange, P.; Devillers, M.; Delsarte, S. Liquid phase aldol condensation of cyclopentanone with valeraldehyde catalysed by oxynitrides possessing tuneable acid–base properties. *Journal of Molecular Catalysis A: Chemical* **2006**, *247*, 116-123.

(30) Ordomsky, V.; Sushkevich, V.; Ivanova, I. Study of acetaldehyde condensation chemistry over magnesia and zirconia supported on silica. *Journal of Molecular Catalysis A: Chemical* **2010**, *333*, 85-93.

(31) Carlini, C.; Girolamo, M. D.; Marchionna, M.; Noviello, M.; Galletti, A. M. R.; Sbrana, G. Selective synthesis of isobutanol by means of the Guerbet reaction: Part 1. Methanol/n-propanol condensation by using copper based catalytic systems. *Journal of Molecular Catalysis A: Chemical* **2002**, *184*, 273-280.

(32) Carlini, C.; Di Girolamo, M.; Macinai, A.; Marchionna, M.; Noviello, M.; Raspolli Galletti, A. M.; Sbrana, G. Selective synthesis of isobutanol by means of the Guerbet reaction: Part 2. Reaction of methanol/ethanol and methanol/ethanol/n-propanol mixtures over copper based/MeONa catalytic systems. *Journal of Molecular Catalysis A: Chemical* **2003**, *200*, 137-146.

(33) Veibel, S.; Nielsen, J. I. On the mechanism of the Guerbet reaction. *Tetrahedron* **1967**, *23*, 1723-1733.

(34) Miller, R.; Bennett, G. Producing 2-Ethylhexanol by the Guerbet Reaction. *Industrial & Engineering Chemistry* **1961**, *53*, 33-36.

(35) Carlini, C.; Girolamo, M. D.; Macinai, A.; Marchionna, M.; Noviello, M.; Galletti, A. M. R.; Sbrana, G. Synthesis of isobutanol by the Guerbet condensation of methanol with n-propanol in the presence of heterogeneous and homogeneous palladium-based catalytic systems. *Journal of Molecular Catalysis A: Chemical* **2003**, *204–205*, 721-728.

(36) Carlini, C.; Macinai, A.; Marchionna, M.; Noviello, M.; Galletti, A. M. R.; Sbrana, G. Selective synthesis of isobutanol by means of the Guerbet reaction: Part 3: Methanol/n-propanol condensation by using bifunctional catalytic systems based on nickel, rhodium and ruthenium species with basic components. *Journal of Molecular Catalysis A: Chemical* **2003**, *206*, 409-418.

(37) Skandan, G.; Singhal, A.; Contescu, C.; Putyera, K.: *Dekker encyclopedia of nanoscience and nanotechnology*; Taylor & Francis, 2009.

(38) Carlini, C.; Flego, C.; Marchionna, M.; Noviello, M.; Raspolli Galletti, A. M.; Sbrana, G.; Basile, F.; Vaccari, A. Guerbet condensation of methanol with n-propanol to isobutyl alcohol over heterogeneous copper chromite/Mg–Al mixed oxides catalysts. *Journal of Molecular Catalysis A: Chemical* **2004**, *220*, 215-220.

(39) Barteau, M. A. Organic Reactions at Well-Defined Oxide Surfaces. *Chemical Reviews* **1996**, *96*, 1413-1430.

(40) Radwan, M. *Performance and knock limits of ethanol-gasoline blends in spark-ignited engines*1985.

(41) Al-Hasan, M. Effect of ethanol–unleaded gasoline blends on engine performance and exhaust emission. *Energy Conversion and Management* **2003**, *44*, 1547-1561.

(42) Zhang, X.; Liu, Z.; Xu, X.; Yue, H.; Tian, G.; Feng, S. Hydrothermal Synthesis of 1-Butanol from Ethanol Catalyzed with Commercial Cobalt Powder. *ACS Sustainable Chemistry & Engineering* **2013**, *1*, 1493-1497.

(43) Ueda, W.; Kuwabara, T.; Ohshida, T.; Morikawa, Y. A low-pressure guerbet reaction over magnesium oxide catalyst. *Journal of the Chemical Society, Chemical Communications* **1990**, 1558-1559.

(44) Ndou, A. S.; Plint, N.; Coville, N. J. Dimerisation of ethanol to butanol over solid-base catalysts. *Applied Catalysis A: General* **2003**, *251*, 337-345.

(45) Ndou, A. S.; Coville, N. J. Self-condensation of propanol over solid-base catalysts. *Applied Catalysis A: General* **2004**, *275*, 103-110.

(46) Ueda, W.; Yokoyama, T.; Moro-Oka, Y.; Ikawa, T. Catalytic synthesis of vinyl ketones over metal oxide catalysts using methanol as the vinylating agent. *Journal of the Chemical Society, Chemical Communications* **1984**, 39-40.

(47) Shen, W.; Tompsett, G. A.; Xing, R.; Conner, W. C.; Huber, G. W. Vapor phase butanal self-condensation over unsupported and supported alkaline earth metal oxides. *Journal of Catalysis* **2012**, *286*, 248-259.

(48) Claridge, J. B.; Green, M. L. H.; Tsang, S. C.; York, A. P. E. Conversion of propanal to pentan-3-one using lanthanide oxides. *Journal of the Chemical Society, Faraday Transactions* **1993**, *89*, 1089-1094.

(49) Nakajima, T.; Nameta, H.; Mishima, S.; Matsuzaki, I.; Tanabe, K. A highly active and highly selective oxide catalyst for the conversion of ethanol to acetone in the presence of water vapour. *Journal of Materials Chemistry* **1994**, *4*, 853-858.

(50) Idriss, H.; Seebauer, E. G. Reactions of ethanol over metal oxides. *Journal of Molecular Catalysis A: Chemical* **2000**, *152*, 201-212.

(51) Sun, J.; Zhu, K.; Gao, F.; Wang, C.; Liu, J.; Peden, C. H. F.; Wang, Y. Direct Conversion of Bio-ethanol to Isobutene on Nanosized ZnxZryOz Mixed Oxides with Balanced Acid–Base Sites. *Journal of the American Chemical Society* **2011**, *133*, 11096-11099.

(52) Simpson, S.; Davis, B. H. Catalytic conversion of alcohols. Relation of hafnium-zirconium mixed oxide catalytic selectivity to surface composition measured by Raman spectroscopic methods. *The Journal of Physical Chemistry* **1987**, *91*, 5664-5668.

(53) Inui, K.; Kurabayashi, T.; Sato, S. Direct Synthesis of Ethyl Acetate from Ethanol Carried Out under Pressure. *Journal of Catalysis* **2002**, *212*, 207-215.

(54) Gines, M. J. L.; Iglesia, E. Bifunctional Condensation Reactions of Alcohols on Basic Oxides Modified by Copper and Potassium. *Journal of Catalysis* **1998**, *176*, 155-172.

(55) Kamimura, Y.; Sato, S.; Takahashi, R.; Sodesawa, T.; Akashi, T. Synthesis of 3-pentanone from 1-propanol over CeO2–Fe2O3 catalysts. *Applied Catalysis A: General* **2003**, *252*, 399-410.

(56) Lietti, L.; Tronconi, E. Mechanistic aspects of the higher alcohol synthesis over unpromoted ZnCrO: 1-Propanol flow microreactor study. *Journal of Molecular Catalysis* **1994**, *94*, 335-346.

(57) Takashi, T.; Shuji, S.; Tatsuya, T.; Wataru, U.: *Direct synthesis of n-butanol from ethanol over nonstoichiometric hydroxyapatite*; American Chemical Society: Washington, DC, ETATS-UNIS, 2006; Vol. 45.

(58) Ogo, S.; Onda, A.; Yanagisawa, K. Selective synthesis of 1-butanol from ethanol over strontium phosphate hydroxyapatite catalysts. *Applied Catalysis A: General* **2011**, *402*, 188-195.

(59) Hanspal, S.; Young, Z. D.; Shou, H.; Davis, R. J. Multiproduct Steady-State Isotopic Transient Kinetic Analysis of the Ethanol Coupling Reaction over Hydroxyapatite and Magnesia. *ACS Catalysis* **2015**, *5*, 1737-1746.

(60) Scalbert, J.; Thibault-Starzyk, F.; Jacquot, R.; Morvan, D.; Meunier, F. Ethanol condensation to butanol at high temperatures over a basic heterogeneous catalyst: How relevant is acetaldehyde self-aldolization? *Journal of Catalysis* **2014**, *311*, 28-32.

(61) Jeong, M. S.; Frei, H. Acetaldehyde as a probe for the chemical properties of aluminophosphate molecular sieves. An in situ FT-IR study. *Journal of Molecular Catalysis A: Chemical* **2000**, *156*, 245-253.

(62) Tichit, D.; Lutic, D.; Coq, B.; Durand, R.; Teissier, R. The aldol condensation of acetaldehyde and heptanal on hydrotalcite-type catalysts. *Journal of Catalysis* **2003**, *219*, 167-175.

(63) Rode, E. J.; Gee, P. E.; Marquez, L. N.; Uemura, T.; Bazargani, M. Aldol condensation of butanal over alkali metal zeolites. *Catal Lett* **1991**, *9*, 103-113.

(64) Dumitriu, E.; Hulea, V.; Fechete, I.; Auroux, A.; Lacaze, J.-F.; Guimon, C. The aldol condensation of lower aldehydes over MFI zeolites with different acidic properties. *Microporous and Mesoporous Materials* **2001**, *43*, 341-359.

(65) Peng, X. D.; Barteau, M. A. Acid-base properties of model magnesium oxide surfaces. *Langmuir* **1991**, *7*, 1426-1431.

(66) Flood, H.; Förland, T. The acidic and basic properties of oxides. *Acta Chem. Scand* **1947**, *1*, 592-604.

(67) Pena, D. A.; Uphade, B. S.; Smirniotis, P. G. TiO 2-supported metal oxide catalysts for low-temperature selective catalytic reduction of NO with NH 3: I. Evaluation and characterization of first row transition metals. *Journal of catalysis* **2004**, *221*, 421-431.

(68) Turek, A. M.; Wachs, I. E.; DeCanio, E. Acidic properties of alumina-supported metal oxide catalysts: an infrared spectroscopy study. *The Journal of Physical Chemistry* **1992**, *96*, 5000-5007.

(69) Boehm, H. Acidic and basic properties of hydroxylated metal oxide surfaces. *Discussions of the Faraday Society* **1971**, *52*, 264-275.

(70) Hattori, H. Catalysis by basic metal oxides. *Materials Chemistry and Physics* **1988**, *18*, 533-552.

(71) Aramendía, M. A.; Borau, V.; Jiménez, C.; Marinas, J. M.; Porras, A.; Urbano, F. J. Chemoselective and regioselective reduction of citral (3,7-dimethyl-2,6-octadienal) by gas-phase hydrogen transfer over acid–basic catalysts. *Applied Catalysis A: General* **1998**, *172*, 31-40.

(72) Satsuma, A.; Kamiya, Y.; Westi, Y.; Hattori, T. Dimethylpyridine-temperature programmed desorption (DMP-TPD) for measurement of strength of Brønsted and Lewis acid sites on metal oxide catalysts. *Applied Catalysis A: General* **2000**, *194–195*, 253-263.

(73) Spitz, R. N.; Barton, J. E.; Barteau, M. A.; Staley, R. H.; Sleight, A. W. Characterization of the surface acid-base properties of metal oxides by titration/displacement reactions. *The Journal of Physical Chemistry* **1986**, *90*, 4067-4075.

(74) Benesi, H. A. Acidity of Catalyst Surfaces. I. Acid Strength from Colors of Adsorbed Indicators. *Journal of the American Chemical Society* **1956**, *78*, 5490-5494.

(75) Walling, C. The Acid Strength of Surfaces. *Journal of the American Chemical Society* **1950**, *72*, 1164-1168.

(76) Auroux, A.; Gervasini, A. Microcalorimetric study of the acidity and basicity of metal oxide surfaces. *Journal of Physical Chemistry* **1990**, *94*, 6371-6379.

(77) Tamura, M.; Shimizu, K.-i.; Satsuma, A. Comprehensive IR study on acid/base properties of metal oxides. *Applied Catalysis A, General* **2012**, *433-434*, 135-145.

(78) Zaki, M. I.; Hasan, M. A.; Al-Sagheer, F. A.; Pasupulety, L. In situ FTIR spectra of pyridine adsorbed on SiO2–Al2O3, TiO2, ZrO2 and CeO2: general considerations for the identification of acid sites on surfaces of finely divided metal oxides. *Colloids and Surfaces A: Physicochemical and Engineering Aspects* **2001**, *190*, 261-274.

(79) Connor, P. A.; Dobson, K. D.; McQuillan, A. J. New sol-gel attenuated total reflection infrared spectroscopic method for analysis of adsorption at metal oxide surfaces in aqueous

solutions. Chelation of TiO2, ZrO2, and Al2O3 surfaces by catechol, 8-quinolinol, and acetylacetone. *Langmuir* **1995**, *11*, 4193-4195.

(80) Tanabe, K.; Sumiyoshi, T.; Shibata, K.; Kiyoura, T.; Kitagawa, J. A new hypothesis regarding the surface acidity of binary metal oxides. *Bulletin of the Chemical Society of Japan* **1974**, *47*, 1064-1066.

(81) Katz, L.; Ward, R. Structure Relations in Mixed Metal Oxides. *Inorganic Chemistry* **1964**, *3*, 205-211.

(82) Calatayud, M.; Ruppert, A. M.; Weckhuysen, B. M. Theoretical study on the role of surface basicity and lewis acidity on the etherification of glycerol over alkaline earth metal oxides. *Chemistry* **2009**, *15*, 10864-10870.

(83) Forni, L. Comparison of the Methods for the Determination of Surface Acidity of Solid Catalysts. *Catalysis Reviews* **1974**, *8*, 65-115.

(84) Snell, R.; Combs, E.; Shanks, B. Aldol Condensations Using Bio-oil Model Compounds: The Role of Acid–Base Bi-functionality. *Topics in Catalysis* **2010**, *53*, 1248-1253.

(85) Cunningham, J.; Hodnett, B. K.; Ilyas, M.; Tobin, J.; Leahy, E. L.; Fierro, J. L. G. Dehydrogenation versus dehydration of aliphatic alcohols on metal oxides. *Faraday Discussions of the Chemical Society* **1981**, *72*, 283-302.

(86) Roy, S.; Mpourmpakis, G.; Hong, D.-Y.; Vlachos, D. G.; Bhan, A.; Gorte, R. J. Mechanistic Study of Alcohol Dehydration on γ-Al2O3. *ACS Catalysis* **2012**, *2*, 1846-1853.

(87) Christiansen, M. A.; Mpourmpakis, G.; Vlachos, D. G. Density Functional Theory-Computed Mechanisms of Ethylene and Diethyl Ether Formation from Ethanol on γ-Al2O3(100). *ACS Catalysis* **2013**, *3*, 1965-1975.

(88) Di Cosimo, J. I.; Apesteguı; amp;´a, C. R.; Ginés, M. J. L.; Iglesia, E. Structural Requirements and Reaction Pathways in Condensation Reactions of Alcohols on MgyAlOx Catalysts. *Journal of Catalysis* **2000**, *190*, 261-275.

(89) Gervasini, A.; Fenyvesi, J.; Auroux, A. Study of the acidic character of modified metal oxide surfaces using the test of isopropanol decomposition. *Catal Lett* **1997**, *43*, 219-228.

(90) Rekoske, J. E.; Barteau, M. A. Competition between acetaldehyde and crotonaldehyde during adsorption and reaction on anatase and rutile titanium dioxide. *Langmuir* **1999**, *15*, 2061-2070.

(91) Mullins, D. R.; Senanayake, S. D.; Chen, T.-L. Adsorption and Reaction of C1− C3 Alcohols over CeO X (111) Thin Films†. *The Journal of Physical Chemistry C* **2010**, *114*, 17112-17119.

(92) Derouane, E. G.; Roberts, S. M.: *Catalysts for fine chemical synthesis, microporous and mesoporous solid catalysts*; John Wiley & Sons, 2006; Vol. 4.

(93) Idriss, H.; Seebauer, E. Reactions of ethanol over metal oxides. *Journal of Molecular Catalysis A: Chemical* **2000**, *152*, 201-212.

(94) Jain, J. R.; Pillai, C. Catalytic dehydration of alcohols over alumina: mechanism of ether formation. *Journal of Catalysis* **1967**, *9*, 322-330.

(95) Padmanabhan, V.; Eastburn, F. Mechanism of ether formation from alcohols over alumina catalyst. *Journal of catalysis* **1972**, *24*, 88-91.

(96) Jenness, G. R.; Christiansen, M. A.; Caratzoulas, S.; Vlachos, D. G.; Gorte, R. J. Site-Dependent Lewis Acidity of γ-Al2O3 and Its Impact on Ethanol Dehydration and Etherification. *The Journal of Physical Chemistry C* **2014**, *118*, 12899-12907.

(97) Kim, K.; Barteau, M.; Farneth, W. Adsorption and decomposition of aliphatic alcohols on titania. *Langmuir* **1988**, *4*, 533-543.

(98) Wade, L. G.: *Organic Chemistry*; 6 ed.; Prentice Hall: Upper, Saddle River, 2005.

(99) Peng, X. D.; Barteau, M. A. Adsorption of formaldehyde on model magnesia surfaces: evidence for the Cannizzaro reaction. *Langmuir* **1989**, *5*, 1051-1056.

(100) Idriss, H.; Kim, K. S.; Barteau, M. A. Carbon□Carbon Bond Formation via Aldolization of Acetaldehyde on Single Crystal and Polycrystalline TiO2 Surfaces. *Journal of Catalysis* **1993**, *139*, 119-133.

(101) Sad, M. E.; Neurock, M.; Iglesia, E. Formation of C–C and C–O Bonds and Oxygen Removal in Reactions of Alkanediols, Alkanols, and Alkanals on Copper Catalysts. *Journal of the American Chemical Society* **2011**, *133*, 20384-20398.

(102) Carotenuto, G.; Tesser, R.; Di Serio, M.; Santacesaria, E. Kinetic study of ethanol dehydrogenation to ethyl acetate promoted by a copper/copper-chromite based catalyst. *Catalysis Today* **2013**, *203*, 202-210.

(103) Tanabe, K.; Saito, K. The conversion of benzaldehyde into benzyl benzoate with alkaline earth metal oxide catalysts. *Journal of Catalysis* **1974**, *35*, 247-255.

(104) Ai, M. The reaction of formaldehyde on various metal oxide catalysts. *Journal of Catalysis* **1983**, *83*, 141-150.

(105) Kiennemann, A.; Idriss, H.; Kieffer, R.; Chaumette, P.; Durand, D. Study of the mechanism of higher alcohol synthesis on copper-zinc oxide-aluminum oxide catalysts by catalytic tests, probe molecules, and temperature programmed desorption studies. *Industrial & Engineering Chemistry Research* **1991**, *30*, 1130-1138.

(106) Tsuji, H.; Yagi, F.; Hattori, H.; Kita, H. Self-Condensation of n-Butyraldehyde over Solid Base Catalysts. *Journal of Catalysis* **1994**, *148*, 759-770.

(107) Berg, L.; Ratanapupech, P.: Separation of ethyl acetate from ethanol and water by extractive distillation. Google Patents, 1983.

(108) Separation of ethyl acetate and ethanol by azeotropic distillation with methanol. Google Patents, 1953.

(109) Murthy, R. S.; Patnaik, P.; Sidheswaran, P.; Jayamani, M. Conversion of ethanol to acetone over promoted iron oxide catalysis. *Journal of Catalysis* **1988**, *109*, 298-302.

(110) Zhang, G.; Hattori, H.; Tanabe, K. Aldol Addition of Acetone, Catalyzed by Solid Base Catalysts: Magnesium Oxide, Calcium Oxide, Strontium Oxide, Barium Oxide, Lanthanum (III) Oxide and Zirconium Oxide. *Applied Catalysis* **1988**, *36*, 189-197.

(111) Zhang, G.; Hattori, H.; Tanabe, K. Aldol addition of butyraldehyde over solid base catalysts. *Bulletin of the Chemical Society of Japan* **1989**, *62*, 2070-2072.

(112) Iwasa, N.; Takezawa, N. Reforming of Ethanol -Dehydrogenation to Ethyl Acetate and Steam Reforming to Acetic Acid over Copper-Based Catalysts. *Bulletin of the Chemical Society of Japan* **1991**, *64*, 2619-2623.

(113) Yang, C.; Meng, Z. Y. Bimolecular Condensation of Ethanol to 1-Butanol Catalyzed by Alkali Cation Zeolites. *Journal of Catalysis* **1993**, *142*, 37-44.

(114) G. A, V.; P. B, H.; G. W, S.; K, K.: Alkali-Promoted Copper-Zinc Oxide Catalysts for Low Alcohol Synthesis. In *Solid State Chemistry in Catalysis*; ACS Symposium Series 279; American Chemical Society, 1985; Vol. 279; pp 295-312.

(115) Xu, M.; Gines, M. J. L.; Hilmen, A.-M.; Stephens, B. L.; Iglesia, E. Isobutanol and Methanol Synthesis on Copper Catalysts Supported on Modified Magnesium Oxide. *Journal of Catalysis* **1997**, *171*, 130-147.

(116) Lietti, L.; Tronconi, E.; Forzatti, P. Mechanistic aspects of the higher alcohol synthesis over K2O-promoted ZnCr oxide: Temperature-programmed reaction and flow experiments of C3, C4, and C5 oxygenates. *Journal of Catalysis* **1992**, *135*, 400-419.

(117) Hamilton, C. A.; Jackson, S. D.; Kelly, G. J. Solid base catalysts and combined solid base hydrogenation catalysts for the aldol condensation of branched and linear aldehydes. *Applied Catalysis A: General* **2004**, *263*, 63-70.

(118) Choudhary, V. R.; Rane, V. H. Acidity/basicity of rare-earth oxides and their catalytic activity in oxidative coupling of methane to C2-hydrocarbons. *Journal of Catalysis* **1991**, *130*, 411-422.

(119) T.-L., C.; R., M. D.: *Adsorption and Reaction of Acetaldehyde over CeO[X](111) Thin Films*; American Chemical Society: Columbus, OH, ETATS-UNIS, 2011; Vol. 115.

(120) Zhang, G.; Hattori, H.; Tanabe, K. Aldol condensation of acetone/acetone d6 over magnesium oxide and lanthanum oxide. *Applied Catalysis* **1988**, *40*, 183-190.

(121) Gurbuz, E. I.; Kunkes, E. L.; Dumesic, J. A. Dual-bed catalyst system for C-C coupling of biomass-derived oxygenated hydrocarbons to fuel-grade compounds. *Green Chemistry* **2010**, *12*, 223-227.

(122) Davis, B. H.; Freeman, G. B.; Watters, J. C.; Collins, D. J. Catalytic conversion of alcohols. 15. Alkene selectivity from the conversion of 2-octanol over hafnium-zirconium mixed oxide catalysts. *The Journal of Physical Chemistry* **1980**, *84*, 55-56.

(123) Climent, M. J.; Corma, A.; Fornés, V.; Guil-Lopez, R.; Iborra, S. Aldol Condensations on Solid Catalysts: A Cooperative Effect between Weak Acid and Base Sites. *Advanced Synthesis & Catalysis* **2002**, *344*, 1090-1096.

(124) Gangadharan, A.; Shen, M.; Sooknoi, T.; Resasco, D. E.; Mallinson, R. G. Condensation reactions of propanal over CexZr1−xO2 mixed oxide catalysts. *Applied Catalysis A: General* **2010**, *385*, 80-91.

(125) Di Cosimo, J. I.; Díez, V. K.; Xu, M.; Iglesia, E.; Apesteguía, C. R. Structure and Surface and Catalytic Properties of Mg-Al Basic Oxides. *Journal of Catalysis* **1998**, *178*, 499-510.

(126) Scalbert, J.; Thibault-Starzyk, F.; Meunier, F.: On the irrelevance of acetaldehyde self-aldolization during ethanol condensation at high temperatures over basic heterogeneous catalysts. In *8th International Conference on Environmental Catalysis*: Asheville, United States, 2014.

(127) Chieregato, A.; Velasquez Ochoa, J.; Bandinelli, C.; Fornasari, G.; Cavani, F.; Mella, M. On the Chemistry of Ethanol on Basic Oxides: Revising Mechanisms and Intermediates in the Lebedev and Guerbet reactions. *ChemSusChem* **2015**, *8*, 377-388.

(128) Parrott, S. L.; Rogers, J.; White, J. The decomposition of ethanol, propanol and acetic acid chemisorbed on magnesium oxide. *Applications of Surface Science* **1978**, *1*, 443-454.

(129) Bowker, M.; Houghton, H.; Waugh, K. C. Temperature-programmed reaction studies of the interaction of methyl formate and ethanol with polycrystalline zinc oxide. *Journal of the Chemical Society, Faraday Transactions 1: Physical Chemistry in Condensed Phases* **1982**, *78*, 2573-2582.

(130) Kakkar, R.; Kapoor, P. N.; Klabunde, K. J. First principles density functional study of the adsorption and dissociation of carbonyl compounds on magnesium oxide nanosurfaces. *The Journal of Physical Chemistry B* **2006**, *110*, 25941-25949.

(131) Zaki, M. I.; Hasan, M. A.; Pasupulety, L. Surface Reactions of Acetone on Al2O3, TiO2, ZrO2, and CeO2: IR Spectroscopic Assessment of Impacts of the Surface Acid−Base Properties. *Langmuir* **2001**, *17*, 768-774.

(132) Tsuchida, T.; Kubo, J.; Yoshioka, T.; Sakuma, S.; Takeguchi, T.; Ueda, W. Reaction of ethanol over hydroxyapatite affected by Ca/P ratio of catalyst. *Journal of Catalysis* **2008**, *259*, 183-189.

(133) Singh, M.; Zhou, N.; Paul, D. K.; Klabunde, K. J. IR spectral evidence of aldol condensation: Acetaldehyde adsorption over TiO2 surface. *Journal of Catalysis* **2008**, *260*, 371-379.

(134) Fouad, N. E.; Thomasson, P.; Knözinger, H. Surface reactions of acetone, acetylene and methylbutynol on a yttrium-modified magnesium oxide catalyst. *Applied Catalysis A: General* **2000**, *196*, 125-133.

(135) C. Chisem, I.; Jones, W.; Martin, I.; Martin, C.; Rives, V. Probing the surface acidity of lithium aluminium and magnesium aluminium layered double hydroxides. *Journal of Materials Chemistry* **1998**, *8*, 1917-1925.

(136) Idriss, H.; Diagne, C.; Hindermann, J. P.; Kiennemann, A.; Barteau, M. A. Reactions of Acetaldehyde on CeO2 and CeO2-Supported Catalysts. *Journal of Catalysis* **1995**, *155*, 219-237.

(137) Iglesia, E.; Barton, D. G.; Biscardi, J. A.; Gines, M. J. L.; Soled, S. L. Bifunctional pathways in catalysis by solid acids and bases. *Catalysis Today* **1997**, *38*, 339-360.

(138) Corma, A.; Iborra, S. Optimization of alkaline earth metal oxide and hydroxide catalysts for base-catalyzed reactions. *Advances in Catalysis* **2006**, *49*, 239-302.

(139) Baigrie, L. M.; Cox, R. A.; Slebocka-Tilk, H.; Tencer, M.; Tidwell, T. T. Acid-catalyzed enolization and aldol condensation of acetaldehyde. *Journal of the American Chemical Society* **1985**, *107*, 3640-3645.

(140) Stefanov, B. I.; Topalian, Z.; Granqvist, C.-G.; Österlund, L. Acetaldehyde adsorption and condensation on anatase TiO 2: Influence of acetaldehyde dimerization. *Journal of Molecular Catalysis A: Chemical* **2014**, *381*, 77-88.

(141) Fierro, J. L. G.: *Metal oxides: chemistry and applications*; CRC press, 2005.

(142) Marcu, I.-C.; Tichit, D.; Fajula, F.; Tanchoux, N. Catalytic valorization of bioethanol over Cu-Mg-Al mixed oxide catalysts. *Catalysis Today* **2009**, *147*, 231-238.

(143) Raskó, J.; Kiss, J. Adsorption and surface reactions of acetaldehyde on TiO2, CeO2 and Al2O3. *Applied Catalysis A: General* **2005**, *287*, 252-260.

(144) Denmark, S. E.; Almstead, N. G. Spectroscopic studies on the structure and conformation of Lewis acid-aldehyde complexes. *Journal of the American Chemical Society* **1993**, *115*, 3133-3139.

(145) Gallezot, P.; Richard, D. Selective Hydrogenation of α,β-Unsaturated Aldehydes. *Catalysis Reviews* **1998**, *40*, 81-126.

(146) Delbecq, F.; Sautet, P. Competitive C□C and C□O Adsorption of α-β-Unsaturated Aldehydes on Pt and Pd Surfaces in Relation with the Selectivity of Hydrogenation Reactions: A Theoretical Approach. *Journal of Catalysis* **1995**, *152*, 217-236.

(147) Aramendía, M. A.; Borau, V.; Jiménez, C.; Marinas, A.; Marinas, J. M.; Porras, A.; Urbano, F. J. Gas-phase hydrogen-transfer reduction of acrolein using 2-propanol over MgO/B2O3 and SiO2/AlPO4 catalysts. *Catal Lett* **1998**, *50*, 173-177.

(148) Ueshima, M.; Shimasaki, Y. Regioselective Reduction of α,β-Unsaturated Carbonyl Compounds to Allylic Alcohols by Vapor Phase Hydrogen Transfer Reaction over MgO-B₂O₃ Catalyst. *Chemistry Letters* **1992**, *21*, 1345-1348.

(149) Wittcoff, H. A.; Reuben, B. G.; Plotkin, J. S.: *Industrial organic chemicals*; John Wiley & Sons, 2012.

(150) Luo, S.; Falconer, J. L. Aldol condensation of acetaldehyde to form high molecular weight compounds on TiO2. *Catal Lett* **1999**, *57*, 89-93.

(151) Yee, A.; Morrison, S. J.; Idriss, H. A Study of ethanol reactions over Pt/CeO 2 by temperature-programmed desorption and in situ FT-IR spectroscopy: evidence of benzene formation. *Journal of Catalysis* **2000**, *191*, 30-45.

(152) Chong, S. V.; Idriss, H. Reactions of acetaldehyde on UO2(111) single crystal surfaces. Evidence of benzene formation. *Journal of Vacuum Science & Technology A* **2001**, *19*, 1933-1937.

(153) Chang, Y.-C.; Ko, A.-N. Vapor phase reactions of acetaldehyde over type X zeolites. *Applied Catalysis A: General* **2000**, *190*, 149-155.

(154) Nadeem, A. M.; Waterhouse, G. I. N.; Idriss, H. The reactions of ethanol on TiO2 and Au/TiO2 anatase catalysts. *Catalysis Today* **2012**, *182*, 16-24.

(155) Calaza, F. C.; Xu, Y.; Mullins, D. R.; Overbury, S. H. Oxygen vacancy-assisted coupling and enolization of acetaldehyde on CeO2 (111). *Journal of the American Chemical Society* **2012**, *134*, 18034-18045.

(156) Burwell Jr, R. L.; Haller, G. L.; Taylor, K. C.; Read, J. F.: Chemisorptive and Catalytic Behavior of Chromia. In *Advances in Catalysis*; D.D. Eley, H. P., Paul, B. W., Eds.; Academic Press, 1969; Vol. Volume 20; pp 1-96.

(157) Ji, W.; Chen, Y.; Kung, H. H. Vapor phase aldol condensation of acetaldehyde on metal oxide catalysts. *Applied Catalysis A: General* **1997**, *161*, 93-104.

(158) Rekoske, J. E.; Barteau, M. A. Kinetics, Selectivity, and Deactivation in the Aldol Condensation of Acetaldehyde on Anatase Titanium Dioxide. *Industrial & Engineering Chemistry Research* **2010**, *50*, 41-51.

(159) Ventosa, E.; Tymoczko, A.; Xie, K.; Xia, W.; Muhler, M.; Schuhmann, W. Low temperature Hydrogen Reduction of High Surface Area Anatase and Anatase/β-TiO2 for High-Charging-Rate Batteries. *ChemSusChem* **2014**, *7*, 2584-2589.

(160) Rekoske, J. E.; Barteau, M. A. Isothermal reduction kinetics of titanium dioxide-based materials. *The Journal of Physical Chemistry B* **1997**, *101*, 1113-1124.

(161) Luo, S.; Falconer, J. L. Acetone and Acetaldehyde Oligomerization on TiO2 Surfaces. *Journal of Catalysis* **1999**, *185*, 393-407.

(162) Idriss, H.; Barteau, M. Selectivity and mechanism shifts in the reactions of acetaldehyde on oxidized and reduced TiO2 (001) surfaces. *Catal Lett* **1996**, *40*, 147-153.

(163) Chizallet, C.; Digne, M.; Arrouvel, C.; Raybaud, P.; Delbecq, F.; Costentin, G.; Che, M.; Sautet, P.; Toulhoat, H. Insights into the Geometry, Stability and Vibrational Properties of OH Groups on γ-Al2O3, TiO2-Anatase and MgO from DFT Calculations. *Topics in Catalysis* **2009**, *52*, 1005-1016.

(164) Hartman, M.; Trnka, O.; Veselý, V. Thermal dehydration of magnesium hydroxide and sintering of nascent magnesium oxide. *AIChE Journal* **1994**, *40*, 536-542.

(165) Biaglow, A. I.; Sepa, J.; Gorte, R. J.; White, D. A 13C NMR Study of the Condensation Chemistry of Acetone and Acetaldehyde Adsorbed at the Brønsted Acid Sites in H-ZSM-5. *Journal of Catalysis* **1995**, *151*, 373-384.

(166) Young, R.; Sheppard, N. Infrared spectroscopic studies of adsorption and catalysis: Acetone and acetaldehyde on silica and silica-supported nickel. *Journal of Catalysis* **1967**, *7*, 223-233.

(167) DeWilde, J. F.; Chiang, H.; Hickman, D. A.; Ho, C. R.; Bhan, A. Kinetics and Mechanism of Ethanol Dehydration on γ-Al2O3: The Critical Role of Dimer Inhibition. *ACS Catalysis* **2013**, *3*, 798-807.

(168) Rauk, A.; Hunt, I. R.; Keay, B. A. Lewis Acidity and Basicity: An Ab Initio Study of Proton and BF3 Affinities of Oxygen-Containing Organic Compounds. *The Journal of Organic Chemistry* **1994**, *59*, 6808-6816.

(169) Shiau, C.-Y.; Chen, S.; Tsai, J. C.; Lin, S. I. Effect of zinc addition on copper catalyst in isoamyl alcohol dehydrogenation. *Applied Catalysis A: General* **2000**, *198*, 95-102.

(170) Church, J. M.; Joshi, H. K. Acetaldehyde by Dehydrogenation of Ethyl Alcohol. *Industrial & Engineering Chemistry* **1951**, *43*, 1804-1811.

(171) Shiau, C.-Y.; Liaw, S.-T. Kinetic Model for Oxidative Dehydrogenation of n-Butanol over Copper-Barium Catalyst. *Journal of Chemical Technology & Biotechnology* **1992**, *53*, 13-19.

(172) Requies, J.; Güemez, M.; Iriondo, A.; Barrio, V.; Cambra, J.; Arias, P. Biobutanol Dehydrogenation to Butyraldehyde over Cu, Ru and Ru–Cu Supported Catalysts. Noble Metal Addition and Different Support Effects. *Catal Lett* **2012**, *142*, 50-59.

(173) Shi, R.; Wang, F.; Mu, X.; Li, Y.; Huang, X.; Shen, W. MgO-supported Cu nanoparticles for efficient transfer dehydrogenation of primary aliphatic alcohols. *Catalysis Communications* **2009**, *11*, 306-309.

(174) Takacs, J. M.; Jiang, X. The Wacker reaction and related alkene oxidation reactions. *Current Organic Chemistry* **2003**, *7*, 369-396.

(175) Kohlpaintner, C.; Schulte, M.; Falbe, J.; Lappe, P.; Weber, J. Aldehydes, aliphatic and araliphatic. *Ullmann's Encyclopedia of Industrial Chemistry* **2000**.

(176) Rioux, R.; Vannice, M. Hydrogenation/dehydrogenation reactions: isopropanol dehydrogenation over copper catalysts. *Journal of Catalysis* **2003**, *216*, 362-376.

(177) Geravand, E.; Shariatinia, Z.; Yaripour, F.; Sahebdelfar, S. Synthesis of copper–silica nanosized catalysts for 2-butanol dehydrogenation and optimization of preparation parameters by response surface method. *Chemical Engineering Research and Design* **2015**, *96*, 63-77.

(178) Crivello, M. E.; Pérez, C. F.; Mendieta, S. N.; Casuscelli, S. G.; Eimer, G. A.; Elías, V. R.; Herrero, E. R. n-Octyl alcohol dehydrogenation over copper catalysts. *Catalysis Today* **2008**, *133–135*, 787-792.

(179) Della Pina, C.; Falletta, E.; Rossi, M. Highly selective oxidation of benzyl alcohol to benzaldehyde catalyzed by bimetallic gold–copper catalyst. *Journal of Catalysis* **2008**, *260*, 384-386.

(180) Ji, D.; Zhu, W.; Wang, Z.; Wang, G. Dehydrogenation of cyclohexanol on Cu–ZnO/SiO2 catalysts: The role of copper species. *Catalysis Communications* **2007**, *8*, 1891-1895.

(181) Davis, J. L.; Barteau, M. A. Decarbonylation and decomposition pathways of alcohol's on Pd(111). *Surface Science* **1987**, *187*, 387-406.

(182) Davis, J. L.; Barteau, M. A. Spectroscopic identification of alkoxide, aldehyde, and acyl intermediates in alcohol decomposition on Pd(111). *Surface Science* **1990**, *235*, 235-248.

(183) Cohen, M. D.; Kargacin, B.; Klein, C. B.; Costa, M. Mechanisms of chromium carcinogenicity and toxicity. *CRC Critical Reviews in Toxicology* **1993**, *23*, 255-281.

(184) Tanabe, K.; Misono, M.; Hattori, H.; Ono, Y.: *New solid acids and bases: their catalytic properties*; Elsevier, 1990.

(185) van der Burg, A.; Doornbos, J.; Kos, N. J.; Ultee, W. J.; Ponec, V. Selectivity of Ni□Cu and Pt□Au alloys in reactions of butanol and related compounds. *Journal of Catalysis* **1978**, *54*, 243-253.

(186) Liu, X.; Madix, R. J.; Friend, C. M. Unraveling molecular transformations on surfaces: a critical comparison of oxidation reactions on coinage metals. *Chemical Society Reviews* **2008**, *37*, 2243-2261.

(187) Keuler, J. N.; Lorenzen, L.; Miachon, S. The dehydrogenation of 2-butanol over copper-based catalysts: optimising catalyst composition and determining kinetic parameters. *Applied Catalysis A: General* **2001**, *218*, 171-180.

(188) Jiao, L.; Regalbuto, J. R. The synthesis of highly dispersed noble and base metals on silica via strong electrostatic adsorption: I. Amorphous silica. *Journal of Catalysis* **2008**, *260*, 329-341.

(189) d'Alnoncourt, R. N.; Kurtz, M.; Wilmer, H.; Löffler, E.; Hagen, V.; Shen, J.; Muhler, M. The influence of ZnO on the differential heat of adsorption of CO on Cu catalysts: a microcalorimetric study. *Journal of Catalysis* **2003**, *220*, 249-253.

(190) Golunski, S. E. Final Analysis: Why Use Platinum in Catalytic Converters? *Platinum Metals Review* **2007**, *51*, 162-162.

(191) Hammer, B.; Morikawa, Y.; Nørskov, J. K. CO chemisorption at metal surfaces and overlayers. *Physical review letters* **1996**, *76*, 2141.

(192) Abild-Pedersen, F.; Andersson, M. CO adsorption energies on metals with correction for high coordination adsorption sites–A density functional study. *Surface Science* **2007**, *601*, 1747-1753.

(193) Delbecq, F.; Sautet, P. Adsorption of aldehydes and ketones on platinum and palladium: influence of steps, open faces and metal nature: A theoretical study. *Surface Science* **1993**, *295*, 353-373.

(194) Shekhar, R.; Barteau, M. A.; Plank, R. V.; Vohs, J. M. Adsorption and Reaction of Aldehydes on Pd Surfaces. *The Journal of Physical Chemistry B* **1997**, *101*, 7939-7951.

(195) Gates, S. M.; Russell Jr, J. N.; Yates Jr, J. T. Bond activation sequence observed in the chemisorption and surface reaction of ethanol on Ni(111). *Surface Science* **1986**, *171*, 111-134.

(196) Sexton, B. A.; Rendulic, K. D.; Huges, A. E. Decomposition pathways of C1□C4 alcohols adsorbed on platinum (111). *Surface Science* **1982**, *121*, 181-198.

(197) Pham, T. T.; Crossley, S. P.; Sooknoi, T.; Lobban, L. L.; Resasco, D. E.; Mallinson, R. G. Etherification of aldehydes, alcohols and their mixtures on Pd/SiO2 catalysts. *Applied Catalysis A: General* **2010**, *379*, 135-140.

(198) Mavrikakis, M.; Barteau, M. A. Oxygenate reaction pathways on transition metal surfaces. *Journal of Molecular Catalysis A: Chemical* **1998**, *131*, 135-147.

(199) Sexton, B. A.; Hughes, A. E.; Avery, N. R. A spectroscopic study of the adsorption and reactions of methanol, formaldehyde and methyl formate on clean and oxygenated Cu(110) surfaces. *Surface Science* **1985**, *155*, 366-386.

(200) Li, R.; Zhang, M.; Yu, Y. A DFT study on the Cu (111) surface for ethyl acetate synthesis from ethanol dehydrogenation. *Applied Surface Science* **2012**, *258*, 6777-6784.

(201) Rioux, R. M.; Vannice, M. A. Dehydrogenation of isopropyl alcohol on carbon-supported Pt and Cu–Pt catalysts. *Journal of Catalysis* **2005**, *233*, 147-165.

(202) Skoda, F.; Astier, M.; Pajonk, G.; Primet, M. Surface characterization of palladium-copper bimetallic catalysts by FTIR spectroscopy and test reactions. *Catal Lett* **1994**, *29*, 159-168.

(203) Xu, B.; Liu, X.; Haubrich, J.; Friend, C. M. Vapour-phase gold-surface-mediated coupling of aldehydes with methanol. *Nat Chem* **2010**, *2*, 61-65.

(204) Chhabra, M.; Naidu, S. Ethanol Dehydrogenation Catalysts A Developmental Approach. *Chem. Ind. Dig* **1996**, *9*, 118-122.

(205) Franckaerts, J.; Froment, G. F. Kinetic study of the dehydrogenation of ethanol. *Chemical Engineering Science* **1964**, *19*, 807-818.

(206) Shiau, C.-Y.; Tsai, J. C. Cu/SiO2 catalyst prepared by electroless method. *Journal of Chemical Technology & Biotechnology* **1998**, *73*, 414-420.

(207) Toupance, T.; Kermarec, M.; Lambert, J.-F.; Louis, C. Conditions of Formation of Copper Phyllosilicates in Silica-Supported Copper Catalysts Prepared by Selective Adsorption. *The Journal of Physical Chemistry B* **2002**, *106*, 2277-2286.

(208) Gong, J.; Yue, H.; Zhao, Y.; Zhao, S.; Zhao, L.; Lv, J.; Wang, S.; Ma, X. Synthesis of Ethanol via Syngas on Cu/SiO2 Catalysts with Balanced Cu0–Cu+ Sites. *Journal of the American Chemical Society* **2012**, *134*, 13922-13925.

(209) Yu, X.; Zhai, S.; Zhu, W.; Gao, S.; Yan, J.; Yuan, H.; Chen, L.; Luo, J.; Zhang, W.; Wang, Z. The direct transformation of ethanol to ethyl acetate over Cu/SiO catalysts that contain copper phyllosilicate. *Journal of Chemical Sciences* **2014**, *126*, 1013-1020.

(210) Sato, A. G.; Volanti, D. P.; de Freitas, I. C.; Longo, E.; Bueno, J. M. C. Site-selective ethanol conversion over supported copper catalysts. *Catalysis Communications* **2012**, *26*, 122-126.

(211) Zhang, Y.; Zheng, N.; Wang, K.; Zhang, S.; Wu, J. Effect of Copper Nanoparticles Dispersion on Catalytic Performance of Cu/SiO2 Catalyst for Hydrogenation of Dimethyl Oxalate to Ethylene Glycol. *Journal of Nanomaterials* **2013**, *2013*, 6.

(212) Yin, A.; Guo, X.; Dai, W.-L.; Fan, K. Effect of initial precipitation temperature on the structural evolution and catalytic behavior of Cu/SiO2 catalyst in the hydrogenation of dimethyloxalate. *Catalysis Communications* **2011**, *12*, 412-416.

(213) Kazachkin, D. V.: Ensemble Size Effect in Catalysis by Platinum-Copper Silica Supported Bimetallic Catalysts. 2006.

(214) Coloma, F.; Marquez, F.; Rochester, C. H.; Anderson, J. A. Determination of the nature and reactivity of copper sites in Cu–TiO 2 catalysts. *Physical Chemistry Chemical Physics* **2000**, *2*, 5320-5327.

(215) Chladek, P.; Croiset, E.; Epling, W.; Hudgins, R. R. Characterization of copper foam as catalytic material in ethanol dehydrogenation. *The Canadian Journal of Chemical Engineering* **2007**, *85*, 917-924.

(216) Rodriguez, J. A.; Goodman, D. W. The Nature of the Metal-Metal Bond in Bimetallic Surfaces. *Science* **1992**, *257*, 897-903.

(217) Doca, N.; Segal, E. Kinetics of dehydrogenation of low aliphatic alcohols on copper catalysts containing small amounts of Cr, Mn, Fe and Ni. *React Kinet Catal Lett* **1985**, *28*, 123-129.

(218) Yin, A.; Wen, C.; Guo, X.; Dai, W.-L.; Fan, K. Influence of Ni species on the structural evolution of Cu/SiO2 catalyst for the chemoselective hydrogenation of dimethyl oxalate. *Journal of Catalysis* **2011**, *280*, 77-88.

(219) Subramanian, P.; Laughlin, D. Cu-Pd (copper-palladium). *Journal of phase equilibria* **1991**, *12*, 231-243.

(220) Subramanian, P.; Perepezko, J. The Ag-Cu (silver-copper) system. *Journal of Phase Equilibria* **1993**, *14*, 62-75.

(221) Shimizu, K.-i.; Shimura, K.; Nishimura, M.; Satsuma, A. Silver cluster-promoted heterogeneous copper catalyst for N-alkylation of amines with alcohols. *RSC Advances* **2011**, *1*, 1310-1317.

(222) Okamoto, H.; Chakrabarti, D.; Laughlin, D.; Massalski, T. The Au– Cu (gold-copper) system. *Journal of Phase Equilibria* **1987**, *8*, 454-474.

(223) Soma-Noto, Y.; Sachtler, W. M. H. Infrared spectra of carbon monoxide adsorbed on silica-supported nickel-copper alloys. *Journal of Catalysis* **1974**, *34*, 162-165.

(224) Zhu, Y.-M.; Shi, X. W. L. Hydrogenation of Ethyl Acetate to Ethanol over Bimetallic Cu-Zn/SiO2 Catalysts Prepared by Means of Coprecipitation. *Bulletin of the Korean Chemical Society* **2014**, *35*.

(225) Tu, Y.-J.; Tu, C.; Li, Y.-W.; Chen. Effect of chromium promoter on copper catalysts in ethanol dehydrogenation. *Journal of chemical technology and biotechnology* **1994**, *59*, 141-147.

(226) He, Z.; Lin, H.; He, P.; Yuan, Y. Effect of boric oxide doping on the stability and activity of a Cu–SiO2 catalyst for vapor-phase hydrogenation of dimethyl oxalate to ethylene glycol. *Journal of Catalysis* **2011**, *277*, 54-63.

(227) Suryanarayana, C. Mechanical alloying and milling. *Progress in materials science* **2001**, *46*, 1-184.

(228) Tu, Y.-J.; Chen, Y.-W. Effects of Alkaline-Earth Oxide Additives on Silica-Supported Copper Catalysts in Ethanol Dehydrogenation. *Industrial & Engineering Chemistry Research* **1998**, *37*, 2618-2622.

(229) Santacesaria, E.; Carotenuto, G.; Tesser, R.; Di Serio, M. Ethanol dehydrogenation to ethyl acetate by using copper and copper chromite catalysts. *Chemical Engineering Journal* **2012**, *179*, 209-220.

(230) Tonner, S. P.; Trimm, D. L.; Wainwright, M. S.; Cant, N. W. Dehydrogenation of methanol to methyl formate over copper catalysts. *Industrial & Engineering Chemistry Product Research and Development* **1984**, *23*, 384-388.

(231) Morgenstern, D. A.; Fornango, J. P. Low-Temperature Reforming of Ethanol over Copper-Plated Raney Nickel: A New Route to Sustainable Hydrogen for Transportation. *Energy & Fuels* **2005**, *19*, 1708-1716.

(232) Cuenya, B. R. Synthesis and catalytic properties of metal nanoparticles: Size, shape, support, composition, and oxidation state effects. *Thin Solid Films* **2010**, *518*, 3127-3150.

(233) Evans, J.; Wainwright, M.; Bridgewater, A.; Young, D. On the determination of copper surface area by reaction with nitrous oxide. *Applied Catalysis* **1983**, *7*, 75-83.

(234) Ma, X.; Yang, Z.; Liu, X.; Tan, X.; Ge, Q. Dynamic redox cycle of Cu0 and Cu+ over Cu/SiO2 catalyst in ester hydrogenation. *RSC Advances* **2015**, *5*, 37581-37584.

(235) Mehta, R. N.; Chakraborty, M.; Mahanta, P.; Parikh, P. A. Evaluation of Fuel Properties of Butanol−Biodiesel−Diesel Blends and Their Impact on Engine Performance and Emissions. *Industrial & Engineering Chemistry Research* **2010**, *49*, 7660-7665.

(236) Pfromm, P. H.; Amanor-Boadu, V.; Nelson, R.; Vadlani, P.; Madl, R. Bio-butanol vs. bio-ethanol: A technical and economic assessment for corn and switchgrass fermented by yeast or Clostridium acetobutylicum. *Biomass and Bioenergy* **2010**, *34*, 515-524.

(237) Patel, A. D.; Telalović, S.; Bitter, J. H.; Worrell, E.; Patel, M. K. Analysis of sustainability metrics and application to the catalytic production of higher alcohols from ethanol. *Catalysis Today* **2015**, *239*, 56-79.

(238) Dias, M. O. S.; Pereira, L. G.; Junqueira, T. L.; Pavanello, L. G.; Chagas, M. F.; Cavalett, O.; Maciel Filho, R.; Bonomi, A. Butanol production in a sugarcane biorefinery using ethanol as feedstock. Part I: Integration to a first generation sugarcane distillery. *Chemical Engineering Research and Design* **2014**, *92*, 1441-1451.

(239) Gabriels, D.; Hernandez, W. Y.; Sels, B.; Van Der Voort, P.; Verberckmoes, A. Review of catalytic systems and thermodynamics for the Guerbet condensation reaction and challenges for biomass valorization. *Catalysis Science & Technology* **2015**, *5*, 3876-3902.

(240) Norman, D. W.; Billodeaux, D. R.; Page, M. D.: Dual catalyst system for the self-condensation of alcohols. Google Patents, 2014.

(241) Ward, R.: Mixed Metal Oxides. In *Progress in Inorganic Chemistry*; John Wiley & Sons, Inc., 2007; pp 465-536.

(242) Evans, M. G.; Polanyi, M. Some applications of the transition state method to the calculation of reaction velocities, especially in solution. *Transactions of the Faraday Society* **1935**, *31*, 875-894.

(243) Panayotov, D. A.; Yates, J. T. Spectroscopic Detection of Hydrogen Atom Spillover from Au Nanoparticles Supported on TiO2: Use of Conduction Band Electrons. *The Journal of Physical Chemistry C* **2007**, *111*, 2959-2964.

(244) Sreekumar, S.; Baer, Z. C.; Pazhamalai, A.; Gunbas, G.; Grippo, A.; Blanch, H. W.; Clark, D. S.; Toste, F. D. Production of an acetone-butanol-ethanol mixture from Clostridium acetobutylicum and its conversion to high-value biofuels. *Nature protocols* **2015**, *10*, 528-537.

(245) Makshina, E. V.; Dusselier, M.; Janssens, W.; Degrève, J.; Jacobs, P. A.; Sels, B. F. Review of old chemistry and new catalytic advances in the on-purpose synthesis of butadiene. *Chemical Society Reviews* **2014**, *43*, 7917-7953.

(246) Huang, H.-J.; Ramaswamy, S.; Tschirner, U. W.; Ramarao, B. V. A review of separation technologies in current and future biorefineries. *Separation and Purification Technology* **2008**, *62*, 1-21.

(247) Mohammadi, M. R.; Cordero-Cabrera, M. C.; Ghorbani, M.; Fray, D. J. Synthesis of high surface area nanocrystalline anatase-TiO2 powders derived from particulate sol-gel route by tailoring processing parameters. *J Sol-Gel Sci Technol* **2006**, *40*, 15-23.

(248) Chen, D.; Huang, F.; Cheng, Y.-B.; Caruso, R. A. Mesoporous Anatase TiO2 Beads with High Surface Areas and Controllable Pore Sizes: A Superior Candidate for High-Performance Dye-Sensitized Solar Cells. *Advanced Materials* **2009**, *21*, 2206-2210.

(249) Haryanto, A.; Fernando, S.; Murali, N.; Adhikari, S. Current Status of Hydrogen Production Techniques by Steam Reforming of Ethanol: A Review. *Energy & Fuels* **2005**, *19*, 2098-2106.

(250) Ni, M.; Leung, D. Y. C.; Leung, M. K. H. A review on reforming bio-ethanol for hydrogen production. *International Journal of Hydrogen Energy* **2007**, *32*, 3238-3247.